

Antenna Showers with One-Loop Matrix Elements

L. Hartgring,^a E. Laenen,^{a,b,c} and P. Skands^d

^a*Nikhef Theory Group, Science Park 105, Amsterdam, The Netherlands*

^b*ITFA, University of Amsterdam, Science Park 904, Amsterdam, The Netherlands*

^c*ITF, Utrecht University, Leuvenlaan 4, Utrecht, The Netherlands*

^d*Theoretical Physics CERN,
CH-1211 Geneva 23, Switzerland*

E-mail: lhartgri@nikhef.nl, Eric.Laenen@nikhef.nl, peter.skands@cern.ch

ABSTRACT: We consider the probability for a colour-singlet $q\bar{q}$ pair to emit a gluon, in strongly and smoothly ordered antenna showers. We expand to second order in α_s and compare to the second-order QCD matrix elements for $Z \rightarrow 3$ jets, neglecting terms suppressed by $1/N_C^2$. We give a prescription that corrects the shower to the matrix-element result at this order for both soft and hard emissions, thereby explicitly reducing its dependence on evolution- and renormalization-scale choices. We confirm that the choice of p_\perp for both of these scales absorbs all logarithms through $\mathcal{O}(\alpha_s^2)$, and contrast this with various alternatives. We include these corrections in the VINCIA shower generator and study the impact on LEP event-shape and fragmentation observables. An uncertainty estimate is provided for each event, in the form of a vector of alternative weights.

KEYWORDS: NLO matching, Parton Shower

ARXIV EPRINT: [1303.4974](https://arxiv.org/abs/1303.4974)

Contents

1	Introduction	1
2	Antenna Showers	3
2.1	The Formal Basis of Antenna Showers	4
2.2	Constructing a Shower Algorithm	6
2.3	Evolution and Ordering	9
2.4	Smooth Ordering	14
3	Matched Antenna Showers	17
3.1	Tree-Level Matching	17
3.2	One-Loop Matching at the Born Level	19
3.2.1	Inclusive Born	20
3.2.2	Exclusive Born	20
3.3	One-Loop Matching for Born + 1 Parton	22
3.4	The Renormalization Term	27
3.5	Leading-Colour One-Loop Correction for $Z \rightarrow 3$ Jets	30
3.6	One-Loop Correction for Born + 2 Partons	32
3.7	One-Loop Matching for Sector Showers	33
4	Sudakov Integrals	35
4.1	Strong Ordering	35
4.1.1	Dipole Virtuality	36
4.1.2	Transverse Momentum	42
4.1.3	Energy	44
4.2	Smooth Ordering	48
4.2.1	Dipole virtuality	49
4.2.2	Transverse momentum	51
4.3	Tables of Infrared Limits	54
5	Results including both LO and NLO corrections	54
5.1	Finite antenna terms and LO matching corrections	55
5.2	LEP Results	58
5.3	Uncertainties	62
5.4	Speed	64
6	Outlook and Conclusions	66
A	Infrared singular operators	68

B	One-Loop Amplitudes	68
B.1	Renormalization	68
B.2	One-loop Matrix Element	68
C	Antenna integrals	70
C.1	Strong Ordering Gluon Emission	70
C.1.1	Dipole Virtuality	71
C.1.2	Transverse Momentum	72
C.1.3	Energy ordering	73
C.2	Strong Ordering Gluon Splitting	73
C.3	Smooth Ordering Gluon Emission	74
C.3.1	Smooth mass ordering	75
C.3.2	Smooth transverse momentum ordering	76
C.4	Smooth Ordering Gluon Splitting	77
C.4.1	Emissions ordered in \mathbf{m}_D , splittings in $\mathbf{m}_{q\bar{q}}$	77
C.4.2	Emissions ordered in \mathbf{p}_\perp , splittings in $\mathbf{m}_{q\bar{q}}$	78
D	NLO Tune Parameters	78

1 Introduction

Modern QCD descriptions of hard-scattering events at particle colliders can be roughly divided into two broad categories. In the first, fixed-order descriptions, matrix elements are computed for all allowed initial states with a given final state, F , plus a limited number of additional partons. The leading-order (LO) description has the minimal number (often zero) of additional partons. For improved accuracy, one includes matrix elements with one extra parton beyond leading order and one loop correction (next-to-leading order) and so forth. The squared matrix elements are numerically integrated over the allowed phase space, after accounting for any divergences. Given the accuracy, i.e. order of the description, the possible number of additional final-state particles is in essence predetermined, and can take one (LO), or two (NLO) etc, values. In the second, parton-shower descriptions, one also starts from matrix elements for the desired hard process, F , but additional radiation is now generated stochastically via a shower algorithm, which is essentially Markovian. This is a unitary process, with probability one, and therefore does not change the probability of the underlying hard process to occur. The number of final-state partons is now not predetermined, and can take an infinity of different values. The two approaches have complementary strengths and weaknesses (for a review, see e.g. [1]). When hard extra emissions (e.g., hard jets) are important to model well, one looks to descriptions of the first category. However, the calculation is then unpredictive for near-collinear and soft radiation (e.g., jet substructure and soft wide-angle jets). The obverse holds for the second category.

Even from this very cursory summary, it is clear that methods to unite the two — combining strengths and eliminating weaknesses — are very important. Two longstanding and very successful approaches for combining one-loop matrix elements with parton showers are MC@NLO [2–6] and POWHEG [7–9]. An important restriction of both of these is that only the spectra of the basic hard-scattering partons are corrected to NLO precision, while those of additional QCD emissions are not. Removing this limitation, fully or partially, has been the focus of much recent effort [10–19], and is also among the main goals of this paper. While most other approaches employ parton-shower algorithms which are based on $1 \rightarrow 2$ splitting kernels, we develop an approach for matching NLO descriptions to showers based on $2 \rightarrow 3$ splittings [20]. The equivalent of the $1 \rightarrow 2$ splitting kernels are, for us, dipole-antenna functions [20–22]. At the practical level, our approach is in the context of the VINCIA framework [23, 24]. Whatever the splitting kernel, the parton-shower approaches rest upon the factorization of both phase space and matrix element when the splitting is either soft or collinear, or both. A technical advantage of our approach is that the $(n + 3)$ -particle phase-space factorizes exactly into a $(n + 2)$ -particle phase space times a $2 \rightarrow 3$ phase space with all momenta on-shell, without need for momentum reshuffling [25]. Phase-space factorization and the antenna-based matrix-element factorization are important to our approach in about equal measure.

The essential bottleneck in such combinations of fixed order and parton shower is how to avoid double counting both real emissions as well as virtual effects. A key aspect of this is how well the NLO emissions are mimicked by parton-shower emissions. Emissions generated by a parton-shower Markov chain in fact produce approximations to tree-level matrix elements up to arbitrary numbers of legs, while the no-emission Sudakov factors generate the equivalent all-orders loop corrections¹. This all-orders resummation of contributions is ordered in a measure of jet resolution, called the evolution scale, which we denote Q_E . It is typically chosen to be a measure of transverse momentum [20] or invariant mass. Its fundamental role is to separate resolved from unresolved emissions, in analogy to a jet-clustering measure. The different evolution variables each have their strengths, depending on the context. As part of our present study, we judge them by how well their fixed-order expansions approximate the NLO matrix elements.

The main purpose of this paper is to define, for e^+e^- initial states, an antenna-based shower algorithm that incorporates multileg NLO corrections for both soft and hard emissions, and to study the quality of the matching for a variety of evolution variables. We strive for next-to-leading logarithmic (NLL) accuracy, in a way we shall detail below.

The leading-logarithmic (LL) structure of antenna showers was discussed in [27, 28], with explicit comparisons of various algorithms to tree-level $\mathcal{O}(\alpha_s^2)$ matrix elements presented in [24, 28, 29]. A prescription for matching the showers to reproduce tree-level matrix elements exactly (over all of phase space) was developed in [24], with uncertainty variations provided in the form of vectors of alternative weights for each event. In [30] and [31] substantial speedups

¹For an introduction to such chains and a description of their properties, see e.g. [1, 26].

of the matching algorithm were obtained by dividing phase space into so-called sectors, and by deriving a formalism for using individual helicity amplitudes to correct the shower evolution, respectively. To further probe the structure of antenna showers, at the subleading-logarithmic level, we shall here consider the expansion of exclusive $2 \rightarrow 3$ splitting probabilities to $\mathcal{O}(\alpha_s^2)$, comparing these to one-loop matrix elements [32] and to corresponding second-order antenna functions [22, 33].

We shall compare six different types of ordering criteria for the shower evolution: 1) strong ordering in transverse momentum, 2) strong ordering in dipole virtuality, 3 & 4) strong ordering in two variants of emission energy (mostly intended as cross-checks), and 5 & 6) so-called smooth ordering in p_\perp and in dipole virtuality, as defined by [24]. We also consider several different choices for the renormalization scale μ_R used in the tree-level antenna functions and discuss how to systematically absorb contributions proportional to the β -function by this choice, elaborating on earlier arguments [34, 35].

Finally, we will present a prescription for how to systematically incorporate the second-order (one-loop) $q\bar{q} \rightarrow qg\bar{q}$ antenna into the shower evolution, for each of the studied evolution variable choices. This will essentially constitute the NLL accuracy mentioned above. The resulting shower algorithm, whose $q\bar{q} \rightarrow qg\bar{q}$ splitting probability should therefore be correct to $\mathcal{O}(\alpha_s^2)$ over all of phase space, has been implemented in the publicly available VINCIA plug-in [23] to the PYTHIA 8 event generator [36].

We have organized the paper as follows. In section 2 we discuss introductory aspects of (antenna) shower algorithms, define the various evolution variables, and the implementation of an ordering prescription that rules the shower evolution. In section 3 we present our matching prescription in detail, initially for 3-parton final states in Z -decay, then generally for n partons. In section 4 we discuss details of the Sudakov integrals required in the matching prescription and compare the infrared limits of those integrals to those of the one-loop matrix elements. In section 5 we combine one-loop and tree-level corrections in a single algorithm, perform speed benchmarking, and study the impact on LEP observables, especially in the context of $\alpha_s(m_Z)$ extractions. We conclude in section 6 and elaborate on technical aspects in the appendices.

2 Antenna Showers

In this section, we recap the basic antenna-shower formalism, as used in the VINCIA shower algorithm. This also serves to introduce the basic notation and conventions that will be used in later sections.

2.1 The Formal Basis of Antenna Showers

Antenna showers are based on the factorization of (squared) colour-ordered QCD amplitudes in soft and collinear limits, which can be expressed as follows

$$|M(\dots, p_i, p_j, \dots)|^2 \xrightarrow{i||j} g_s^2 \mathcal{C} \frac{P(z)}{s_{ij}} |M(\dots, p_i + p_j, \dots)|^2 \quad (2.1)$$

$$|M(\dots, p_i, p_j, p_k, \dots)|^2 \xrightarrow{jg \text{ soft}} g_s^2 \mathcal{C} A_g(s_{ij}, s_{jk}, s_{ijk}) |M(\dots, p_i, p_k, \dots)|^2, \quad (2.2)$$

with $g_s^2 = 4\pi\alpha_s$ the strong coupling and the subscript g in the second line emphasizing that the soft limit is only relevant for gluons.

In the collinear limit (first line), $P(z)$ are the Altarelli-Parisi splitting kernels [37], z is the energy fraction taken by parton i (with a fraction $(1 - z)$ going to parton j), and \mathcal{C} is a colour factor, which we discuss below. This limit forms the basis for traditional parton showers, such as those in the PYTHIA generator [38].

In the soft-gluon limit (second line), the function A has dimension GeV^{-2} , and is called an antenna function. For unpolarized massless partons², its leading term is the so-called eikonal or dipole factor,

$$A_{\text{Eik}}(s_{ij}, s_{jk}, s_{ijk}) = \frac{2s_{ik}}{s_{ij}s_{jk}}, \quad (2.3)$$

where $s_{ik} = s_{ijk} - s_{ij} - s_{jk}$ for massless partons. It was found early on that this factor can be reproduced by a traditional parton shower by imposing the requirement of angular ordering of subsequent emissions [40]. This gave rise to the angular-ordered showers [41, 42] in the HERWIG and HERWIG++ generators [43, 44] as well as the imposition of an angular-ordering constraint [38, 45] in the JETSET and PYTHIA generators [36, 46].

In fixed-order calculations, dipole [47] and antenna [21, 22, 25] functions are frequently used to define subtraction terms. These functions include additional subleading terms, beyond the eikonal one, which are necessary to correctly describe both soft and collinear limits in all regions of phase space. In the parametrization we shall use, their most general forms, for the branching process $IK \rightarrow ijk$, are

$$A_{\text{Emit}}(s_{ij}, s_{jk}, m_{IK}^2) = \frac{1}{m_{IK}^2} \left(\frac{2y_{ik}}{y_{ij}y_{jk}} + \frac{y_{jk}(1 - y_{jk})^{\delta_{ig}}}{y_{ij}} + \frac{y_{ij}(1 - y_{ij})^{\delta_{kg}}}{y_{jk}} + F_{\text{Emit}} \right) \quad (2.4)$$

$$A_{\text{Split}}(s_{ij}, s_{jk}, m_{IK}^2) = \frac{1}{m_{IK}^2} \left(\frac{y_{jk}^2 + y_{ik}^2}{2y_{ij}} + F_{\text{Split}} \right), \quad (2.5)$$

for gluon-emission and gluon-splitting processes, respectively, with the parent antenna invariant mass, $m_{IK}^2 = (p_I + p_K)^2 = (p_i + p_j + p_k)^2$ and the scaled invariants,

$$y_{ij} = \frac{s_{ij}}{m_{IK}^2}; \quad y_{jk} = \frac{s_{jk}}{m_{IK}^2}, \quad (2.6)$$

²In the context of massive particles, replace s_{ab} by $2p_a \cdot p_b$ in all expressions. For a more complete treatment, see [39].

and we use the notation $\delta_{ig} = 1$ if parton i is a gluon and zero otherwise. The functions F_{Emit} and F_{Split} allow for the presence of non-singular terms, which are in principle arbitrary. A logical choice would be $F = 0$, but this would not be invariant under reparametrizations of the antenna functions across the gluon-collinear singular limits [24]. Since the F functions can anyway be made useful in the context of uncertainty estimates [23, 24], we therefore leave them as functions whose forms we are free to choose.

In the soft-gluon limit, the eikonal factor is reproduced by the first term in in eq. (2.4). In the collinear $q \rightarrow qg$ limit, the AP splitting kernel also is reproduced. For collinear $g \rightarrow gg$ and $g \rightarrow q\bar{q}$ branchings, one must sum over the contributions from two neighbouring antennae, which together reproduce the AP splitting kernel. Limits that are both soft and collinear are also correctly reproduced [22].

In the antenna context, the colour factors are $2C_F$ for $q\bar{q} \rightarrow qq\bar{q}$, C_A for $gg \rightarrow ggg$ ³, and $2T_R$ for gluon splitting to $q\bar{q}$, again using the normalization convention adopted in [24]. However, for $gg \rightarrow ggg$ there is a genuine subleading ambiguity whether to prefer, say, $2C_F$, C_A , or something interpolating between them [48]. At fixed order, the question of subleading colour can in fact be dealt with quite elegantly, by using C_A for all antennae and then including an additional $q\bar{q}$ antenna with a negative colour factor, $-C_A/N_C^2$, spanned between the two endpoint quarks, for each $gg \dots \bar{q}$ chain [49]. In the context of an antenna-based shower, however, it is desirable to use only positive-definite antenna functions, and a prescription for absorbing the negative one into the positive ones was given in [24]. In the context of this work, however, we shall largely ignore subleading-colour aspects and, unless explicitly stated otherwise, assign a colour factor C_A to the $gg \rightarrow ggg$ antenna function, thereby overcounting the collinear limit in the quark direction by a factor $C_A/(2C_F) \simeq 1 + 1/N_C^2$.

The renormalization scale used to evaluate the strong coupling in the antenna function, $g_s^2 = 4\pi\alpha_s(\mu_{\text{PS}})$, is typically chosen proportional to p_\perp (following [34]). As alternatives, we shall also consider $\mu_{\text{PS}}^2 \propto m_D^2 = 2\min(s_{ij}, s_{jk})$, and, as an extreme case which connects with fixed-order calculations, the invariant mass of the antenna, $\mu_{\text{PS}}^2 \propto m_{IK}^2$.

A final aspect concerns the phase-space factorization away from the collinear limit. Within the framework of collinear factorization (and hence, in traditional parton showers), the momentum fraction, z , is only uniquely defined in the exactly collinear limit; outside that limit, the choice of z is not unique. In addition, a prescription must be adopted for ensuring overall momentum conservation, leading to the well-known ambiguities concerning recoil strategies (see e.g. [1]). In antenna showers, on the other hand, the antenna function is defined in terms of the unique branching invariants, s_{ij} and s_{jk} , over all of phase space, and the phase space itself has an exact Lorentz-invariant and momentum-conserving factorization,

$$d\Phi_n = d\Phi_{n-1} \times d\Phi_{\text{Ant}} , \quad (2.7)$$

³Note that in a process like $H^0 \rightarrow gg$, there are two gg antennae at the Born level, and hence the antenna approximation to $H^0 \rightarrow ggg$ is twice as large as the single $gg \rightarrow ggg$ antenna. Likewise, the collinear limit of a gluon is obtained by summing over the contributions from both of the dipoles/antennae it is connected to. One must also include a sum over permutations of the final-state gluons, if comparing to a summed matrix-element expression.

with

$$d\Phi_{\text{Ant}} = \frac{1}{16\pi^2 m_{IK}^2} ds_{ij} ds_{jk} \frac{d\phi}{2\pi} \quad (2.8)$$

for massless partons (for massive ones, see [39]), with the ϕ angle parametrizing rotations around the antenna axis, in the CM of the antenna. Note the equality signs; no approximation is involved in this step. The only remaining phase-space ambiguity, outside the singular limits, is present when specifying how the post-branching momenta are related to the pre-branching ones. This is defined by a kinematics map, the antenna equivalent of a recoil strategy, which we here take to be of the class defined by [21, 23].

2.2 Constructing a Shower Algorithm

In a shower context, the amplitude and phase-space factorizations above imply that we can interpret the radiation functions (AP splitting kernels or dipole/antenna functions) as the probability for a radiator (parton or dipole/antenna) to undergo a branching, per unit phase-space volume,

$$\frac{dP(\Phi)}{d\Phi} = g_s^2 \mathcal{C} A(\Phi) , \quad (2.9)$$

where we use Φ as shorthand to denote a phase-space point. (If there are several partons/dipoles/antennae, the total probability for branching of the event as a whole is obtained as a sum of such terms.)

An equally fundamental object in both analytical resummations and in parton showers is the Sudakov form factor, which defines the probability for a radiator *not* to emit anything, as a function of the shower evolution parameter, Q (i.e., similarly to a jet veto, with Q playing the role of the jet clustering scale; we return to the choice of functional form for the shower evolution scale in section 2.3). In the all-orders shower construction, these factors generate the sum over virtual amplitudes plus unresolved real radiation, and hence their first-order expansions play a crucial role in matching to next-to-leading order matrix elements. We here recap some basic properties. The Sudakov factor, giving the no-emission probability between two values of the shower evolution parameter, Q_1 and Q_2 (with $Q_1 > Q_2$), is defined by

$$\Delta(Q_1^2, Q_2^2) = \exp \left(- \int_{Q_2^2}^{Q_1^2} \frac{dP(\Phi)}{d\Phi} d\Phi \right) = \exp \left(- \int_{Q_2^2}^{Q_1^2} g_s^2 \mathcal{C} A(\Phi) d\Phi \right) , \quad (2.10)$$

where it is understood that the integral boundaries must be imposed either as step functions on the integrand or by a suitable transformation of integration variables, accompanied by Jacobian factors.

This description has a very close analogue in the simple process of nuclear decay, in which the probability for a nucleus to undergo a decay, per unit time, is given by the nuclear decay constant,

$$\frac{dP(t)}{dt} = c_N . \quad (2.11)$$

The probability for a nucleus existing at time t_1 to remain undecayed before time t_2 , is

$$\Delta(t_2, t_1) = \exp \left(- \int_{t_1}^{t_2} c_N dt \right) = \exp(-c_N \Delta t) . \quad (2.12)$$

This case is especially simple, since the decay probability per unit time, c_N , is constant. By conservation of the total number of nuclei (unitarity), the activity per nucleon at time t , equivalent to the “resummed” decay probability per unit time, is minus the derivative of Δ ,

$$\frac{dP_{\text{res}}(t)}{dt} = -\frac{d\Delta}{dt} = c_N \Delta(t, t_1) . \quad (2.13)$$

In QCD, the emission probability varies over phase space, hence the probability for an antenna not to emit has the more elaborate integral form of eq. (2.10). By unitarity, the resummed branching probability is again minus the derivative of the Sudakov factor,

$$\frac{dP_{\text{res}}(\Phi)}{d\Phi} = g_s^2 \mathcal{C} A(\Phi) \Delta(Q_1^2, Q^2(\Phi)) , \quad (2.14)$$

with $Q^2(\Phi)$ the shower evolution scale (typically chosen as a measure of invariant mass or transverse momentum, see section 2.3), evaluated at the phase-space point Φ .

In shower algorithms, branchings are generated with this distribution, starting from a uniformly distributed random number $\mathcal{R} \in [0, 1]$, by solving the equation,

$$\mathcal{R} = \Delta(Q_1^2, Q^2) \quad (2.15)$$

for Q^2 . For an initial distribution of “trial” branching scales, we do not use the full antenna function, eq. (2.4), as the evolution kernel, but only its leading singularity,

$$A_T = \frac{2m_{IK}^2}{s_{ij}s_{jk}} = \frac{2}{p_{\perp A}^2} , \quad (2.16)$$

where $p_{\perp A}$ is the ARIADNE definition of transverse momentum [50], which is also the one used in VINCIA. This reflects the universal $1/p_{\perp}^2$ behaviour of soft-gluon emissions. In addition to the trial scale, Q , two complementary phase-space variables are also generated (which we usually label ζ and ϕ [24]), according to the shape of A_T over a phase-space contour of constant Q . From these, the model-independent set of trial phase-space variables (s_{ij}, s_{jk}, ϕ) are determined by inversion of the defining relations $Q(s_{ij}, s_{jk})$ and $\zeta(s_{ij}, s_{jk})$, and the full kinematics (i.e., four-momenta) of the trial branching can then be constructed [23].

To decide whether to accept the trial or not, we note that the function A_T differs from the eikonal in eq. (2.3) by the replacement of s_{ik} in the numerator by m_{IK}^2 . By accepting the trial scales generated by A_T with the probability

$$P_{\text{eik}} = \frac{A_{\text{eik}}}{A_T} = \frac{s_{ik}}{m_{IK}^2} \leq 1 , \quad (2.17)$$

the eikonal approximation can be recovered, by virtue of the veto algorithm [1, 51, 52]. Crucially, any other function that has the eikonal as its soft-collinear limit could equally well

be imprinted on the trial distribution by a similar veto. Two particularly relevant choices are the full physical antenna function, eq. (2.4) (which includes additional collinear-singular terms in addition to the eikonal) and the GKS-corrected antenna function (which also incorporates a multiplicative factor that represents tree-level matching in VINCIA),

$$P_{\text{accept}}^{\text{LL}} = \frac{A_{\text{Emit}}}{A_T} , \quad (2.18)$$

$$P_{\text{accept}}^{\text{LO}} = P_{\text{accept}}^{\text{LL}} R_n , \quad (2.19)$$

with A_{Emit} given in eq. (2.4) and R_n the n -parton tree-level GKS matching factor [24], to which we return in section 3.1.

Note that, for gluon-splitting antenna functions ($Xg \rightarrow Xq\bar{q}$), we use $Q = m_{q\bar{q}}$, with a trial function $\propto 1/m_{q\bar{q}}^2$, and again implement the physical antenna function, eq. (2.5), and LO matching corrections by vetos. We also include the so-called ARIADNE factor, P_{Ari} , defined by

$$A_{\text{Split}} \rightarrow P_{\text{Ari}} A_{\text{Split}} = \frac{2s_N}{s_P + s_N} A_{\text{Split}} , \quad (2.20)$$

with s_N the invariant mass squared of the colour neighbour on the other side of the splitting gluon and $s_P = m_{IK}^2$ the invariant mass squared of the parent (splitting) antenna. This does not modify the singular behavior (as will be elaborated upon below), and was shown to give significantly better agreement with the $Z \rightarrow qq\bar{q}$ matrix element in [30].

Explicit solutions to eq. (2.15) using the trial function defined by eq. (2.16) were presented in [24], for fixed and first-order running couplings. In the context of the present work, two-loop running has been implemented using a simple numerical trick, as follows: given a value of $\alpha_s(M_Z)$, we determine the corresponding two-loop value of $\Lambda_{\text{QCD}}^{2\text{-loop}}$. We then use that Λ value in the one-loop solutions in [24], and correct the resulting distribution by inserting an additional trial accept veto:

$$P_{\text{accept}}^{2\text{-loop}} = \frac{\alpha_s^{2\text{-loop}}(Q, \Lambda_{\text{QCD}}^{2\text{-loop}})}{\alpha_s^{1\text{-loop}}(Q, \Lambda_{\text{QCD}}^{2\text{-loop}})} . \quad (2.21)$$

Due to the faster pace of 2-loop running, $\alpha_s^{2\text{-loop}}(Q, \Lambda) < \alpha_s^{1\text{-loop}}(Q, \Lambda)$, hence this accept probability is guaranteed to be smaller than or equal to unity.

A final point concerns if there are several “competing” radiators (equivalent to several competing nuclei, and/or several competing available decay channels for each nucleus). In this case, the trial with the highest value of Q is selected (corresponding to the one happening at the earliest time, t), and consideration of any other branchings (decays) are postponed temporarily. After a branching, any partons involved in that branching are replaced by the post-branching ones, and any postponed trial branchings involving those partons are deleted. The evolution is then restarted, from the scale Q of the new configuration, until there are no radiators left with trial branching scales larger than a fixed, lower, cutoff, normally identified with the hadronization scale, $Q_{\text{had}} \sim 1 \text{ GeV}$.

2.3 Evolution and Ordering

In order to solve eq. (2.15) we need to specify the form of eq. (2.10), which takes us from one scale Q_1^2 to a lower scale Q_2^2 . We change variables to parametrize the integral by the ordering variable, Q , and another, complementary (but otherwise arbitrary), phase-space variable which we denote by ζ . The generic evolution integral now reads

$$\mathcal{A}(Q_1^2, Q_2^2) = \int_{Q_2^2}^{Q_1^2} g_s^2 \mathcal{C} dQ^2 d\zeta |J| A(Q^2, \zeta) \quad (2.22)$$

with $|J|$ denoting the Jacobian of this transformation. For branchings involving gluon emission, we consider three possible choices for the ordering variable: dipole virtuality m_D , transverse momentum, and the energy of the emitted parton, E_j^* (in the CM of the parent antenna), with the following definitions,

$$Q_{E1}^2 = m_D^2 = 2m_{IK}^2 \min(y_{ij}, y_{jk}) , \quad (2.23)$$

$$Q_{E2}^2 = 4p_\perp^2 = 4m_{IK}^2 y_{ij} y_{jk} , \quad (2.24)$$

$$Q_{E3}^2 = 4E_j^{*2} = m_{IK}^2 (y_{ij} + y_{jk})^2 = x_j^2 m_{IK}^2 , \quad (2.25)$$

with the energy fraction $x_j = 2E_j^*/m_{IK}$.

All three options are available as ordering variables in the VINCIA shower Monte Carlo. They are illustrated in figure 1, where contours of constant value of $y_E = Q_E^2/m_{IK}^2$ are shown for each variable, as a function of y_{ij} and y_{jk} . For completeness, we show both the case of a linear (top row) and quadratic (bottom row) dependence on the branching invariants, for each variable. Since the ordering variable raised to any positive power will result in the same relative ordering of emissions within a given antenna, the distinction between linear and quadratic forms does not affect individual antenna Sudakov factors. It does, however, affect the “competition” between different antennae, and the choice of restart scale for subsequent evolution after a branching has taken place, as will be discussed further below.

In labeling the columns in figure 1, we have also emphasized that mass-ordering, as defined here, corresponds to choosing the smallest of the daughter antenna masses as the “resolution scale” of the branching, whereas p_\perp and energy correspond to using the geometric and arithmetic means of the daughter invariants, respectively. Naively, each of these could be taken as a plausible measure of the resolution scale of a given phase-space point. We shall see below which ones lead to better agreement with the one-loop matrix elements.

We consider two possible definitions for the complementary phase-space variable ζ ,

$$\zeta_1 = \frac{y_{ij}}{y_{ij} + y_{jk}} \quad (2.26)$$

$$\zeta_2 = y_{ij} . \quad (2.27)$$

We emphasize that the choice of ζ has no physical consequences, it merely serves to reparametrize the Lorentz-invariant phase space. We may therefore let the choice be governed purely by

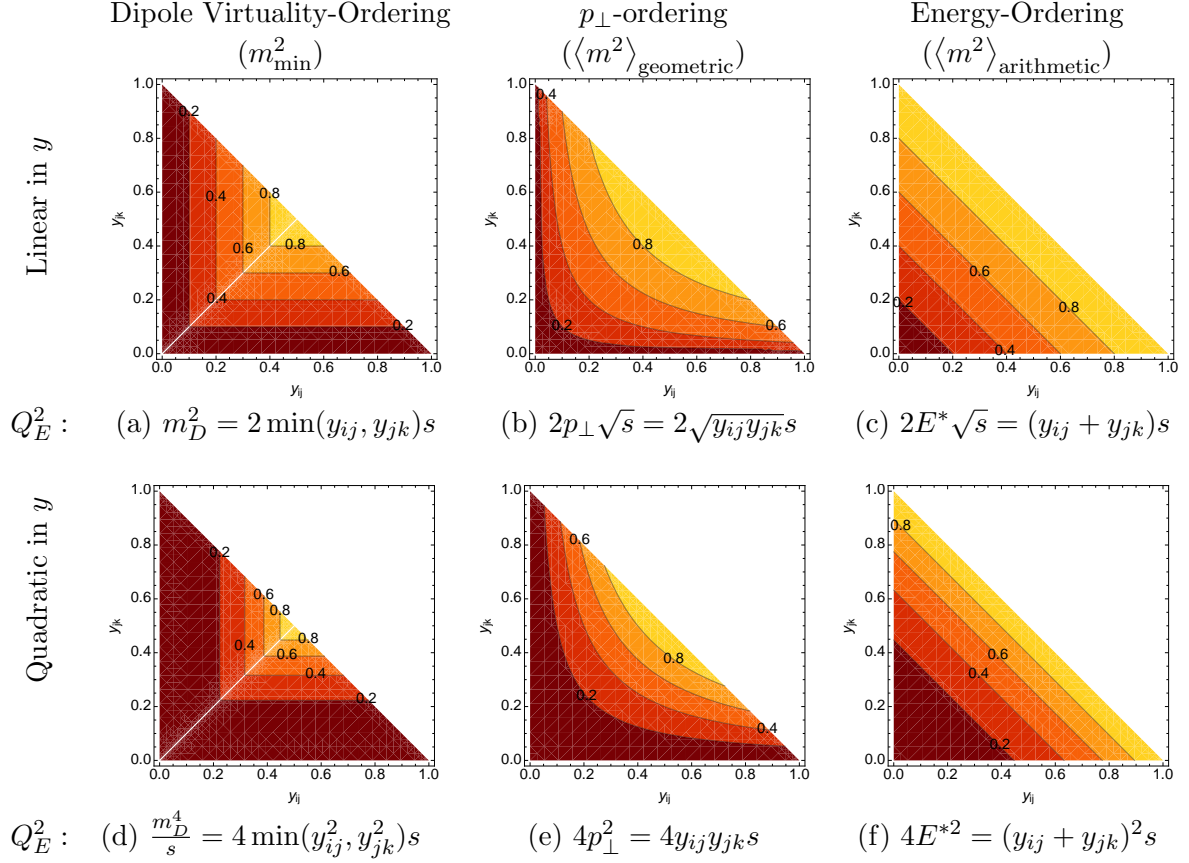


Figure 1. Contours of constant value of $y_E = Q_E^2/m_{IK}^2$ for evolution variables linear (top) and quadratic (bottom) in the branching invariants, for virtuality-ordering (left), p_{\perp} -ordering (middle), and energy-ordering (right). Note that the energy-ordering variables intersect the phase-space boundaries, where the antenna functions are singular, for finite values of the evolution variable. They can therefore only be used as evolution variables together with a separate infrared regulator, such as a cut in invariant mass, not shown here.

$y_E = \frac{Q^2}{s_{ijk}}$	$= \frac{m_{jk}^2}{s}$	$\frac{m_D^2}{s}$	$\frac{m_D^4}{s^2}$	$\frac{2p_{\perp}}{\sqrt{s}}$	$\frac{4p_{\perp}^2}{s}$	$\frac{2E^*}{\sqrt{s}}$	$\frac{4E^{*2}}{s}$
$ J(y_E, \zeta_1) $	$= \frac{y_E}{(1-\zeta_1)^2}$	$\frac{y_E}{4(1-\zeta_1)^2}$	$\frac{1}{8(1-\zeta_1)^2}$	$\frac{y_E}{4\zeta_1(1-\zeta_1)}$	$\frac{1}{8\zeta_1(1-\zeta_1)}$	y_E	$\frac{1}{2}$
$ J(y_E, \zeta_2) $	$= 1$	$\frac{1}{2}$	$\frac{1}{4\sqrt{y_E}}$	$\frac{y_E}{2\zeta_2}$	$\frac{1}{4\zeta_2}$	1	$\frac{1}{2\sqrt{y_E}}$

Note : $|J(Q^2, \zeta)| = s_{ijk}|J(y_E, \zeta)|$

Table 1. Jacobian factors for all combinations of evolution variables and ζ choices.

convenience, and, for each antenna integral, select whichever of the above definitions give the simplest final expressions. The corresponding Jacobian factors, for each of the evolution-variable choices we shall consider, are listed in tab. 1.

Note that, for the special case of the m_D^2 and m_D^4 variables, which contain the non-analytic

function $\min(y_{ij}, y_{jk})$, the ζ definitions in eqs. (2.26) and (2.27) apply to the branch with $y_{ij} > y_{jk}$. For the other branch, y_{ij} and y_{jk} should be interchanged. With this substitution, the Jacobians listed in tab. 1 apply to both branches⁴.

For branchings involving gluon splitting, $g \rightarrow q\bar{q}$, we restrict our attention to two possibilities, ordering in p_\perp , defined as above, and ordering in gluon virtuality, defined as

$$Q_{E4}^2 = m_{g^*}^2 = m_{q\bar{q}}^2 \quad (\text{for gluon splitting}) . \quad (2.28)$$

Note that the normalization factors for the ordering variables have in all cases been chosen such that the maximum value of the ordering variable is m_{IK}^2 .

Since the phase space for subsequent branchings is limited both by the scale Q_E of the previous branching (according to strong ordering) and by the invariant mass of the antenna m_j , the effective “restart scale”, after a branching in a strongly ordered shower, is given by

$$Q_{Rj}^2 = \min(Q^2, m_j^2) , \quad (2.29)$$

for each antenna j .

Depending on the choice and value of Q , one or both daughter antennae after a splitting may have a non-trivial restriction on the phase space available for subsequent branching. Conversely, if $Q > m_j$, there is no such restriction. Physically, we distinguish between the case in which the strong-ordering condition implies a non-trivial constraint on the evolution of the produced antennae, eating into the phase-space that would otherwise be accessible, and the case in which the strong-ordering condition does not imply such a constraint.

The regions of $q\bar{q} \rightarrow qg\bar{q}$ phase space in which either zero, one, or both of the daughter antennae (qg and $g\bar{q}$ respectively) are constrained by the ordering condition are illustrated in figure 2, for each of the choices of evolution variable under consideration. The black shaded areas correspond to regions in which both the qg and $g\bar{q}$ antennae are restricted, by having $Q < m_j$. The darker gray shaded areas show regions in which only one of the antennae is restricted, while the other will still be allowed to evolve over its full phase space. In the light-gray shaded areas, both of the antennae are allowed to evolve over all of their available phase spaces, equivalent to the ordering condition imposing no constraint on the subsequent evolution. We recall that we are here discussing the *upper* boundary on the subsequent evolution, hence the infrared⁵ (IR) poles are not affected.

To further clarify the meaning of the plots in figure 2, let us discuss panel (e) as an example. The coordinates, (y_{ij}, y_{jk}) , represent the 3-parton state before it evolves to a 4-parton state, and each point corresponds to a specific value of the evolution variable at hand, cf. figure 1. Assuming ordering in p_\perp and using subscript (3) for quantities evaluated in the 3-parton state, the value of the evolution variable for a specific (y_{ij}, y_{jk}) point is $Q_{E(3)}^2 = 4p_{\perp(3)}^2 = 4y_{ij}y_{jk}s$, with $s = m_Z^2$ at the Z pole. The further evolution of the shower, from a 3- to a 4-parton state, involves a sum over all possible branchings of the qg and $g\bar{q}$

⁴This corresponds to replacing y_{ij} by $\max(y_{ij}, y_{jk})$ in the numerator of eq. (2.26) and in eq. (2.27).

⁵Note: we use the word infrared to refer collectively to soft and/or collinear regions of phase space.

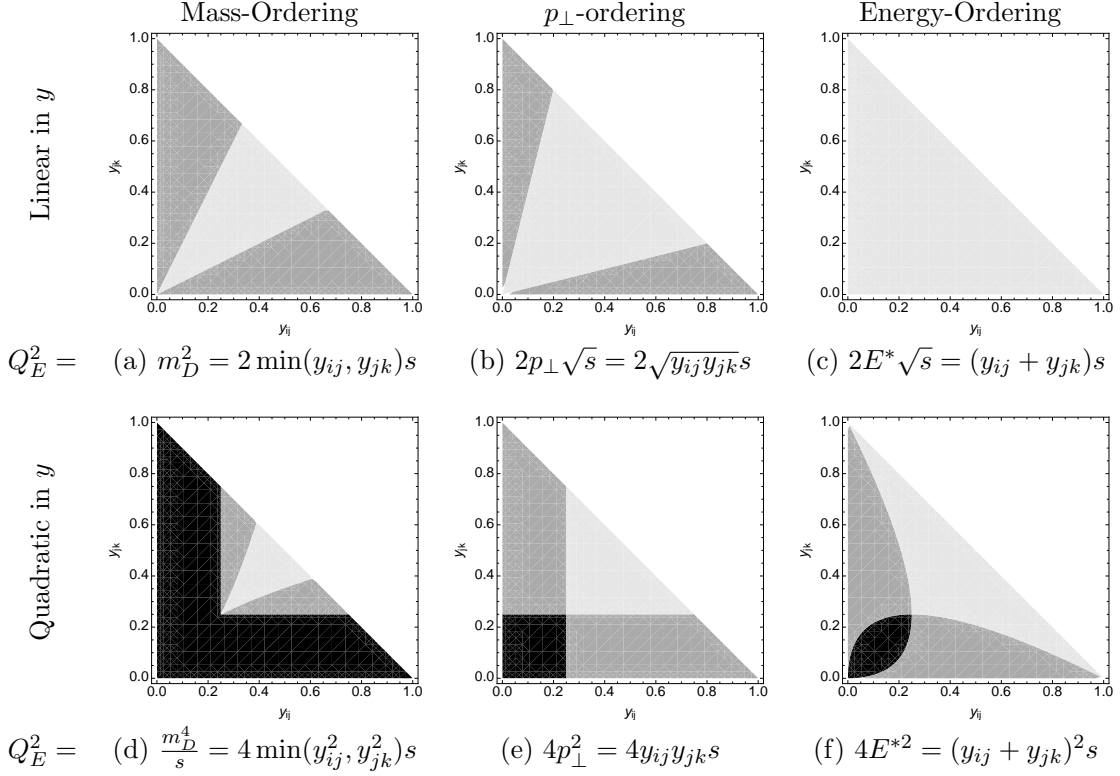


Figure 2. Illustration of the regions of 3-parton phase space in which the subsequent evolution of the qg and $g\bar{q}$ antennae is restricted (from above) by the strong-ordering condition. See the text for further clarification of this plot. *Black*: both antennae restricted. *Dark Gray*: one antenna restricted, the other unrestricted. *Light Gray*: both antennae unrestricted. *Top/Bottom*: Q^2 linear/quadratic in the branching invariants, for mass-ordering (left), p_\perp -ordering (middle), and energy-ordering (right).

antennae. Consider the qg one. Its branchings can again be characterized by two invariants (s_1, s_2) , both of which will be smaller than m_{qg}^2 . However, depending on the value of m_{qg}^2 (or, equivalently, y_{ij}) the p_\perp of the new configuration, $4p_{\perp(4)}^2 = 4s_1s_2/m_{qg}^2$ may actually be *larger* than $4p_{\perp(3)}^2$. In a strongly ordered shower, such configurations are not allowed, and would be discarded. Whether this situation can occur or not, for one or both of the qg and $g\bar{q}$ antennae, as a function of (y_{ij}, y_{jk}) , is what figure 2 reveals, for each type of ordering variable.

The mathematical consequence is that, in the dark- and black-shaded regions, respectively, the upper boundary of one or both of the qg and $g\bar{q}$ antenna integrals is set by the evolution variable, rather than by phase space. This creates an important difference between the integrals generated by a shower algorithm and those used for IR subtractions in traditional fixed-order applications for which the integrals often run over all of phase space, although some subtraction schemes feature parameters that allow restrictions on the phase space for the subtraction terms [53, 54]. In particular, we see that the strong-ordering condition will generate additional logarithms involving $s_{ij}/Q_{E(3)}^2$ as argument. For a “good” choice of evolution variable, these logarithms should explicitly cancel against ones present in the one-loop

Ordering type		Q_E^2	$\zeta_{\min}(Q_E^2)$	$\zeta_{\max}(Q_E^2)$	$3 \rightarrow 4$ restriction
p_\perp -ordering	linear	$2m_{IK}^2 \sqrt{y_{ij}y_{jk}}$	$\frac{1 \mp \sqrt{1 - Q_E^4/m_{IK}^4}}{2}$		$\theta(m_{\text{ant}}^2 - 2\sqrt{s_{ij}s_{jk}})$
	squared	$4m_{IK}^2 y_{ij}y_{jk}$	$\frac{1 \mp \sqrt{1 - Q_E^2/m_{IK}^2}}{2}$		$\theta(m_{\text{ant}}^2 - 4\frac{s_{ij}s_{jk}}{s})$
m_D -ordering	linear	$2m_{IK}^2 \min(y_{ij}, y_{jk})$	$\frac{Q_E^2}{2m_{IK}^2}$	$1 - \frac{Q_E^2}{2m_{IK}^2}$	$\theta(m_{\text{ant}}^2 - 2\min(s_{ij}, s_{jk}))$
	squared	$4m_{IK}^2 \min(y_{ij}^2, y_{jk}^2)$	$\sqrt{\frac{Q_E^2}{4m_{IK}^2}}$	$1 - \sqrt{\frac{Q_E^2}{4m_{IK}^2}}$	$\theta\left(m_{\text{ant}}^2 - 4\frac{\min(s_{ij}^2, s_{jk}^2)}{s}\right)$
E^* -ordering	linear	$m_{IK}^2 (y_{ij} + y_{jk})$	0	1	1
	squared	$m_{IK}^2 (y_{ij} + y_{jk})^2$	0	1	$\theta\left(m_{\text{ant}}^2 - \frac{(s_{ij} + s_{jk})^2}{s}\right)$

Table 2. Boundaries corresponding to the ordering variables portrayed in figure 1, with m_{ant}^2 corresponding to the active $3 \rightarrow 4$ dipole s_{qg} or $s_{g\bar{q}}$, and $s = m_Z^2$ at the Z pole. We have chosen ζ_2 as the energy sharing variable for m_D and p_\perp ordering and ζ_1 for E^* ordering, with ζ defined as in eq. (2.26) and eq. (2.27). The energy variable will lead to infinities if the hadronization scale is not imposed as a cut-off.

matrix elements, a question we shall return to in detail in section 4.

Several interesting structures can be seen in figure 2. Firstly, the linearized variables imply less severe constraints on the subsequent evolution than the quadratic ones. This is easy to understand given that the linearized variables, Q_{lin} , are related to the quadratic ones, Q_{qdr} , by

$$Q_{\text{lin}}^2 = Q_{\text{qdr}} m_{IK} , \quad (2.30)$$

and hence $Q_{\text{lin}} > Q_{\text{qdr}}$, implying a higher absolute restart scale for the linearized ordering variables.

It is also apparent that, for a given choice of linearity, mass-ordering reduces the phase-space for further evolution more than p_\perp -ordering does, which in turn is more constraining than energy-ordering. In this comparison, however, it becomes important to recall that the traditional ordering variables used, e.g., in VINCIA, are the *linearized* mass-ordering and the *quadratic* p_\perp and energy-ordering variables⁶. Within that group, p_\perp -ordering appears to be the most restrictive, followed by energy-ordering, with (traditional, linearized) mass-ordering leading to the most open phase space for the subsequent evolution.

We are now able to fully specify the boundaries of the evolution integrals in eq. (2.22). For each Q_E contour (see figure 1), the integration limits in ζ are listed in tab. 2. Combined with a Q_E interval and an antenna function, these boundaries account for the integrated tree-level splitting probability when going from one scale Q_1^2 to another Q_2^2 , as expressed by eq. (2.22). The last column in tab. 2 tells when the $3 \rightarrow 4$ ordering condition is active. In figure 2 this corresponds to a region darkening due to the restriction, with its shade determined by the amount of restricted dipoles.

⁶This distinction comes about from using quantities that are similar to a squared mass, squared transverse momentum, and squared energy, respectively.

Finally, we note that the dependence on Q in eq. (2.29) causes explicit non-Markovian behavior at the 4-parton level and beyond, since the value of Q then depends explicitly on which branching was the last to occur. A more strictly Markovian variant of this is obtained by letting the $\min()$ function act on all possible Q values (corresponding to all possible colour-connected clusterings) of the preceding topology. In that case, a single Q value can be used to characterize an entire n -parton topology, irrespective of which branching was the last to occur. Since the distinction between Markovian and non-Markovian shower restart conditions only enters starting from the $4 \rightarrow 5$ parton evolution step, it will not affect our discussion of the second-order $2 \rightarrow 3$ branching process. For completeness, we note that the strongly ordered showers in VINCIA are of the ordinary non-Markovian type, while the smoothly ordered ones are Markovian.

2.4 Smooth Ordering

In addition to traditional (strongly ordered) showers, we shall also consider so-called smooth ordering [24]: applying the ordering criterion as a smooth dampening factor instead of as a step function. This is not as radical as it may seem at first. Applying a jet algorithm to any set of events will in general result in some small fraction of unordered clustering sequences. This is true even if the events were generated by a strongly ordered shower algorithm, if the jet clustering measure is not strictly identical to the shower ordering variable. An example of this, for strong ordering in p_\perp and in m_D , clustered with the k_T algorithm, can be found in [55].

In smooth ordering, the only quantity which must still be strictly ordered are the antenna invariant masses, a condition which follows from the nested antenna phase spaces and momentum conservation. Within each individual antenna, and between competing ones, the measure of evolution time is still provided by the ordering variable, which we therefore typically refer to as the “evolution variable” in this context (rather than the “ordering variable”), in order to prevent confusion with the strong-ordering case. The evolution variable can in principle still be chosen to be any of the possibilities given above, though we shall typically use $2p_\perp$ for gluon emission and $m_{q\bar{q}}$ for gluon splitting.

In terms of an arbitrary evolution variable, Q , the smooth-ordering factor is [55]

$$P_{\text{imp}} = \frac{\hat{Q}^2}{\hat{Q}^2 + Q^2}, \quad (2.31)$$

where Q is the evolution scale associated with the current branching, and \hat{Q} measures the scale of the parton configuration before branching. A comparison to the strong-ordering step function is given in figure 3, on a log-log scale.

In the strongly-ordered region of phase-space, $Q \ll \hat{Q}$, we may rewrite the P_{imp} factor as

$$P_{\text{imp}} = \frac{1}{1 + \frac{Q^2}{\hat{Q}^2}} \stackrel{Q \ll \hat{Q}}{\approx} 1 - \frac{Q^2}{\hat{Q}^2} + \dots \quad (2.32)$$

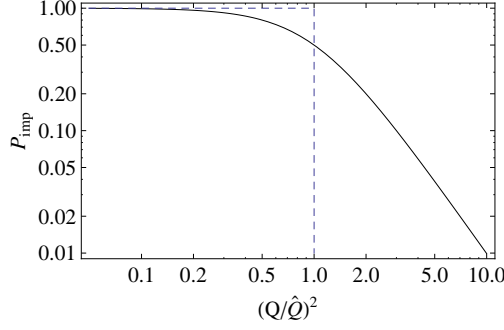


Figure 3. The smooth-ordering factor (*solid*) compared to a strong-ordering Θ function (*dashed*).

Applying this to the $2 \rightarrow 3$ antenna function whose leading singularity, eq. (2.16), is proportional to $1/Q^2$, we see that the overall correction arising from the Q^2/\hat{Q}^2 and higher terms is finite and of order $1/\hat{Q}^2$; a power correction. The LL singular behaviour is therefore not affected. However, at the multiple-emission level, the $1/\hat{Q}^2$ terms do modify the *subleading* logarithmic structure, starting from $\mathcal{O}(\alpha_s^2)$, as we shall return to below.

In the *unordered* region of phase-space, $Q > \hat{Q}$, we rewrite the P_{imp} factor as

$$P_{\text{imp}} = \frac{\hat{Q}^2}{Q^2} \frac{1}{1 + \frac{\hat{Q}^2}{Q^2}} \stackrel{Q > \hat{Q}}{=} \frac{\hat{Q}^2}{Q^2} \left(1 - \frac{\hat{Q}^2}{Q^2} + \dots \right), \quad (2.33)$$

which thus effectively modifies the leading singularity of the LL $2 \rightarrow 3$ function from $1/Q^2$ to $1/Q^4$, removing it from the LL counting. The only effective terms $\propto 1/Q^2$ arise from finite terms in the radiation functions, if any such are present, multiplied by the P_{imp} factor. Only a matching to the full tree-level $2 \rightarrow 4$ functions would enable a precise control over these terms. Up to any given fixed order, this can effectively be achieved by matching to tree-level matrix elements, as will be discussed in section 3.1. Matching beyond the fixed-order level is beyond the scope of this paper. We thus restrict ourselves to the observation that, at the LL level, smooth ordering is equivalent to strong ordering, with differences only appearing at the subleading level.

The effective $2 \rightarrow 4$ probability in the shower arises from a sum over two different $2 \rightarrow 3 \otimes 2 \rightarrow 3$ histories, each of which has the tree-level form

$$\hat{A} P_{\text{imp}} A \propto \frac{1}{\hat{Q}^2} \frac{\hat{Q}^2}{\hat{Q}^2 + Q^2} \frac{1}{Q^2} = \frac{1}{\hat{Q}^2 + Q^2} \frac{1}{Q^2}, \quad (2.34)$$

thus we may also perceive the combined effect of the modification as the addition of a mass term in the denominator of the propagator factor of the previous splitting. In the strongly ordered region, this correction is negligible, whereas in the unordered region, there is a large suppression from the necessity of the propagator in the previous topology having to be very off-shell, which is reflected by the P_{imp} factor. Using the expansion for the unordered region,

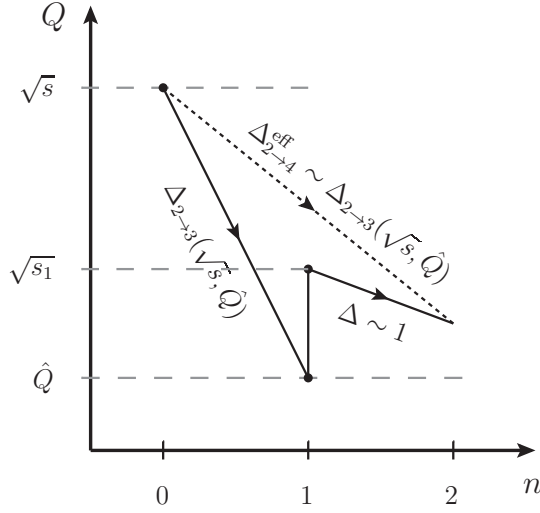


Figure 4. Illustration of scales and Sudakov factors involved in an unordered sequence of two $2 \rightarrow 3$ branchings, representing the smoothly ordered shower’s approximation to a hard $2 \rightarrow 4$ process.

eq. (2.33), we also see that the effective $2 \rightarrow 4$ radiation function, obtained from iterated $2 \rightarrow 3$ splittings, is modified as follows,

$$P_{2 \rightarrow 4} \propto \frac{1}{\hat{Q}^2} \frac{\hat{Q}^2}{Q^2} \frac{1}{Q^2} \rightarrow \frac{1}{Q^4} + \mathcal{O}(\dots) , \quad (2.35)$$

in the unordered region. That is, the intermediate low scale \hat{Q} , is *removed* from the effective $2 \rightarrow 4$ function, by the application of the P_{imp} factor.

Finally, to illustrate what happens to the Sudakov factors, we illustrate the path through phase space taken by an unordered shower history in figure 4. An antenna starts showering at a scale equal to its invariant mass, \sqrt{s} , and a first $2 \rightarrow 3$ branching occurs at the evolution scale \hat{Q} . This produces the overall Sudakov factor $\Delta_{2 \rightarrow 3}(\sqrt{s}, \hat{Q})$. A daughter antenna, produced by the branching, then starts showering at a scale equal to its own invariant mass, labeled $\sqrt{s_1}$. However, for all scales larger than \hat{Q} , the P_{imp} factor suppresses the evolution in this new dipole so that no leading logs are generated. To leading approximation, the effective Sudakov factor for the combined $2 \rightarrow 4$ splitting is therefore given by

$$\Delta_{2 \rightarrow 4}^{\text{eff}} \sim \Delta_{2 \rightarrow 3}(\sqrt{s}, \hat{Q}) , \quad (2.36)$$

in the unordered region. Thus, we see that a dependence on the intermediate scale \hat{Q} still remains in the effective Sudakov factor generated by the smooth-ordering procedure. Since $\hat{Q} < Q$ in the unordered region, the effective Sudakov suppression of these points might be “too strong”. The smooth ordering therefore allows for phase space occupation in regions corresponding to dead zones in a strongly ordered shower, but it does suggest that a correction

to the Sudakov factor may be desirable, in the unordered region. A study of $Z \rightarrow 4$ jets at one loop would be required to shed further light on this question.

Having presented introductory aspects of (antenna) showers, we now turn to a detailed discussion of how we match them to higher fixed-order calculations.

3 Matched Antenna Showers

3.1 Tree-Level Matching

The strategy for matching to tree-level matrix elements used in VINCIA was defined by GKS in [24] and is tightly related to the veto algorithm outlined above. The philosophy is to view the shower produced by the smoothly ordered antenna functions as generating an all-orders approximation to QCD, which can be systematically improved, order by order, by including one more factor in the accept probability, called the matrix-element correction. For a given trial branching, the full trial accept probability, up to the highest matched number of partons, is then obtained as a product of the ordinary trial-accept probability in the shower, multiplied by this extra correction factor.

Since the shower is already correct in the soft and collinear limits, the matrix-element correction factor will tend to unity in those limits, but it can deviate on either side of unity outside those limits. As long as the combined accept probability is still smaller than unity, a probabilistic accept/reject step can still be applied, without having to worry about reweighting the events (which would be required if the total accept probability should exceed unity). It is also important to define the factor only in terms of physical cross sections (here represented by LO matrix elements), which guarantees positivity. (Again, if it were allowed to become negative, one would have to introduce negative-weight events, but this is avoided in the GKS strategy as defined in [24]).

As we have seen, the shower furnishes an all-orders approximation to QCD. The aim is, for each resolved parton/jet multiplicity, to match the answer provided by the shower to an, ideally, all-orders exact expression, by applying a multiplicative correction factor, schematically [24, 38]

$$\text{Matched} = \text{Approximate} \frac{\text{Exact}}{\text{Approximate}} . \quad (3.1)$$

At tree level, we in fact know only the first term in the expansion of the numerator, and we therefore expand the shower approximation to the same level. For n partons, assuming the approximation has already (recursively) been matched to the preceding order,

$$\text{Exact} \rightarrow |M_n|^2 \quad (3.2)$$

$$\text{Approximate} \rightarrow \sum_j g_{Tj}^2 \mathcal{C}_{Tj} A_{Tj} P_{\text{accept}} |M_{n-1j}|^2 = \sum_j g_j^2 \mathcal{C}_j P_{\text{imp}} P_{\text{Ari}} A_j |M_{n-1j}|^2 , \quad (3.3)$$

where the subscript “T” indicates trial quantities (cf. section 2.2), we have suppressed the dependence on phase-space points, Φ , and the subscript j in the $(n-1)$ -parton matrix element

indicates the configuration obtained by performing the inverse shower step that removes parton j from the n -parton state.

The factors in eq. (3.3) are easy to calculate if a tree-level matrix-element (ME) generator is available to provide the $|M|^2$ factors. The total ME-corrected accept probability is thus simply eq. (2.19),

$$P_{\text{accept}}^{\text{LO}} = P_{\text{accept}} R_n = P_{\text{accept}} \frac{|M_n|^2}{\sum_j g_j^2 \mathcal{C}_j P_{\text{imp}} P_{\text{Ari}} A_j |M_{n-1_j}|^2} . \quad (3.4)$$

As mentioned above, this factor should be positive and smaller than unity, in order to avoid having to reweight any events. In practice, we have found the trial function defined in eq. (2.16) to guarantee this for all processes we have so far considered, mainly consisting of $Z \rightarrow n$ and $H \rightarrow n$ partons. As shown in [24], it is also possible to absorb subleading-colour corrections into this matching factor in a positive-definite way, but since subleading colour goes beyond the scope of our study we do not reproduce the arguments here.

The fact that these factors change the distribution of the final set of generated events to the correct matrix-element answer can be explained by following the steps of the algorithm and summing over all possible branching histories. We start from Born-level matrix-element events, and generate trial shower branchings, for a trial approximation to the $(B+1)$ -parton matrix element of:

$$|M_{B+1}^{\text{Trial}}|^2 = \sum_i g_{Ti}^2 \mathcal{C}_{Ti} A_{Ti} |M_{B_i}^{\text{LO}}|^2 , \quad (3.5)$$

with i running over all possible single-parton clusterings that correspond to allowed shower branchings. Applying the LO accept probability, eq. (3.4), changes this to

$$\begin{aligned} & \rightarrow \sum_i g_{Ti}^2 \mathcal{C}_{Ti} A_{Ti} P_{\text{accept}}^{\text{LO}} |M_{B_i}^{\text{LO}}|^2 \\ & = \sum_i g_i^2 \mathcal{C}_i P_{\text{imp}} P_{\text{Ari}} A_i \frac{|M_{B+1}^{\text{LO}}|^2}{\sum_j g_{sj}^2 \mathcal{C}_j P_{\text{imp}} P_{\text{Ari}} A_j |M_{B_j}^{\text{LO}}|^2} |M_{B_i}^{\text{LO}}|^2 \\ & = |M_{B+1}^{\text{LO}}|^2 . \end{aligned} \quad (3.6)$$

That is, summed over shower histories, numerators and denominators are designed to cancel exactly, leaving only the LO matrix element for $B+1$ partons, as desired. Due to the full phase-space coverage and explicitly Markovian nature of the smoothly ordered shower algorithm, this procedure is straightforward to iterate for Born + 2, 3, etc partons⁷.

To provide a connection with antenna subtraction, which will be useful when we extend to NLO matching below, we can rewrite the ratio in eq. (3.1) by a trivial rearrangement,

$$\text{Matched} = \text{Approximate} \left(1 + \frac{\text{Exact} - \text{Approximate}}{\text{Approximate}} \right) . \quad (3.7)$$

⁷That is not the case for ordinary strongly ordered frameworks, due to the presence of dead zones in phase space and to the generally non-Markovian shower restart conditions. For such algorithms, addition of events in the dead zones [56], with CKKW-like Sudakov-factor prescriptions for multi-leg matching [57, 58], would presumably be necessary.

The numerator in this equation is very similar to a standard antenna-subtracted matrix element, though we emphasize that our antennae are of course modified by the presence of the P_{imp} and P_{Ari} factors.

Let us finally re-emphasize that since we apply the correction factor to the antenna functions themselves, thereby modifying the probability for a branching to occur, the probability for a branching *not* to occur is also modified. These corrections will therefore also be present in the Sudakov factors generated by the corrected shower evolution. The fact that the correction factor, R_n , is unity in all LL singular limits (since the shower functions are guaranteed to match the matrix-element singularities there) implies that the LL properties of the Sudakov factors are not affected by this modification. However, the tower of subleading logarithms *is* changed, for better or worse. While it is known that finite terms do not exponentiate our corrections here also include a more subtle aspect, namely a resummation of the subleading logarithms present in the higher-order matrix elements. At this level, however, we cannot be sure that this procedure produces the *correct* subleading logarithms of a formally higher-order resummation. Therefore, we view it at present merely as an interesting, and hopefully beneficial, side-effect of unitarity-based matching. The examination of formally subleading terms carried out in this paper is a first step towards a more rigorous study of these aspects.

3.2 One-Loop Matching at the Born Level

For the Born level, at NLO, the GKS matching strategy [24] reduces to the POWHEG one [7–9]. We nonetheless begin by recapitulating the steps used to derive the one-loop correction to the Born-level matrix element, in our notation. We then continue to higher multiplicities.

As our basis for one-loop matching we take the tree-level strategy described in section 3.1. Since the corrections are applied as modifications to the branching probabilities, without adding, subtracting, or reweighting events, the total inclusive rate after tree-level matching to any number of partons, is still just the leading-order, Born-level one. By the same token, after one-loop matching, at the integrated level, the total NLO correction to the inclusive rate must therefore just be the NLO “ K -factor”,

$$K^{\text{NLO}} = \frac{\sigma_{\text{inc}}^{\text{NLO}}}{\sigma_{\text{inc}}^{\text{LO}}} . \quad (3.8)$$

For processes like Z decay, where the NLO correction has no dependence on the Born-level kinematics, this is trivial to implement as an overall reweighting factor on the Born-level events,

$$K_Z^{\text{NLO}} = 1 + V_Z = 1 + \frac{\alpha_s}{\pi} , \quad (3.9)$$

where we have introduced the notation V for the NLO correction term, anticipating a similar notation for the multileg case below. Note that one could equally trivially normalize to NNLO or to data, as desired for the application at hand (we note though that such a normalization choice does not, by itself, ensure NNLO precision for any quantity besides the total inclusive rate).

However, when the amount of final state particles exceeds two, the NLO correction depends on the Born-level kinematics, therefore it is worth illustrating the general procedure for deriving a fully differential K-factor, for each phase-space point. This also serves as a useful warm-up exercise for the multi-leg case below.

At NLO, we may distinguish between inclusive and exclusive rates for the first time. Either can in principle be used to derive matching equations between showers and fixed-order calculations, but the exclusive one is best suited for deriving expressions at the fully differential level. We recall that the exclusive n -jet cross section is defined as the cross section for observing n *and only* n jets, while the inclusive n -jet cross section counts the number of events with n *or more* jets. One therefore has the trivial relation

$$\sigma_n^{\text{incl}}(Q) = \sum_{k \geq n} \sigma_k^{\text{excl}}(Q) . \quad (3.10)$$

with Q the resolution scale of whatever (IR safe) algorithm is used to define the jets.

3.2.1 Inclusive Born

The total inclusive rate produced by the tree-level matched shower is just the Born-level matrix element,

$$\text{Approximate} \rightarrow |M_2^0|^2 , \quad (3.11)$$

where the subscript indicates the parton multiplicity (2 for $Z \rightarrow q\bar{q}$ decay) and the superscript indicates the loop order beyond the Born level (0 indicates the Born loop order). Because cancellation of real and virtual corrections is exact in both the unmatched shower as well as in the tree-level matching scheme described above, there are no further corrections to consider for the inclusive rate. In other words, the total integrated cross section produced by the shower is obtained merely by integrating eq. (3.11) over all of the Born-level phase space. We now seek a correction term, V_2 , such that

$$\text{Matched} \rightarrow (1 + V_{2Z}) |M_2^0|^2 \quad (3.12)$$

gives the correct inclusive NLO rate. From eq. (3.9), we know that the correction term for Z decay is

$$V_{2Z} = \frac{\alpha_s}{\pi} . \quad (3.13)$$

A systematic way of deriving this result, which can be applied to arbitrary processes, is provided by considering the cross section at the exclusive level.

3.2.2 Exclusive Born

The shower expression for the exclusive $Z \rightarrow q\bar{q}$ rate (defined at the hadronization cut-off, which is the lowest meaningful resolution scale in the perturbative shower) is

$$|M_2^0|^2 \Delta(s, Q_{\text{had}}^2) = |M_2^0|^2 \left(1 - \int_{Q_{\text{had}}^2}^s d\Phi_{\text{ant}} g_s^2 C A_{g/q\bar{q}} + \mathcal{O}(\alpha_s^2) \right) , \quad (3.14)$$

where we have expanded the Sudakov factor Δ to first order. Due to the presence of the hadronization scale, this expression is IR finite and can be defined in 4 dimensions.

We remark here on the validity of this expansion in α_s for the exclusive cross section. For the purpose of constructing the matching factor to order α_s the expansion is a parametric one. In the ratio of the exact and approximate exclusive cross section, since the singularities match to the shower accuracy, divergences or large logarithms (depending on whether one choose zero or finite resolution scale) cancel and the resulting factor has a well-behaved expansion in α_s .

The colour factor for $q\bar{q} \rightarrow qg\bar{q}$ is

$$C_{g/q\bar{q}} = 2C_F , \quad (3.15)$$

and we assume that the antenna function, A , is either the one derived from Z decay [20] or has been matched to it, using LO matching. That is,

$$g_s^2 2C_F A_{g/q\bar{q}} = \frac{|M_3^0|^2}{|M_2^0|^2} . \quad (3.16)$$

We first consider the limit $Q_{\text{had}} \rightarrow 0$, in which case the expression becomes

$$|M_2^0|^2 \Delta(s, 0) = |M_2^0|^2 \left(1 - \int_0^s d\Phi_{\text{ant}} g_s^2 2C_F A_{g/q\bar{q}} + \mathcal{O}(\alpha_s^2) \right) , \quad (3.17)$$

which can only be defined in the presence of an IR regularization scheme. We shall here use dimensional regularization, working in $d = 4 - 2\epsilon$ dimensions. Below, we rederive the matching equations in 4 dimensions, for $Q_{\text{had}} \neq 0$, and show that the *same* final matching factors are obtained in both cases.

At NLO, the exclusive $Z \rightarrow q\bar{q}$ rate at “infinite” perturbative resolution is

$$|M_2^0|^2 + 2 \text{Re}[M_2^0 M_2^{1*}] = |M_2^0|^2 \left(1 + \frac{2 \text{Re}[M_2^0 M_2^{1*}]}{|M_2^0|^2} \right) , \quad (3.18)$$

where we have written the right-hand side in a form similar to eq. (3.17), in d dimensions. Because the resolution scale has been taken to zero, there are no unresolved 3-parton configurations to include. The virtual matrix element is

$$\frac{2 \text{Re}[M_2^0 M_2^{1*}]}{|M_2^0|^2} = \frac{\alpha_s}{2\pi} 2C_F (2I_{q\bar{q}}(\epsilon, \mu^2/s) - 4) , \quad (3.19)$$

with the function $I_{q\bar{q}}$ used to classify the ϵ divergences [22, 33, 59]. Note that we have modified the definition of I to make it explicitly dimensionless, see appendix A. On the shower side, the integral of the $Z \rightarrow qg\bar{q}$ antenna in eq. (3.17) is [22]

$$\int_0^s d\Phi_{\text{ant}} 2C_F g_s^2 A_{g/q\bar{q}} = \frac{\alpha_s}{2\pi} 2C_F \left(-2I_{q\bar{q}}(\epsilon, \mu^2/s) + \frac{19}{4} \right) , \quad (3.20)$$

and, not surprisingly, the difference comes out to be exactly $\alpha_s/\pi \times |M_2^0|^2$. Writing this correction as a multiplicative K -factor, we obtain eq. (3.9).

As a cross-check, we now repeat the derivation in 4 dimensions, reinstating the hadronization scale. The fixed-order side is then

$$|M_2^0|^2 \left(1 + \frac{2 \operatorname{Re}[M_2^0 M_2^{1*}]}{|M_2^0|^2} + \int_0^{Q_{\text{had}}^2} d\Phi_{\text{ant}} g_s^2 \mathcal{C} A_{g/q\bar{q}} \right), \quad (3.21)$$

where the integral that has been added corresponds to unresolved 3-parton configurations, with A again given by eq. (3.16). Though eq. (3.14) is now defined entirely in 4 dimensions, we still need dimensional regularization to regulate the two last terms in the fixed-order expression. In principle, the integral in the last term could be carried out explicitly, but it is simpler to rewrite it as

$$\int_0^{Q_{\text{had}}^2} d\Phi_{\text{ant}} g_s^2 \mathcal{C} A_{g/q\bar{q}} = \int_0^{m_Z^2} d\Phi_{\text{ant}} g_s^2 \mathcal{C} A_{g/q\bar{q}} - \int_{Q_{\text{had}}^2}^{m_Z^2} d\Phi_{\text{ant}} g_s^2 \mathcal{C} A_{g/q\bar{q}} \quad (3.22)$$

where the first term is just the full antenna integral, eq. (3.20), and the second term is identical to the one appearing in eq. (3.14), with which it cancels completely, cf. the definition of the tree-level matching, eq. (3.16). The final correction term is therefore again exactly equal to $\alpha_s/\pi \times |M_2^0|^2$.

Note that the scale and scheme dependence of the α_s/π correction is not specified since its ambiguity is formally of order α_s^2 . For definiteness we take the renormalization scale for this correction to be proportional to the invariant mass of the system, $\mu_R = k_\mu^{\text{inc}} \sqrt{\hat{s}}$ (so that $\mu_R = k_\mu^{\text{inc}} m_Z$ at the Z pole), with k_μ^{inc} thus representing the free parameter that governs the choice of renormalization scale for the total inclusive rate for $Z \rightarrow \text{hadrons}$. We shall consider both one-loop and two-loop running options. The value of $\alpha_s(m_Z)$ will be determined from LEP data in section 5.

3.3 One-Loop Matching for Born + 1 Parton

The approximation to the 3-parton exclusive rate produced by a shower matched to (at least) NLO for the 2-parton inclusive rate and to LO for the 3-parton one, is

$$\text{Approximate} \rightarrow (1 + V_2) |M_3^0|^2 \Delta_2(m_Z^2, Q_3^2) \Delta_3(Q_{R3}^2, Q_{\text{had}}^2), \quad (3.23)$$

where M_3^0 is the tree-level $Z \rightarrow qg\bar{q}$ matrix element and Q_{R3} denotes the “restart scale”. For strong ordering, Q_{R3} is equal to Q_3 , while, for smooth ordering, it is given by the nested antenna phase spaces, i.e., by the successive antenna invariant masses. The subscripts on the two Sudakov factors Δ_2 and Δ_3 make it explicit that they refer to the event as a whole, see the illustration in figure 5. Again, we have the choice whether we wish to work in 4 dimensions, with a non-zero hadronization scale, Q_{had} , or in d dimensions with the hadronization scale taken to zero. We have maintained the hadronization scale in eq. (3.23), though we shall see below that the dependence on it does indeed cancel in the final result.

The 2-parton Sudakov factor, Δ_2 , is generated by the (matched) evolution from 2 to 3 partons,

$$\Delta_2(m_Z^2, Q_3^2) = 1 - \int_{Q_3^2}^{m_Z^2} d\Phi_{\text{ant}} g_s^2 2C_F A_{g/q\bar{q}} + \mathcal{O}(\alpha_s^2), \quad (3.24)$$

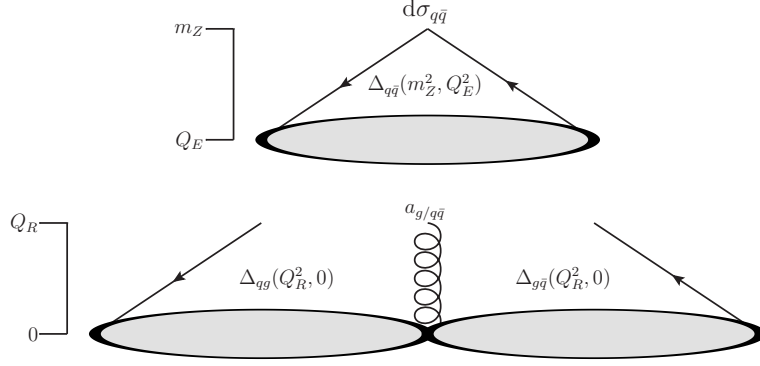


Figure 5. Illustration of the evolution scales and Sudakov factors appearing in the exclusive 3-jet cross section, eq. (3.23).

with $A_{g/q\bar{q}}$ again defined by eq. (3.16). Notice that the integral only runs from the starting scale, m_Z^2 , to the 3-parton resolution scale, Q_3^2 , hence this integral is IR finite, though it does contain logarithms. In the remainder of this paper, we shall work only with the leading-colour part of the Sudakov and matrix-element expressions, hence from now on we replace $2C_F$ in the above expression by C_A ,

$$\Delta_2^{\text{LC}}(m_Z^2, Q_3^2) = 1 - \int_{Q_3^2}^{m_Z^2} d\Phi_{\text{ant}} g_s^2 C_A A_{g/q\bar{q}} + \mathcal{O}(\alpha_s^2). \quad (3.25)$$

The 3-parton Sudakov factor, Δ_3 , imposes exclusivity and is given by

$$\Delta_3(Q_{R3}^2, Q_{\text{had}}^2) = 1 - \sum_{j=1}^2 \int_{Q_{\text{had}}^2}^{Q_{R3}^2} d\Phi_{\text{ant}} g_s^2 (C_A A_{Ej} + 2T_R A_{Sj}) + \mathcal{O}(\alpha_s^2), \quad (3.26)$$

where the index j runs over the qg and $g\bar{q}$ antennae, and we use subscripts E and S for gluon emission and gluon splitting, respectively. We have implicitly assumed smooth ordering here, which implies that the upper boundaries on the integrals are given by the respective dipole invariant masses (squared), s_j . Note also that we must take into account all modifications that are applied to the LL antenna functions, including P_{imp} , P_{Ari} , and LO matrix-element matching factors. (We do not write out these factors here, to avoid clutter.) I.e., the antenna functions in the above expression must be the ones actually generated by the shower algorithm, including the effect of any modifications imposed by vetos.

For strong ordering, there are no P_{imp} factors, and the upper integral boundary is instead $\min(Q_3^2, s_j)$,

$$\Delta_3(Q_3^2, Q_{\text{had}}^2) = 1 - \sum_{j=1}^2 \int_{Q_{\text{had}}^2}^{\min(Q_3^2, s_j)} d\Phi_{\text{ant}} g_s^2 (C_A A_{Ej} + 2T_R A_{Sj}) + \mathcal{O}(\alpha_s^2). \quad (3.27)$$

However, since strong ordering is not able to fill the entire 4-parton phase space [24, 29], full NLO matching can only be obtained for the smoothly ordered variant. It is nonetheless

interesting to examine both types of shower algorithms, since even in the strongly ordered case, we may compare the Sudakov logarithms arising at $\mathcal{O}(\alpha_s^2)$ to those present in the fixed-order calculation.

On the fixed-order side, the expression for the 3-parton exclusive rate is simply

$$\text{Exact} \rightarrow |M_3^0|^2 + 2 \text{Re}[M_3^0 M_3^{1*}] + \int_0^{Q_{\text{had}}^2} \frac{d\Phi_4}{d\Phi_3} |M_4^0|^2, \quad (3.28)$$

where the last term represents 4-parton configurations in which a single parton is unresolved with respect to the hadronization scale. For Z decay, d -dimensional expressions for the virtual matrix element have been available since long [22, 32, 33, 60]. Details on the calculation and in particular its renormalization, are given in appendix B, in a notation convenient for our purposes.

We now seek a fully differential matching factor, $K_3 = 1 + V_3$, such that the expansion of

$$\text{Matched} = (1 + V_3) \text{Approximate}, \quad (3.29)$$

reproduces the exact expression, eq. (3.28), to one-loop order. (“Approximate” here stands for the tree-level matched shower approximation, eq. (3.23).) Trivial algebra yields

$$\begin{aligned} V_3^{\text{LC}} &= \left[\frac{2 \text{Re}[M_3^0 M_3^{1*}]}{|M_3^0|^2} \right]^{\text{LC}} - V_2 \\ &+ \int_{Q_3^2}^{m_Z^2} d\Phi_{\text{ant}} g_s^2 C_A A_{g/q\bar{q}} + \sum_{j=1}^2 \int_0^{s_j} d\Phi_{\text{ant}} g_s^2 (C_A A_{Ej} + 2T_R A_{Sj}) \\ &+ \int_0^{Q_{\text{had}}^2} \frac{d\Phi_4}{d\Phi_3} \frac{|M_4^0|^2}{|M_3^0|^2} - \sum_{j=1}^2 \int_0^{Q_{\text{had}}^2} d\Phi_{\text{ant}} g_s^2 (C_A A_{Ej} + 2T_R A_{Sj}), \quad (3.30) \end{aligned}$$

where we have reinstated d -dimensional forms of the one-loop matrix element and of the divergent $3 \rightarrow 4$ terms. For a shower matched to $|M_4^0|^2$ at leading order, the last two terms will cancel, by definition of the matched antenna functions (even for an unmatched shower, the difference could at most be a finite power correction in the hadronization scale, since the matrix element and the shower antenna functions have the same singularities), yielding:

$$\begin{aligned} V_{3Z}^{\text{LC}} &= \left[\frac{2 \text{Re}[M_3^0 M_3^{1*}]}{|M_3^0|^2} \right]^{\text{LC}} - V_{2Z} \\ &+ \int_{Q_3^2}^{m_Z^2} d\Phi_{\text{ant}} g_s^2 C_A A_{g/q\bar{q}} + \sum_{j=1}^2 \int_0^{s_j} d\Phi_{\text{ant}} g_s^2 (C_A A_{Ej} + 2T_R A_{Sj}) \quad (3.31) \end{aligned}$$

Rewriting the remaining integrals in terms of a set of standardized antenna subtraction terms, writing out the ordering functions for gluon emission and gluon splitting, O_E and

O_S , explicitly, and denoting the ARIADNE factor for gluon splitting by P_A , we arrive at the following master equation for the second-order correction to the 3-jet rate:

$$\begin{aligned}
V_{3Z}^{\text{LC}} = & \left[\frac{2 \text{Re}[M_3^0 M_3^{1*}]}{|M_3^0|^2} \right]^{\text{LC}} - V_{2Z} + \sum_{j=1}^2 \int_0^{s_j} d\Phi_{\text{ant}} g_s^2 \left(C_A A_{Ej}^{\text{std}} + n_F A_{Sj}^{\text{std}} \right) \\
& + \int_{Q_3^2}^{m_Z^2} d\Phi_{\text{ant}} g_s^2 C_A A_{g/q\bar{q}}^{\text{std}} + \int_{Q_3^2}^{m_Z^2} d\Phi_{\text{ant}} g_s^2 C_A \delta A_{g/q\bar{q}} \\
& - \sum_{j=1}^2 \int_0^{s_j} d\Phi_{\text{ant}} g_s^2 \left(C_A (1 - O_{Ej}) A_{Ej}^{\text{std}} + n_F (1 - O_{Sj}) P_{A_j} A_{Sj}^{\text{std}} \right) \\
& + \sum_{j=1}^2 \int_0^{s_j} d\Phi_{\text{ant}} g_s^2 (C_A \delta A_{Ej} + n_F \delta A_{Sj}) - \sum_{j=1}^2 \int_0^{s_j} d\Phi_{\text{ant}} g_s^2 n_F (1 - P_{A_j}) A_{Sj}^{\text{std}} ,
\end{aligned} \tag{3.32}$$

with the standardized Gehrmann-Gehrmann-de Ridder-Glover (GGG) subtraction terms defined by [22]:

$$\begin{aligned}
A_{g/q\bar{q}}^{\text{std}} &= a_3^0 \quad (= A_3^0) , \quad \int_0^s d\Phi_{\text{ant}} g_s^2 A_{g/q\bar{q}}^{\text{std}} = \frac{\alpha_s}{2\pi} \left(-2I_{q\bar{q}}^{(1)}(\epsilon, \mu^2/s) + \frac{19}{4} \right) \\
A_{g/qg}^{\text{std}} &= d_3^0 , \quad \int_0^s d\Phi_{\text{ant}} g_s^2 A_{g/qg}^{\text{std}} = \frac{\alpha_s}{2\pi} \left(-2I_{qg}^{(1)}(\epsilon, \mu^2/s) + \frac{17}{3} \right) \\
A_{\bar{q}/qg}^{\text{std}} &= e_3^0 \quad (= \tfrac{1}{2} E_3^0) , \quad \int_0^s d\Phi_{\text{ant}} g_s^2 A_{\bar{q}/qg}^{\text{std}} = \frac{\alpha_s}{2\pi} \left(-2I_{qg,F}^{(1)}(\epsilon, \mu^2/s) - \frac{1}{2} \right)
\end{aligned} \tag{3.33}$$

whose IR limits and integrated pole structures were examined thoroughly in [22, 33, 59], though we have here rewritten the IR singularity operators $I^{(1)}$ in explicitly dimensionless forms, see appendix A. (The alphabetical labeling in eqs. (3.33) corresponds to the notation used in [22].)

The first line combined with the first term on the second line in eq. (3.32) represent a standard antenna-subtracted one-loop matrix element, normalized to the Born level, with the standardized subtraction terms tabulated in eq. (3.33), and the additional finite term V_{2Z} originating from the NLO matching at the preceding order; see section 3.2, eq. (3.13).

The subsequent terms express the difference between the simple fixed-order subtraction carried out in the first line and the actual terms that are generated by a matched Markovian antenna shower. Physically, these terms represent the difference between the evolution of a single dipole (the original $q\bar{q}$ system) and evolution of two dipoles (the post-branching $qg\bar{q}$ system), with a transition occurring at the branching scale Q_3 . As mentioned above, the O_{Ej} and O_{Sj} factors in the third line represent the ordering criterion imposed in the evolution, either strong or smooth. For smooth ordering, they are

$$1 - O_{Ej} = 1 - \frac{Q_3^2}{Q_{Ej}^2 + Q_3^2} , \tag{3.34}$$

$$1 - O_{Sj} = 1 - \frac{Q_3^2}{m_{q\bar{q}}^2 + Q_3^2} , \tag{3.35}$$

with Q_{Ej} the evolution variable used for gluon emissions, while for strong ordering, the factor $(1 - O_j)$ can be removed if the integral boundaries are replaced by $[Q_3^2, s_j]$ (note: this replacement should only be done in the third line).

The last term in eq. (3.32) is an artifact of the ARIADNE factor, P_{Ari} , which was introduced in section 2.2 and is applied to gluon-splitting antennae in VINCIA. Summed over the two “sides” of the splitting gluon, this produces the same collinear singularities as the standard gluon-splitting antenna, but in highly asymmetric configurations in which the splitting gluon is near-collinear to a neighbouring colour line, the ARIADNE factor produces a strong suppression, which improves the agreement with the tree-level 4-parton matrix element [30], and which then generates an additional logarithm.

Notice that all but the δA terms are defined in terms of standardized antenna functions, and the corresponding integrals can be carried out analytically, once and for all. We give explicit forms for each of these terms, for each choice of evolution variable, in the following section.

The only terms of eq. (3.32) that need to be integrated numerically are thus the δA terms, which express the difference between the standardized antenna functions and those generated by the actual (matched) shower evolution, which may have different finite terms and/or be matched to the LO 4-parton matrix element. Nonetheless, since the previous lines already contain most of the structure, we expect these functions to be relatively well-behaved and numerically sub-leading. Specifically, the δA terms for gluon emission and gluon splitting, respectively, are defined by

$$\delta A_{Ej}^{\text{LC}} = O_{Ej} \left(R_{4E}^{\text{LC}} A_{Ej}^{\text{LL}} - A_{Ej}^{\text{std}} \right), \quad (3.36)$$

$$\delta A_{Sj}^{\text{LC}} = O_{Sj} P_{Aj} \left(R_{4S} A_{Sj}^{\text{LL}} - A_{Sj}^{\text{std}} \right), \quad (3.37)$$

with A^{LL} the unmatched shower antenna function (as defined in [30, 39]) and the second-order LO matching factors, R_{4E} and R_{4S} (for $Z \rightarrow qgg\bar{q}$ and $Z \rightarrow q\bar{q}'q'\bar{q}$, respectively), defined as in eq. (3.4), but including only the leading-colour terms in R_{4E}^{LC} . For strong ordering, similarly to above, the O_j factors can be removed by changing the integration boundaries of the δA terms to $[0, Q_3^2]$.

Finally, we note that one could in principle equally well have defined eq. (3.32) without the terms on the third line. The δA terms in eqs. (3.36) and (3.37) would then likewise have to be defined without P_{imp} and P_{Ari} factors. However, while this would give a seemingly cleaner relation with standard fixed-order subtraction, the behaviour of the (numerical) integrals over the δA terms would be more difficult, due to over-subtraction in the unordered regions. (Showers without either a strong-ordering condition or a smooth-ordering suppression greatly overestimate the real-radiation matrix elements in the unordered region [24, 28, 30].) Numerically, it is therefore more convenient to integrate the contributions represented by the third line in eq. (3.32) analytically, leaving only the suppressed terms in eq. (3.37) to be integrated over numerically.

To be specific, the numerical integration over the δA terms is performed by rewriting the δA integrals in dimensionless MC form, as:

$$\frac{\alpha_s}{2\pi} C_A \sum_{j=1}^2 \frac{1}{4} \frac{1}{N} \sum_{i=1}^N (s_j \delta A_j(\Phi_i)) , \quad (3.38)$$

and similarly for the gluon-splitting terms, with Φ_i a number of random (uniformly distributed) antenna phase-space points. The common factor $1/4$ arises from combining the prefactor $8\pi^2$ above with the area of the phase-space triangle, $1/2$, and the factor $1/(16\pi^2)$ from the phase-space factorization, $d\Phi_{\text{ant}}$. For smooth p_\perp -ordering with an arbitrary normalization factor N_\perp (so $Q_E^2 = N_\perp p_\perp^2$), the ordering factors, O_j , reduce to:

$$O_E(q_i g_j, \bar{q}_k \rightarrow q_a g_b g_c, \bar{q}_k) = \frac{y_{jk}}{y_{jk} + x_{ab} x_{bc}} , \quad (3.39)$$

$$O_E(q_i, g_j \bar{q}_k \rightarrow q_i, g_a g_b \bar{q}_c) = \text{same with } i \leftrightarrow k , \quad (3.40)$$

$$O_S(q_i g_j, \bar{q}_k \rightarrow q_a \bar{q}'_b q'_c, \bar{q}) = \frac{N_\perp y_{jk}}{N_\perp y_{jk} + x_{bc}} , \quad (3.41)$$

$$O_S(q_i, g_j \bar{q}_k \rightarrow q_i, \bar{q}'_c q'_b \bar{q}_a) = \text{same with } i \leftrightarrow k , \quad (3.42)$$

where we have used y with ijk indices for the scaled invariants in the original $qg\bar{q}$ topology and x with abc indices for the integration variables in the antenna phase space. Note also that the y values are normalized to the full 3-parton CM energy (squared), while the x values are normalized to their respective dipole CM energies (squared).

3.4 The Renormalization Term

A further ingredient to be discussed is the choice of renormalization scale on both the fixed order and parton shower sides of the calculation, as these scales are in general chosen differently in both sides. Hence a translation term arises at second order, which must account for this difference, keeping in mind that, as the scale evolves from one to the other, flavour thresholds are passed. Our aim is to have the flexibility to use fixed order matrix elements renormalized according to their usual scheme, while maintaining the freedom to make a different choice on the shower side.

The fixed order calculations for Z -decay to jets to which we match are customarily renormalized in a version of the $\overline{\text{MS}}$ scheme called the Zero-Mass Variable Flavour Number Scheme (ZM-VFNS). In this scheme the bare QCD coupling is renormalized as

$$g_b = \mu^\epsilon g(\mu_R^2) \left[1 + \frac{\alpha_s(\mu_R^2)}{8\pi} \left\{ \left(-\frac{1}{\epsilon} + \gamma_E - \ln 4\pi + \ln \frac{\mu_R^2}{\mu^2} \right) \beta_0 \right\} \right] \quad (3.43)$$

with $\beta_0 = (11C_A - 2n_F)/3 \equiv \beta_0^F$ and n_F is the number of light flavours. One thus ignores flavours that are heavier than the scale of the calculation, both in the virtual and in the real calculations. Once all the UV poles are cancelled, one has a running coupling that depends on

the number of light flavours for the scale μ_R at hand. One then changes the flavour number when a threshold is crossed. For our present case of Z boson decay to jets we take $n_F = 5$ for μ_R not too different from the Z -boson mass.

Let us be more specific about the matching of α_s across flavour thresholds. At one loop,

$$\alpha_s^{(n_F)}(\mu_R) = \frac{4\pi/\beta_0^F}{\ln(\mu_R^2/\Lambda_F^2)}. \quad (3.44)$$

The value of Λ_F depends on the number of active flavours, as follows. When passing flavour thresholds the following one-loop matching conditions are imposed

$$\alpha_s^{(5)}(m_b) = \alpha_s^{(4)}(m_b), \quad \alpha_s^{(4)}(m_c) = \alpha_s^{(3)}(m_c). \quad (3.45)$$

These conditions can be satisfied if Λ_F obeys the matching conditions

$$\ln \frac{\Lambda_F^2}{\Lambda_{F+1}^2} = \frac{2}{3\beta_0^F} \ln \frac{m_{F+1}^2}{\Lambda_{F+1}^2}. \quad (3.46)$$

With these conditions one can also express α_s values for different flavour numbers into each other. E.g. if $m_c < \mu_R < m_b$, one can express $\alpha_s^{(4)}(\mu_R)$ in terms of $\alpha_s^{(5)}(\mu_R)$ by the relation

$$\alpha_s^{(4)}(\mu_R) = \alpha_s^{(5)}(\mu_R) \frac{1}{\frac{\beta_0^4}{\beta_0^5} + \left(1 - \frac{\beta_0^4}{\beta_0^5}\right) \frac{\alpha_s^{(5)}(\mu_R)}{\alpha_s^{(5)}(m_b)}}. \quad (3.47)$$

For completeness we briefly review how this n_F -dependent UV singularity occurs in the context of the (inclusive) 3-jet rate, in the case where we only consider massless quarks [32, 60]. In the virtual contribution, the only one-loop diagram for $Z \rightarrow q\bar{q}g$ that is sensitive to the number of flavours is the quark self-energy correction on the external gluon. The self-energy diagram itself, being scaleless, is zero in dimensional regularization. However, renormalization of the coupling amounts to adding a n_F counterterm on the external gluon line proportional to

$$n_F \frac{2}{3\epsilon} \left(\frac{\mu^2}{\mu_R^2} \right)^\epsilon. \quad (3.48)$$

The real contribution contributes a n_F dependent (collinear) $1/\epsilon$ pole as well, from gluon-splitting

$$- n_F \frac{2}{3\epsilon} \left(\frac{\mu^2}{s} \right)^\epsilon. \quad (3.49)$$

In the sum over real and virtual contributions the poles cancel, as guaranteed by the KLN theorem, leaving a logarithm of the form

$$n_F \frac{2}{3} \ln \left(\frac{s}{\mu_R^2} \right). \quad (3.50)$$

On the shower side a related prescription is used, in which the running coupling is evaluated at a shower scale μ_{PS} , such that the scale again depends on the number of flavours.

Depending on the value of μ_{PS} , a corresponding value of n_F is chosen, as well as of the QCD scale Λ_F . This is often different from that for a fixed order calculation. To give a specific example, matrix elements will typically be renormalized at a scale characteristic of the total CM energy, i.e., $\mu_{\text{ME}}^2 = s$ an event-independent value, while resummation arguments imply one best chooses a running scale, such as $\mu_{\text{PS}} = p_\perp$, for shower applications [34, 35], which can differ per event.

Shifting to a different scale for α_s of a given flavour number is quite straightforward. Translating from a shower scale μ_{PS} to a matrix-element scale μ_{ME} amounts to replacing, for an antenna function

$$a_{g/q\bar{q}}|_{\mu_R=\mu_{\text{PS}}} \rightarrow \left(1 + \frac{\alpha_s}{2\pi} \frac{11N_C - 2n_F}{6} \ln\left(\frac{\mu_{\text{ME}}^2}{\mu_{\text{PS}}^2}\right) + \mathcal{O}(\alpha_s^2)\right) a_{g/q\bar{q}}|_{\mu_R=\mu_{\text{ME}}} . \quad (3.51)$$

A further aspect is that shower Monte Carlos normally switch to 4-flavour (3-flavour) running for scales $\mu < m_b$ ($\mu < m_c$), matching the α_s value across the thresholds to obtain a continuous running. For a consistent treatment, such thresholds must be taken into account when translating α_s from the shower scale to the matrix-element one. At one-loop order (which is all that is relevant for the NLO expansion), this can be done by inserting an additional term for each flavour threshold in the region $[\mu_{\text{PS}}, \mu_{\text{ME}}]$,

$$+ \frac{\alpha_s}{2\pi} \frac{1}{3} \ln\left(\frac{m_{\text{thres}}^2}{\mu_{\text{PS}}^2}\right) , \quad (3.52)$$

with m_{thres} the flavour threshold. Physically, eq. (3.51) expresses running with n_F flavours all the way from μ_{PS} to μ_{ME} . The correction term, eq. (3.52), expresses that the number of flavours was effectively lower below each flavour threshold passed on the way. Note that this can also be used to account for a larger number of flavours in the shower calculation, e.g., at scales $\mu_{\text{PS}} > m_t$, with the sign change of the correction then automatically reflected by the logarithm.

For coherent parton-shower models, the arguments presented in [35] also motivate a change to a “Monte Carlo” scheme for α_s , in which Λ_{QCD} is rescaled, for each n_F , by the so-called CMW factor ~ 1.5 (with some mild flavour dependence), relative to its $\overline{\text{MS}}$ value. If the shower model being matched employs this scheme, then a further rescaling of the renormalization-scale argument, $\mu_{\text{PS}} \rightarrow \mu_{\text{PS}}/k_{\text{CMW}}$, should be used in eq. (3.51), with

$$k_{\text{CMW}} = \exp\left(\frac{67 - 3\pi^2 - 10n_F/3}{2(33 - 2n_F)}\right) = \begin{cases} 1.513 & n_F = 6 \\ 1.569 & n_F = 5 \\ 1.618 & n_F = 4 \\ 1.661 & n_F = 3 \end{cases} \quad (3.53)$$

for $N_C = 3$. The translation of renormalization scale (and scheme) yields then an additional term to be added to the definition of V_3 in eq. (3.32),

$$V_{3\mu} = -\frac{\alpha_s}{2\pi} \frac{11N_C - 2n_F}{6} \ln\left(\frac{\mu_{\text{ME}}^2}{\mu_{\text{PS}}^2}\right) = -\frac{\alpha_s}{2\pi} \frac{\beta_0}{2} \ln\left(\frac{\mu_{\text{ME}}^2}{\mu_{\text{PS}}^2}\right) , \quad (3.54)$$

plus any additional flavour-threshold correction terms, cf. eq. (3.52). By inserting these terms, which enter at overall order $\alpha_s^2 \ln(\mu_{\text{ME}}^2/\mu_{\text{PS}}^2)$, the two calculations can be compared consistently at one-loop accuracy.

Note that if several different shower paths populate the same fixed-order phase-space point, then each path will in general be associated with a distinct μ_{PS} value. Thus, one $V_{3\mu}$ term arises for each shower path, weighted by the relative contribution of each path to the total. Since for our case there is only one antenna contributing to $Z \rightarrow qg\bar{q}$, this particular complication does not arise here.

We finally alert the reader regarding the use of different flavour number α_s 's in the master equation (3.32). In that equation cancellation of $1/\epsilon$ divergences take place, already in the first line of the right hand side. For this cancellation it is important that the subtraction terms, originating from the shower expansion and listed in eq. (3.33), use $\alpha_s^{(5)}$ renormalized as in the fixed order calculation. All subsequent terms in the master equation are finite, and constitute differences of unordered and strongly ordered shower based terms, which are also finite, and beyond NLO.

3.5 Leading-Colour One-Loop Correction for $Z \rightarrow 3$ Jets

Combining the results above, in particular eqs. (3.32), (3.33), and (3.54), we obtain the complete expression for the leading-colour⁸ one-loop correction for $Z \rightarrow 3$ Jets,

$$\begin{aligned}
V_{3Z}(q, g, \bar{q}) = & \left[\frac{2 \operatorname{Re}[M_3^0 M_3^{1*}]}{|M_3^0|^2} \right]^{\text{LC}} - \frac{\alpha_s}{\pi} - \frac{\alpha_s}{2\pi} \left(\frac{11N_C - 2n_F}{6} \right) \ln \left(\frac{\mu_{\text{ME}}^2}{\mu_{\text{PS}}^2} \right) \\
& + \frac{\alpha_s C_A}{2\pi} \left[-2I_{qg}^{(1)}(\epsilon, \mu^2/s_{qg}) - 2I_{qg}^{(1)}(\epsilon, \mu^2/s_{g\bar{q}}) + \frac{34}{3} \right] \\
& + \frac{\alpha_s n_F}{2\pi} \left[-2I_{qg,F}^{(1)}(\epsilon, \mu^2/s_{qg}) - 2I_{g\bar{q},F}^{(1)}(\epsilon, \mu^2/s_{g\bar{q}}) - 1 \right] \\
& + \frac{\alpha_s C_A}{2\pi} \left[8\pi^2 \int_{Q_3^2}^{m_Z^2} d\Phi_{\text{ant}} A_{g/q\bar{q}}^{\text{std}} + 8\pi^2 \int_{Q_3^2}^{m_Z^2} d\Phi_{\text{ant}} \delta A_{g/q\bar{q}} \right. \\
& \quad \left. - \sum_{j=1}^2 8\pi^2 \int_0^{s_j} d\Phi_{\text{ant}} (1 - O_{Ej}) A_{g/qg}^{\text{std}} + \sum_{j=1}^2 8\pi^2 \int_0^{s_j} d\Phi_{\text{ant}} \delta A_{g/qg} \right] \\
& + \frac{\alpha_s n_F}{2\pi} \left[- \sum_{j=1}^2 8\pi^2 P_{Aj} \int_0^{s_j} d\Phi_{\text{ant}} (1 - O_{Sj}) A_{\bar{q}/qg}^{\text{std}} + \sum_{j=1}^2 8\pi^2 \int_0^{s_j} d\Phi_{\text{ant}} \delta A_{\bar{q}/qg} \right. \\
& \quad \left. - \frac{1}{6} \frac{s_{qg} - s_{g\bar{q}}}{s_{qg} + s_{g\bar{q}}} \ln \left(\frac{s_{qg}}{s_{g\bar{q}}} \right) \right], \tag{3.55}
\end{aligned}$$

where:

⁸We use the usual MC definition of leading colour and include terms $\propto C_A$ and $\propto n_F$ but neglect ones $\propto 1/C_A$.

- the first line contains the full (leading-colour) one-loop matrix element, the V_{2Z} correction from one-loop matching at the preceding order, and the $V_{3\mu}$ term from the choice of shower renormalization scale;
- the second line contains the standardized subtraction term arising from the $qg \rightarrow qgg$ and $g\bar{q} \rightarrow gg\bar{q}$ antennae;
- the third line contains the standardized subtraction term arising from the $qg \rightarrow q\bar{q}'q'$ and $g\bar{q} \rightarrow q'q'\bar{q}$ antennae;
- the fourth to last lines contain the terms arising from the difference between the (matched) shower evolution and the standardized subtraction terms, including the consequences of ordering choices and modification factors such as those arising from the Ariadne factor and from matching to the LO matrix elements.

We denote the singular subtracted 1-loop matrix element by SVirtual

$$\begin{aligned} \text{SVirtual} = & \left[\frac{2 \text{Re}[M_3^0 M_3^{1*}]}{|M_3^0|^2} \right]^{\text{LC}} + \frac{\alpha_s C_A}{2\pi} \left[-2I_{qg}^{(1)}(\epsilon, \mu^2/s_{qg}) - 2I_{qg}^{(1)}(\epsilon, \mu^2/s_{g\bar{q}}) + \frac{34}{3} \right] \\ & + \frac{\alpha_s n_F}{2\pi} \left[-2I_{qg,F}^{(1)}(\epsilon, \mu^2/s_{qg}) - 2I_{g\bar{q},F}^{(1)}(\epsilon, \mu^2/s_{qg}) - 1 \right] \end{aligned} \quad (3.56)$$

In section 4, we compute the analytical integrals corresponding to each of the shower-generated terms, for different choices of evolution variable, ordering criterion, and antenna functions.

With the one-loop matrix element expressed as in appendix B.2, it is easy to see that the infrared singularity operators in eq. (3.56) cancel, leaving only explicitly finite remainders (which may still contain logarithms of resolved scales). This then constitutes the description of the one-loop matching for $Z \rightarrow 3$ jets, having already discussed the case for two jets. In the context of eq. (3.10) we have now corrected the first two terms on the rhs to NLO accuracy.

We round off with a few remarks on the normalizations of the various $Z \rightarrow n$ -parton rates that are obtained by our procedure, since this is a point on which the various approaches to multileg NLO corrections differ. We make the following observations:

1. *The total inclusive Z decay rate:* the matrix-element correction scheme derived in this paper maintains a strict unitarity between the real and virtual corrections that are applied beyond Born level. An important consequence is that the total inclusive Z decay rate is not changed by switching on the V_{3Z} correction⁹.

⁹The theoretically most sensible choice would be to normalize the inclusive $Z \rightarrow 2$ -parton rate to the full NNLO result, but at the level we work at, one could equally well normalize to NLO or to data. In either case, the total normalization of the generated sample is left unchanged by the V_{3Z} correction.

2. *The inclusive $Z \rightarrow 3$ jets rate:* both the virtual (one-loop) correction to the 3-jet rate and the real (tree-level) correction to the 4-jet rate are included here. Hence the inclusive 3-jet rate is NLO correct. Without these corrections, it would only be LO correct. Thus, the 3-jet inclusive rate *does* change when switching on the V_{3Z} term¹⁰.
3. *The exclusive $Z \rightarrow 2$ jets rate:* The strict unitarity imposed by our correction method implies that every 3-jet event begins life as a 2-jet one. Since the V_{3Z} term modifies the probability for a 2-jet event to evolve to become a 3-jet one, at the $\mathcal{O}(\alpha_s^2)$ level, the 2-jet exclusive rate receives an equal and opposite correction. This represents an $\mathcal{O}(\alpha_s^2)$ ambiguity on the exclusive 2-jet rate, which is not addressed in our paper (though it could be removed by normalizing to the full NNLO result for $Z \rightarrow 2$, cf. the inclusive 2-jet rate above).
4. *The exclusive $Z \rightarrow 3$ jets rate:* for a given 3-parton configuration, the evolution to 4 partons and beyond is not changed by V_{3Z} (though it *is* changed by the application of the 4-parton tree-level corrections, which we take to be included throughout this paper). Thus, while switching V_{3Z} on does change the total amount of 3-jet events (cf. the inclusive 3-jet rate above), it does not directly change the fraction of those events which will develop a fourth or more jets.

3.6 One-Loop Correction for Born + 2 Partons

To illustrate how the formalism presented here generalizes to higher multiplicities, we take the case of the NLO correction to $Z \rightarrow 4$ partons. For simplicity, however, we continue to restrict our analysis of the correction factor to the leading-colour level. At NLO, the exclusive $Z \rightarrow 4$ partons rate at “infinite” perturbative resolution (similarly to above) is

$$\text{Exact} \rightarrow |M_4^0|^2 + 2\text{Re}[M_4^0 M_4^{1*}] . \quad (3.57)$$

Labeling the 4 partons by $Z \rightarrow i, j, k, \ell$, there are two possible antenna-shower histories leading to each 4-parton configuration, with j and k the last emitted parton, respectively. Those two contributions both enter in the definition of the tree-level 4-parton matching factor,

$$R_4 = \frac{|M_4^0(i, j, k, \ell)|^2}{A_{j/IK}|M_3^0(I, K, \ell)|^2 + A_{k/JL}|M_3^0(i, J, L)|^2} , \quad (3.58)$$

such that their sum reproduces the full 4-parton matrix element. Note that a separate such factor is applied to $Z \rightarrow qgg\bar{q}$ and $Z \rightarrow q\bar{q}'q'\bar{q}$, and that we have suppressed colour and coupling factors here, for compactness (we ignore the small, non-singular extra interference terms for the special case where all four quarks have the same flavour). The antenna functions, A , are understood to include all such factors, as well as any P_{imp} and P_{ari} factors appropriate

¹⁰In section 5.2 below (comparisons to LEP measurements), this is seen most easily in figure 15, where the “(NLO off)” curves undershoot the “(NLO on)” ones, for observable regions dominated by 3 or more jets.

to the branchings at hand. For a general n -parton matrix element, the denominator contains one term for each possible clustering.

Labeling the $IK \rightarrow ijk$ history by A and the $JL \rightarrow jk\ell$ one by B , the sum over the two histories yields

$$R_4 \Delta_4(Q_4, 0) \sum_{\alpha \in A, B} A_{3 \rightarrow 4}^\alpha |M_3^\alpha|^2 \Delta_2(m_Z^2, Q_3^\alpha) \Delta_3(Q_3^\alpha, Q_4^\alpha) \prod_{m=2}^3 (1 + V_m^\alpha), \quad (3.59)$$

where it is understood that α is an index, not a power, and the last product factor takes into account the NLO matching at the preceding multiplicities. Expanding the Sudakov factors to first order and using the definition of the NLO correction factor at the preceding multiplicity, eq. (3.31), this becomes

$$R_4 \left(1 - \sum_k \int_0^{s_k} d\Phi_{\text{ant}} R_5 A_{4 \rightarrow 5} \right) \sum_{\alpha \in A, B} A_{3 \rightarrow 4}^\alpha |M_3^\alpha|^2 \left[1 + \frac{2\text{Re}[M_3^0 M_3^{1*}]^\alpha}{|M_3^\alpha|^2} + \sum_j \int_0^{Q_4^\alpha} d\Phi_{\text{ant}} A_{3 \rightarrow 4}^\alpha \right], \quad (3.60)$$

which we can rewrite as

$$\begin{aligned} & |M_4|^2 \left(1 - \sum_k \int_0^{s_k} d\Phi_{\text{ant}} R_5 A_{4 \rightarrow 5} \right) \\ & + R_4 \sum_{\alpha \in A, B} A_{3 \rightarrow 4}^\alpha |M_3^\alpha|^2 \left(\frac{2\text{Re}[M_3^0 M_3^{1*}]^\alpha}{|M_3^\alpha|^2} + \sum_j \int_0^{Q_4^\alpha} d\Phi_{\text{ant}} A_{3 \rightarrow 4}^\alpha \right), \end{aligned} \quad (3.61)$$

where we again emphasize that the antenna functions are understood to include all relevant coupling, P_{imp} , and P_{ari} factors. The first term represents the new subtraction that the shower generates at 4 partons, while the second represents part of the NLO correction to the preceding multiplicity. For one of the histories (the one followed by the “current” event), this correction has already been evaluated and can be reused. The contribution from the other history will have to be recomputed, however. In general, there will be one subtraction to perform at the n -parton level, and there will be $m \sim n - n_{\text{Born}} - 1$ new subtractions that have to be done at the $(n - 1)$ -parton level, in addition to the one that was already done during the evolution of the current event.

Clearly, there is an undesirable scaling behavior built into this, which will make NLO matching at many partons quite computing intensive. An alternative, which eliminates the sum over histories, is that of sector showers, see e.g., [30, 61]. Though this is not the main avenue pursued in this paper, we nevertheless give some comments below on how a sector-based NLO matching scheme could be constructed.

3.7 One-Loop Matching for Sector Showers

The matching conditions derived above may also be applied to so-called sector showers [30, 61], with a few relatively minor modifications. The expansion of the Sudakov factors generated

by the LO matched shower will now contain integrals over ratios of matrix elements (which are the LO matched sector antenna functions), multiplied by sector vetos. The presence of the sector vetos makes analytical phase-space integration more difficult.

However, since the sector approach merely represents a different way of decomposing the same singularities as the global one, we may effectively recycle the integrals carried out for the global case by adding and subtracting the terms produced by a smoothly ordered “standard” shower (i.e., using the GGG functions). The first four lines of eq. (3.32) then remain unchanged. The definition of the δA terms in the last line, however, changes to

$$\sum_{j=1}^2 \int_0^{s_j} d\Phi_{\text{ant}} g_s^2 C_A \left(\Theta_j^{\text{sct}} A_{g/qg}^{\text{sct}} - A_{g/qg}^{\text{std}} \right), \quad (3.62)$$

for the terms arising from the $qg\bar{q} \rightarrow qgg\bar{q}$ Sudakov factor, with analogous ones arising from the gluon-splitting contributions. The step function, Θ_j , represents the sector veto applied to the sector antenna functions. The sector antenna function, up to the tree-level matched orders, is just

$$g_s^2 \mathcal{C} A^{\text{sct}} = \frac{|M_n^0|^2}{|M_{n-1}^0|^2}. \quad (3.63)$$

Since the individual sector and global antenna functions have different singularity structures (they are only guaranteed to have the same singularities at the summed level), the integrals in eq. (3.62) are divergent, and cannot be carried out numerically. In order to obtain numerically convergent integrals, we must divide up the contributions of the global terms onto each sector, and perform a set of correlated integrals in which the singularities explicitly cancel in the divergent limits,

$$\begin{aligned} \rightarrow & \int_0^{s_{qg}} d\Phi_{\text{ant}} g_s^2 C_A \Theta_1^{\text{sct}} \left(A_{g/qg}^{\text{sct}} - A_{g/qg}^{\text{std}} \right) - \int_0^{s_{g\bar{q}}} d\Phi_{\text{ant}} g_s^2 C_A \Theta_1^{\text{sct}} A_{g/g\bar{q}}^{\text{std}} \\ & + \int_0^{s_{g\bar{q}}} d\Phi_{\text{ant}} g_s^2 C_A \Theta_2^{\text{sct}} \left(A_{g/g\bar{q}}^{\text{sct}} - A_{g/g\bar{q}}^{\text{std}} \right) - \int_0^{s_{qg}} d\Phi_{\text{ant}} g_s^2 C_A \Theta_2^{\text{sct}} A_{g/qg}^{\text{std}}, \end{aligned} \quad (3.64)$$

where each line now corresponds to the sum of contributions to a single sector, for which the difference between sector and global antennae is finite. The individual integrals are of course still divergent, but they can now be treated numerically by collecting the terms on each line under a single integral sign. Analytically, this is complicated since the two integrals on each line are not associated with the same kinematics map¹¹. Numerically, however, we may still ensure a point-by-point cancellation in the singular limits by keeping the two integrals formally separate, but carrying them out simultaneously, in a correlated way, as follows.

For each antenna, generate a random uniformly distributed phase-space point,

$$[y_{ij}, y_{jk}, \phi], \quad (3.65)$$

¹¹In the example here, for $Z \rightarrow 3$ partons, one term is associated with branchings in the qg antenna, while the other is associated with branchings in the $g\bar{q}$ one.

and evaluate the first term in eq. (3.64). (If the point is outside the relevant sector, this term is zero for the time being). If the pair (jk) , say, corresponds to a sector shared with a neighboring antenna (as in our example), check whether the correlated phase-space point defined by

$$[y_{jk}, 1 - y_{jk} - y_{ij}, \phi], \quad (3.66)$$

in the neighboring antenna passes the same sector veto as before, and if so, subtract the global term corresponding to the second term on the first line of eq. (3.64). The sampling represented by eq. (3.66) is uniform, as long as that used to generate the original point, eq. (3.65), is uniform. The replacement of y_{ij} by $1 - y_{jk} - y_{ij}$ corresponds precisely to the mapping $z \rightarrow 1 - z$ in the collinear limit, which is what is required to reestablish a point-by-point cancellation of the sector and global singularities.

4 Sudakov Integrals

In this section, we work out the standardized Sudakov integrals appearing in the second and third line of eq. (3.32), for each choice of evolution variable. We also study the soft and collinear limits of the Sudakov integrals and compare them to those of the one-loop matrix element. This provides an explicit check of whether the first-order expansion of the Sudakov factors generates the correct logarithms present in the fixed-order calculation.

Given our choice of the GGG antenna functions as our standard ones, the relevant terms are

$$g_s^2 \left[C_A \int_{Q_3^2}^s a_3^0 d\Phi_{\text{ant}} - \sum_{j=1}^2 C_A \int_0^{s_j} (1 - O_{E_j}) d_3^0 d\Phi_{\text{ant}} - \sum_{j=1}^2 2T_R n_F P_{A_j} \int_0^{s_j} (1 - O_{S_j}) e_3^0 d\Phi_{\text{ant}} \right] \quad (4.1)$$

The general form of the first term, which originates from the $2 \rightarrow 3$ branching step, is

$$g_s^2 C_A \int_{Q_3^2}^s a_3^0 d\Phi_{\text{ant}} = \frac{\alpha_s C_A}{2\pi} \left(\sum_{i=1}^5 K_i I_i(s, Q_3^2) \right) \quad (4.2)$$

where the definitions for the K_i and the I_i functions are given in appendix C, for each type of antenna function and ordering variable. Their derivation and soft/collinear structure will be discussed more closely below, for each choice of ordering and evolution variable. The form of the $3 \rightarrow 4$ integrals depends on whether we work in the context of strong or smooth ordering. We shall now consider each of those cases in turn, beginning with strong ordering.

4.1 Strong Ordering

For strong ordering, the inverted ordering conditions in eq. (3.32), $(1 - O_{E_j/S_j})$, reduce to step functions expressing integration over the unordered region. The integration surface is

thus limited from below by the phase-space contour defined by the evolution scale of the first branching, Q^2 , and from above by the edge defined by the invariant mass of the antenna.

The expression generated by the $3 \rightarrow 4$ splitting case for gluon emission is

$$-g_s^2 \sum_{j=1}^2 C_A \int_0^{s_j} (1-O_{E_j}) d_3^0 d\Phi_{\text{ant}} = -\frac{\alpha_s C_A}{2\pi} \left(\sum_{i=1}^5 K_i I_i(s_{qg}, Q_3^2) \right) - \frac{\alpha_s C_A}{2\pi} \left(\sum_{i=1}^5 K_i I_i(s_{g\bar{q}}, Q_3^2) \right). \quad (4.3)$$

where K_i and I_i are the same as those for the $2 \rightarrow 3$ term above, though they here appear with different arguments. The remaining case is the $3 \rightarrow 4$ gluon splitting defined by

$$-g_s^2 \sum_{j=1}^2 n_F P_{A_j} \int_0^{s_j} (1-O_{S_j}) e_3^0 d\Phi_{\text{ant}} = -\frac{\alpha_s n_F}{2\pi} P_{A_{qg}} H(s_{qg}, Q_3^2) - \frac{\alpha_s n_F}{2\pi} P_{A_{g\bar{q}}} H(s_{g\bar{q}}, Q_3^2). \quad (4.4)$$

with H defined in appendix C and P_{A_j} as defined in eq. (2.20). We will discuss the derivation of these terms in more detail in the following three subsections, for strong m_D -, p_\perp -, and energy-ordering, respectively.

4.1.1 Dipole Virtuality

We begin with dipole virtuality as evolution variable, which is perhaps the simplest case. We start by repeating the integrals of eq. (3.32) with the one-particle phase space defined as in eq. (2.8). In the case of dipole virtuality the contours are triangular (figure 2.3). We recall that, for the $g \rightarrow q\bar{q}$ terms, it is the $q\bar{q}$ invariant mass that is used as evolution variable, regardless of what choice is made for gluon emissions. The m_D scale of the previous emission still enters, however, since that defines the ordering scale applied to both emissions and splittings. The explicit forms of the terms in eq. (4.1) are:

$$\begin{aligned} &= \frac{\alpha_s}{4\pi} \left[\frac{C_A}{s} \int_{\min(s_{qg}, s_{g\bar{q}})}^{s-\min(s_{qg}, s_{g\bar{q}})} ds_1 \int_{\min(s_{qg}, s_{g\bar{q}})}^{s-s_1} ds_2 a_3^0(s_1, s_2) \right. \\ &- \left\{ \frac{C_A}{s_{g\bar{q}}} \Theta(s_{g\bar{q}} - 2s_{qg}) \int_{s_{qg}}^{s_{g\bar{q}}-s_{qg}} ds_1 \int_{s_{qg}}^{s_{g\bar{q}}-s_1} ds_2 + \frac{C_A}{s_{qg}} \Theta(s_{qg} - 2s_{g\bar{q}}) \int_{s_{g\bar{q}}}^{s_{qg}-s_{g\bar{q}}} ds_1 \int_{s_{g\bar{q}}}^{s_{qg}-s_1} ds_2 \right\} d_3^0(s_1, s_2) \\ &- \left. \left\{ \frac{n_F}{s_{qg}} \Theta(s_{qg} - s_{g\bar{q}}) P_{A_1} \int_{s_{g\bar{q}}}^{s_{qg}} ds_1 \int_0^{s_{qg}-s_1} ds_2 + \frac{n_F}{s_{g\bar{q}}} \Theta(s_{g\bar{q}} - s_{qg}) P_{A_2} \int_{s_{qg}}^{s_{g\bar{q}}} ds_1 \int_0^{s_{g\bar{q}}-s_1} ds_2 \right\} e_3^0(s_1, s_2) \right], \quad (4.5) \end{aligned}$$

with $P_{A_j} = \frac{2s_{qg}}{s_{qg}+s_{g\bar{q}}}$ and $P_{A_2} = \frac{2s_{g\bar{q}}}{s_{qg}+s_{g\bar{q}}}$ as defined in eq. (2.20) and the gluon-splitting antenna e_3^0 has its singularities in s_1 .

For compactness, we only show the integration for the double-pole (soft-collinear eikonal) terms present in both a_3^0 and d_3^0 here, which are the only sources of transcendentality-2 terms.

The full antenna integrals, including also the lower-transcendentality terms originating from single poles and finite terms, are given in appendix C. The $T = 2$ part of the a_3^0 integral is

$$\frac{\alpha_s C_A}{4\pi} \left[\int_{\min(s_{qg}, s_{g\bar{q}})}^{s - \min(s_{qg}, s_{g\bar{q}})} ds_1 \int_{\min(s_{qg}, s_{g\bar{q}})}^{s - s_1} ds_2 \frac{2}{s_1 s_2} \right]. \quad (4.6)$$

To evaluate this expression, we first rewrite it in a dimensionless form in terms of the rescaled integration variables $y_i = s_i / (s - \frac{1}{2}Q_3^2)$, with upper boundary 1 and lower boundary

$$\xi_{\min} = \frac{\min(s_{qg}, s_{g\bar{q}})}{s - \min(s_{qg}, s_{g\bar{q}})}. \quad (4.7)$$

The integration is over a triangular surface. The lower integration boundary cuts off the evolution variable at the value of the 3-parton evolution scale. The other boundary is determined by the total energy of the dipole before branching which here is \sqrt{s} . We use the integral

$$\int_x^1 \frac{dy}{y} \ln \left(\frac{1 - y + x}{x} \right) = \ln^2(x) - \ln(x) \ln(1 + x) - \text{Li}_2 \left(\frac{1}{1 + x} \right) + \text{Li}_2 \left(\frac{x}{1 + x} \right). \quad (4.8)$$

to obtain

$$\begin{aligned} \frac{\alpha_s C_A}{2\pi} & \left[\ln \left(\frac{s}{\min(s_{qg}, s_{g\bar{q}})} \right) \ln \left(\frac{s - \min(s_{qg}, s_{g\bar{q}})}{\min(s_{qg}, s_{g\bar{q}})} \right) \right. \\ & \left. - \text{Li}_2 \left(\frac{s - \min(s_{qg}, s_{g\bar{q}})}{s} \right) + \text{Li}_2 \left(\frac{\min(s_{qg}, s_{g\bar{q}})}{s} \right) \right]. \end{aligned} \quad (4.9)$$

To discuss the $3 \rightarrow 4$ Sudakov terms, let us for definiteness assume that we are in a 3-parton phase-space point with $s_{qg} > s_{g\bar{q}}$. The opposite case is symmetric. Again we only include the $T = 2$ terms explicitly here, with the details of the full antenna integrals relegated to appendix C.

$$\frac{\alpha_s C_A}{4\pi} \left[\int_{s_{g\bar{q}}}^{s_{qg} - s_{g\bar{q}}} ds_1 \int_{s_{g\bar{q}}}^{s_{qg} - s_1} ds_2 \frac{2}{s_1 s_2} \right]. \quad (4.10)$$

The integration is again over a triangular surface. The total energy of the dipole before branching is now s_{qg} . The integral in eq. (4.10) corresponding to the sum over antenna integrals only contains one d_3^0 integral because the other has equal upper and lower integration boundaries. Note that this integral actually vanishes for $s_{qg} \leq Q_3^2$, which amounts to the dipole-virtuality ordering allowing the $3 \rightarrow 4$ branchings to populate their full respective phase spaces (i.e. no correction term is necessary).

Focusing on the case $s_{qg} > 2s_{g\bar{q}}$ for which the second integral is nonvanishing (which now amounts to the ordering condition imposing a nontrivial restriction on the $3 \rightarrow 4$ phase space, see figure 2.3), we obtain, including the $2 \rightarrow 3$ term

$$\frac{\alpha_s C_A}{4\pi} \left[\int_{\xi_{\min}}^1 dy_1 \int_{\xi_{\min}}^{1 - y_1 + \xi_{\min}} dy_2 \frac{2}{y_1 y_2} - \int_{\xi'_{\min}}^1 dy'_1 \int_{\xi'_{\min}}^{1 - y'_1 + \xi'_{\min}} dy'_2 \frac{2}{y'_1 y'_2} \right], \quad (4.11)$$

$y'_i = s_i/(s_{qg} - s_{g\bar{q}})$ and boundaries

$$\xi'_{\min} = \frac{s_{g\bar{q}}}{s_{qg} - s_{g\bar{q}}} . \quad (4.12)$$

with lower-transcendentality terms again available in appendix C. For the mirror case $s_{g\bar{q}} > 2s_{qg}$ essentially symmetric expressions are obtained, while for the intermediate cases in which the two invariants are within a factor 2 of each other, the second integral in eq. (4.11) simply vanishes.

The full double-logarithmic term from the expanded Sudakov terms in eq. (4.5), for strong ordering in dipole virtuality, is then

$$\begin{aligned} & \frac{\alpha_s C_A}{2\pi} \left[\ln \left(\frac{s}{\frac{1}{2}Q_3^2} \right) \ln \left(\frac{s - \frac{1}{2}Q_3^2}{\frac{1}{2}Q_3^2} \right) - \text{Li}_2 \left(\frac{s - \frac{1}{2}Q_3^2}{s} \right) + \text{Li}_2 \left(\frac{\frac{1}{2}Q_3^2}{s} \right) \right. \\ & \left. + \Theta(s_{\max} - Q_3^2) \left(-\ln \left(\frac{s_{\max}}{\frac{1}{2}Q_3^2} \right) \ln \left(\frac{s_{\max} - \frac{1}{2}Q_3^2}{\frac{1}{2}Q_3^2} \right) + \text{Li}_2 \left(\frac{s_{\max} - \frac{1}{2}Q_3^2}{s_{\max}} \right) - \text{Li}_2 \left(\frac{\frac{1}{2}Q_3^2}{s_{\max}} \right) \right) \right] , \end{aligned} \quad (4.13)$$

where the Θ function ensures that the second term is only active if

$$s_{\max} = \max(s_{qg}, s_{g\bar{q}}) > 2 \min(s_{qg}, s_{g\bar{q}}) = Q_3^2 , \quad (4.14)$$

so that the expression applies over all of phase space.

We shall now consider the infrared limits of this result, and compare them to those of the one-loop matrix element. For this comparison we keep only terms that involve logarithms of the invariants. The soft limit corresponds to vanishing Q_3^2 ($\xi_{\min} \rightarrow 0$). The first line of eq. (4.13) represents the contribution of the $2 \rightarrow 3$ expanded Sudakov. To find the contribution in the soft limit, we choose to approach the limit along the diagonal of the phase space triangle. Parametrizing this by $s_{qg}/s = s_{g\bar{q}}/s \rightarrow y$ we find for this term

$$\ln^2(y) - \frac{\pi^2}{6} .$$

The contributions of the $3 \rightarrow 4$ Sudakovs in the soft limit are examined in two separate cases corresponding to the two regions in figure 2.3. In the first case given by $s_{\max} < 2s_{\min}$, corresponding to the light grey area in the figure, the step function in eq. (4.13) yields zero. In the second case given by $s_{\max} > 2s_{\min}$, corresponding to the dark grey area in the figure, the step function is equal to one. The double logs and dilogarithms now yield a finite contribution that does not diverge in the soft limit. We can understand this by parametrizing the soft limit by λ

$$s_{qg} = \lambda s \quad s_{g\bar{q}} = p\lambda s \quad s'_1 = \lambda\kappa s \quad s'_2 = \lambda\mu s \quad p > 2 , \quad (4.15)$$

so that the integral becomes

$$\int_{s_{\min}}^{s_{\max}-s_{\min}} ds_1 \int_{s_{\min}}^{s_{\max}-s_1} ds_2 \frac{1}{s_1 s_2} \rightarrow \int_1^{p-1} d\kappa \int_1^{p-\kappa} d\mu \frac{1}{\kappa\mu} . \quad (4.16)$$

This implies that the integration variable scales with the integration limits and is independent of the soft limit. We can also expect this behaviour from examining figure 2.3. The shape of the different regions does not change for different values of Q_3^2 , in contrast with the case of transverse momentum, as we will see below.

After the poles cancel in eq. (3.55), the pole-subtracted version of the one-loop matrix element, SVirtual , defined in eq. (3.56), contains all the relevant terms on the matrix-element side. The transcendentality-2 terms of SVirtual are given by

$$-R(y_1, y_2) = \text{Li}_2(y_1) + \text{Li}_2(y_2) - \frac{\pi^2}{6} - \ln y_1 \ln y_2 + \ln y_1 \ln(1 - y_1) + \ln y_2 \ln(1 - y_2) . \quad (4.17)$$

Including the transcendentality-1 terms (see appendix B), taking the soft limit by sending $s_{qg}/s = s_{g\bar{q}}/s = y \rightarrow 0$, and keeping only logarithmic terms, the pole-subtracted matrix element (ME) reduces to

$$\text{ME:} \quad s_{qg}/s = s_{g\bar{q}}/s = y \rightarrow 0 \quad \frac{\alpha_s C_A}{2\pi} \left[-\ln^2(y) - \frac{10}{3} \ln(y) \right] + \frac{\alpha_s n_F}{6\pi} \ln(y), \quad (4.18)$$

The single log proportional to C_A originates from the renormalization term and the single log of the closed quark loops (proportional to n_F) arises due to the definition of the infrared singularity operator, defined in the appendix in eq. (A.3).

Taking the same limit of the Sudakov integrals for dipole virtuality eq. (4.5), but omitting for the time being the renormalization term, $V_{3\mu}$, we find for the parton shower (PS),

$$-\text{PS:} \quad s_{qg}/s = s_{g\bar{q}}/s = y \rightarrow 0 \quad \frac{\alpha_s C_A}{2\pi} \left[\ln^2 y + \frac{3}{2} \ln(y) \right] . \quad (4.19)$$

We see that the soft limit almost cancels against eq. (4.18). For an NLL-accurate shower, however, all divergent terms should match precisely, leaving at most a finite remainder in the final matching correction, eq. (3.55). In the expressions above, this holds for the $\ln^2(y)$ term but not for the single logarithms (different coefficient). Interestingly, the remainder is proportional to the QCD β function, specifically

$$\text{ME} - \text{PS} \rightarrow -\frac{\alpha_s}{2\pi} \frac{1}{2} \beta_0 \ln(y) . \quad (4.20)$$

It can therefore be absorbed in the choice of renormalization scale by solving for μ_{PS} in $V_{3\mu}$, which yields:

$$\mu_{\text{PS}}^2 \propto y s . \quad (4.21)$$

This tells us that, in the soft limit, the specific choice of a renormalization scale that is linear in the branching invariants will absorb all logarithms up to and including $\alpha_s^2 \ln(y)$. Interestingly, this reasoning would rule out $\mu_R^2 \propto p_\perp^2$, since our p_\perp -definition is quadratic in the invariants, $p_\perp^2 = s_{ij}s_{jk}/s$. A better choice of renormalization scale would appear to be $\mu_R \propto m_D$, specifically

$$\mu_{\text{PS}}^2 = \min(s_{ij}, s_{jk}) = \frac{1}{2} m_D^2 . \quad (4.22)$$

Taken at face value, this seems to contradict the standard literature [34] on p_\perp as the optimal universal renormalization-scale choice. However, as we shall see below in figure 6, there is in fact no choice of renormalization scale that absorbs *all* logarithms for this particular evolution variable; the choice $\mu_R \propto m_D$ merely manages to reabsorb the additional logarithms that are generated by the ordering condition as $y \rightarrow 0$, but leftover logs in other parts of phase space will remain uncanceled, ruining the NLL precision. In that sense, choosing $\mu_R \propto p_\perp$ would simply leave a different set of uncanceled logs, nonvanishing as $y \rightarrow 0$.

Before we show the results over all of phase space however, we first investigate a complementary interesting limit, the hard-collinear one, which is characterized by one of the invariants becoming maximal while the other vanishes. In this limit, the pole-subtracted one-loop matrix element, SVirtual , becomes

$$\text{ME:} \quad s_{qg}/s \rightarrow 1, s_{g\bar{q}}/s = y \rightarrow 0 \quad \frac{\alpha_s}{2\pi} \left[-\frac{5}{3}C_A + \frac{1}{6}n_F \right] \ln(y) \quad (4.23)$$

There are no log-squared terms in this limit, and both of the single-log terms are half as large here as they were in the soft limit.

The Sudakov integrals for m_D -ordering yield one divergent term, $-\frac{1}{6}C_A \ln(y)$, in the hard-collinear region, modulo a factor $\alpha_s/(2\pi)$. The Sudakov integral for gluon splitting in the neighbouring antenna, represented by the first term on the second-to-last line of eq. (3.55) is specified in the last line of eq. (4.5). The step function is only non-zero for the first term in the hard-collinear limit $s_{qg} \rightarrow s, s_{g\bar{q}} \rightarrow 0$ and produces a term $\frac{1}{6}P_{A_j}n_F \ln(y)$. The numerator of the corresponding Ariadne factor contains the invariant of the neighboring dipole $s_{g\bar{q}}$ which vanishes in this limit and causes the dipole splitting contribution to reduce to zero. The n_F -dependent contribution is instead shifted to the last term of eq. (3.55), which has the same limit but without the Ariadne pre-factor. The hard-collinear limit of the shower terms, including only terms involving logarithms of the invariants and not including the $V_{3\mu}$ term, is therefore

$$\text{-PS:} \quad s_{qg}/s \rightarrow 1, s_{g\bar{q}}/s = y \rightarrow 0 \quad \frac{\alpha_s}{2\pi} \left[-\frac{1}{6}C_A + \frac{1}{6}n_F \right] \ln(y) . \quad (4.24)$$

Again, the combination (ME–PS) relevant for computing the correction factor is proportional to the QCD β function, and in fact has exactly the same form as eq. (4.20). The conclusion is therefore that, also in this limit, all logarithms through $\alpha_s^2 \ln(y)$ can be absorbed by choosing a renormalization scale which is linear in the vanishing invariant. The particular choice which is linear in both the soft and collinear limits is $\mu_{\text{PS}} \propto m_D$. To illustrate this, we show the full NLO $Z \rightarrow 3\text{jets}$ correction factors, $(1 + V_{3Z})$, for m_D -ordering with a few different choices of renormalization scale and scheme, in figure 6. Note that the axes are logarithmic, in $\ln(y_{ij}) = \ln(s_{ij}/s)$, to make the infrared limits clearly visible.

Without the $V_{3\mu}$ term, the correction factor looks as depicted in the top left-hand plot in figure 6. The increasing contours towards the axes indicate uncanceled logarithms in the correction factor. The middle pane shows the correction factor derived for $\mu_{\text{PS}} = p_\perp$. As

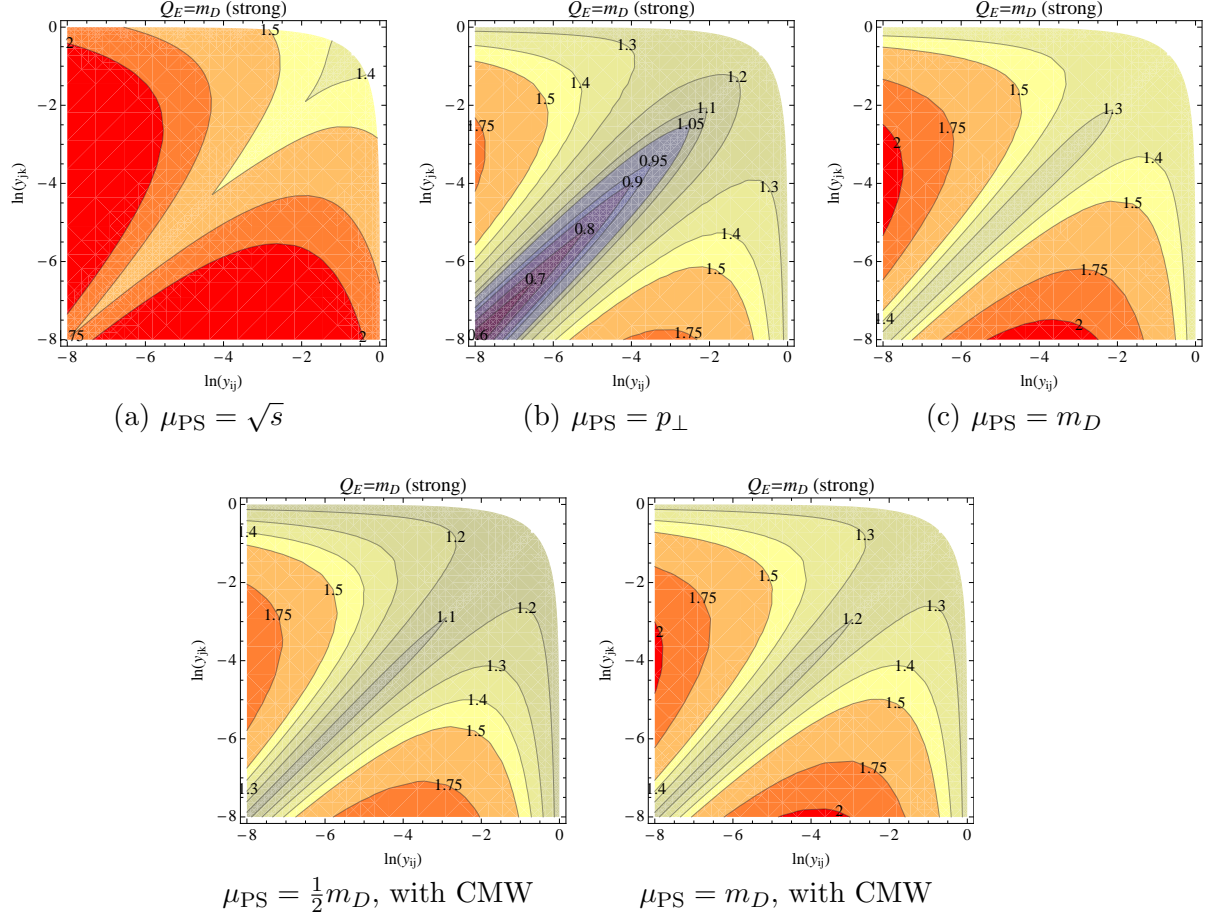


Figure 6. NLO correction factor for strong m_D -ordering, with GGG antennae. *Top row:* $\mu_R = \sqrt{s}$ (left), $\mu_R = p_\perp$ (middle), and $\mu_R = m_D$ (right). *Bottom row:* using the CMW Λ_{MC} , with $\mu_R = \frac{1}{2}m_D$ (left) and $\mu_R = m_D$ (right). For all plots, $\alpha_s = 0.12$, $n_F = 5$, and gluon splittings were evolved in m_{qq} .

discussed above, there is an uncanceled logarithm in the soft limit (lower left-hand corner of the plot), since p_\perp is quadratic in the vanishing invariants there. However, in the hard-collinear limits (upper left-hand and lower right-hand corners), p_\perp is linear in the vanishing invariant, and hence the contours remain bounded there. In the right-hand pane, we show the choice $\mu_{PS} = m_D$, which can be seen to lead to bounded correction factors (below ~ 1.3) in all three phase-space corners. Nonetheless, there is still an uncanceled divergence *between* the soft and hard collinear limits. We shall see in the section on p_\perp -ordering below that the cure for this is basically to choose a better evolution variable.

In the bottom row of figure 6, we show a few variations on $\mu_{PS} = m_D$, specifically we include the CMW rescaling of Λ_{QCD} , as defined by eq. (3.53), and show how a variation of the renormalization scale by a factor of 2 affects the correction factor. In the left-hand pane, we show $\mu_{PS} = \frac{1}{2}m_D$ and in the right-hand one $\mu_{PS} = m_D$. Of these, the choice $\mu_{PS} = \frac{1}{2}m_D$,

with CMW rescaling, leads to the smallest correction factors (best LO behaviour), and this could therefore be taken as a useful default for m_D -ordering, e.g. for uncertainty estimates.

4.1.2 Transverse Momentum

For a shower ordered in p_\perp , the antenna phase-space integrals in eq. (3.32) are performed over contours such as those depicted for p_T squared in figure 1. The curved contours motivate a coordinate transformation from (s_1, s_2) to a basis defined as the dimensionless evolution variable $y = \frac{Q^2}{s} = \frac{4s_1s_2}{s^2}$, complemented by an energy-sharing variable, which we define as $z = \frac{s_1}{s}$. Note that the coordinate transformation depends explicitly on the total invariant mass s of the $2 \rightarrow 3$ dipole. For the $3 \rightarrow 4$ integrations, the invariant mass s is replaced by the invariant mass of the appropriate dipole (either s_{qg} or $s_{g\bar{q}}$). The integration boundaries in z are determined by the intersection of the invariant mass of the dipole with the evolution parameter Q^2 . The choice of y and its integration boundaries make the effect of strong ordering especially clear since we see integration from Q^2 to the total invariant mass of the dipole (the unordered region). As before, the integration over the gluon-splitting antenna (e_3^0) makes use of a different phase space integration, in $m_{q\bar{q}}$, and only uses the evolution parameter as a cut-off in the singularity of the corresponding dipole.

The contributing terms are:

$$\begin{aligned}
& g_s^2 \left[C_A \int_{Q_3^2}^s d_3^0 d\Phi_{\text{ant}} - \sum_{j=1}^2 C_A \int_0^{s_j} (1 - O_{E_j}) d_3^0 d\Phi_{\text{ant}} - \sum_{j=1}^2 2T_R n_F P_{A_j} \int_0^{s_j} (1 - O_{S_j}) e_3^0 d\Phi_{\text{ant}} \right] \\
&= \frac{\alpha_s}{4\pi} \left[C_A s \mathcal{A}_1 \left[\frac{Q_3^2}{s}, 1 \right] - C_A s_{qg} \mathcal{A}_2 \left[\frac{4s_{g\bar{q}}}{s}, \max \left(\frac{4s_{g\bar{q}}}{s}, 1 \right) \right] - s_{g\bar{q}} C_A \mathcal{A}_3 \left[\frac{4s_{qg}}{s}, \max \left(\frac{4s_{qg}}{s}, 1 \right) \right] \right. \\
&\quad \left. - n_F \left(\frac{P_{A_1}}{s_{qg}} \int_{Q_3^2}^{\max(Q_3^2, s_{qg})} ds_1 \int_0^{s_{qg}-s_1} ds_2 + \frac{P_{A_2}}{s_{g\bar{q}}} \int_{Q_3^2}^{\max(Q_3^2, s_{g\bar{q}})} ds_1 \int_0^{s_{g\bar{q}}-s_1} ds_2 \right) e_3^0(s_1, s_2) \right] \quad (4.25)
\end{aligned}$$

with

$$\mathcal{A}_n[a, b] = \int_a^b dy_n \int_{z_{\min}^n}^{z_{\max}^n} dz_n |\mathcal{J}_n| A_n(y_n, z_n) \quad \text{for } n = 1, 2, 3, \quad (4.26)$$

and

$$y_n = 4 \frac{s_1 s_2}{m_{IK}^4}, \quad z_n = \frac{s_1}{m_{IK}^2}, \quad |\mathcal{J}_1| = \frac{m_{IK}^4}{4z_n}, \quad z_{\min}^n = \frac{1}{2} \left(1 \pm \sqrt{1 - y_n} \right). \quad (4.27)$$

For $n = 1$ we set $m_{IK}^2 = s$, for $n = 2$ $m_{IK}^2 = s_{qg}$ and for $n = 3$ $m_{IK}^2 = s_{g\bar{q}}$. The Ariadne factor P_{A_j} is defined in eq. (2.20). The max condition on the outer integration boundary of \mathcal{A}_2 and \mathcal{A}_3 reflect that the correction term disappears if the generated Q_3^2 is larger than the invariant mass of the dipole. As for m_D -ordering, we here work out the most divergent behavior explicitly, by focussing on the double log terms arising from the eikonal term in the

antenna, and relegate the full form of the antenna integrals to appendix C. The double poles give rise to terms

$$\frac{\alpha_s C_A}{2\pi} \int_{\frac{Q_3^2}{s}}^1 dy_1 \int_{z_{\min}}^{z_{\max}} dz_1 \frac{1}{y_1 z_1} ,$$

which lead to the following generic transcendentality-2 integrals,

$$\begin{aligned} \int_x^1 \frac{dy_1}{y_1} \ln \left(\frac{1 + \sqrt{1 - y_1}}{1 - \sqrt{1 - y_1}} \right) &= \text{Li}_2 \left(\frac{1}{2} (1 - \sqrt{1 - x}) \right) - \text{Li}_2 \left(\frac{1}{2} (1 + \sqrt{1 - x}) \right) \\ &+ \frac{1}{2} \ln \left(\frac{x}{4} \right) \ln \left[- \left(\frac{-2 + 2\sqrt{1 - x} + x}{x} \right) \right] . \end{aligned} \quad (4.28)$$

The double logarithm in the shower expansion is generated by a combination of the $2 \rightarrow 3$ and $3 \rightarrow 4$ Sudakov integrals, with the respective pieces adding up to

$$\frac{\alpha_s C_A}{2\pi} \left[-\frac{\pi^2}{6} + \frac{1}{2} \ln \left(\frac{s_{qg} s_{g\bar{q}}}{s^2} \right)^2 + \frac{\pi^2}{3} - \frac{1}{2} \ln \left(\frac{s_{qg}}{s} \right)^2 - \frac{1}{2} \ln \left(\frac{s_{g\bar{q}}}{s} \right)^2 \right] . \quad (4.29)$$

We see that a partial cancellation arises between the first two terms (which come from the $2 \rightarrow 3$ Sudakov expansion) and the last three (which come from the $3 \rightarrow 4$ expansion). What remains is a log squared in both invariants $\ln(s_{qg}/s) \ln(s_{g\bar{q}}/s)$.

At the single-log level, the $3 \rightarrow 4$ terms give a numerically larger coefficient than the $2 \rightarrow 3$ ones, leading to a single log remainder. The gluon-splitting term also reduces to a single log. The overall result in the soft limit is then

$$-\text{PS:} \quad s_{qg} = s_{g\bar{q}} = y \rightarrow 0 \quad \frac{\alpha_s C_A}{2\pi} \left[\ln^2(y) - \frac{1}{3} \ln(y) \right] + \frac{\alpha_s n_F}{6\pi} \ln(y) \quad (4.30)$$

Comparing with the result of the virtual correction in the soft limit, eq. (4.18), we see that the shower generates the double log terms correctly, and, similarly to the case of m_D -ordering, there is a single-log remainder which is proportional to the QCD β function. However, for p_\perp -ordering the constant of proportionality is 1, rather than $\frac{1}{2}$, a difference which translates to the optimal renormalization-scale choice being quadratic in the invariants in this case, rather than linear. Before commenting further on this difference, let us first consider the complementary, hard-collinear, limit.

In the hard-collinear limit, we find the same as for m_D -ordering,

$$-\text{PS:} \quad s_{qg} = y \rightarrow 0, s_{g\bar{q}} \rightarrow s \quad \frac{\alpha_s}{2\pi} \left[-\frac{1}{6} C_A + \frac{1}{6} n_F \right] \ln(y) . \quad (4.31)$$

Double logs (eikonal parts of the antenna) also appear at both the $2 \rightarrow 3$ and $3 \rightarrow 4$ levels, but cancel among each other as almost all other antenna terms do; what remains at the single-log level is the integrated difference between a quark-antiquark antenna and a quark-gluon antenna, plus the n_F -dependent ‘Ariadne Log’. The only contributing Sudakov gluon

splitting contribution is the second term in the last line of eq. (4.25). Integration over the $s_{g\bar{q}}$ dipole, however, is associated with an Ariadne factor carrying s_{qg} in the numerator and therefore reduces to zero. As before, we can write the remainder as half the QCD β function, which implies that a renormalization scale linear in the vanishing invariants can absorb the logarithm.

To summarize, for p_\perp -ordering we find that the optimal renormalization-scale choice must be quadratic in the vanishing invariants in the soft limit and linear in the hard-collinear limit. Those conditions are fulfilled by p_\perp itself, thus

$$\mu_{\text{PS}}^2 \propto p_\perp^2 = \frac{s_{ij}s_{jk}}{s_{ijk}} \quad (4.32)$$

absorbs all logarithmic terms up to and including $\alpha_s^2 \ln(y)$ in the LO couplings.

Illustrations of the full NLO correction factors, $(1 + V_{3Z})$, are given in figure 7. The ordering of the plots in the top row are the same as in figure 7, showing, from left to right, $\mu_{\text{PS}} = \sqrt{s}$, $\mu_{\text{PS}} = p_\perp$, $\mu_{\text{PS}} = m_D$. Similarly to the case of strong m_D -ordering, both of the latter two choices exhibit no logarithmic divergences in the hard-collinear regions (top left and bottom right corners of the plots), but in the soft region (bottom left corner) it is here $\mu_{\text{PS}} = p_\perp$ which leaves the correction factor free of logarithms. Indeed, we see that the combination of evolution and renormalization in p_\perp leads to a rather flat correction factor over all of phase space, showing that this combination is indeed “better” than m_D -ordering.

In the bottom row of plots in figure 7, we include the CMW factor and show the correction factors for $\mu_{\text{PS}} = p_\perp$ (left) and $\mu_{\text{PS}} = 2p_\perp$ (right). In particular on the left-hand pane, the NLO correction factor is essentially unity in the soft limit, while the corrections in the hard-collinear regions remain less than $\sim 20\%$. This gives some additional weight to the arguments for p_\perp -ordered showers with p_\perp as renormalization scale being the best default choice for strongly ordered dipole-antenna showers. It also provides some rationale why one typically finds a rather large value of $\alpha_s(m_Z) \sim 0.13$ (with CMW rescaling, or $\alpha_s(m_Z) \sim 0.14$ without it) when tuning such models to LEP event shapes; there is still a genuine order 20% NLO correction in the hard resolved region (upper right-hand corner). We return to this in more detail in the context of full LO + NLO matching in section 5.

4.1.3 Energy

To put the differences between m_D and p_\perp in context, we now briefly examine the case of energy ordering, which is known to produce the wrong DGLAP evolution in the collinear limit [27, 28, 62], and hence we should find larger (possibly divergent) NLO corrections.

Slicing phase space with the energy variable $Q_3^2 = s_{ijk}(y_{ij} + y_{jk})^2$, see figure 1, requires the use of an explicit infrared cut-off because the contours otherwise allow for the invariants to hit singular regions for every value of the contour. We will here use a cut-off in transverse momentum (a cut-off in dipole virtuality is also possible). The cutoff motivates us to switch to a different choice of integration variables. Therefore integration is transformed from (s_1, s_2) to the dimensionless evolution parameters $y_E^2 = \frac{Q^2}{s} = \frac{(s_1+s_2)^2}{m_{iK}^2}$ and completed with the energy

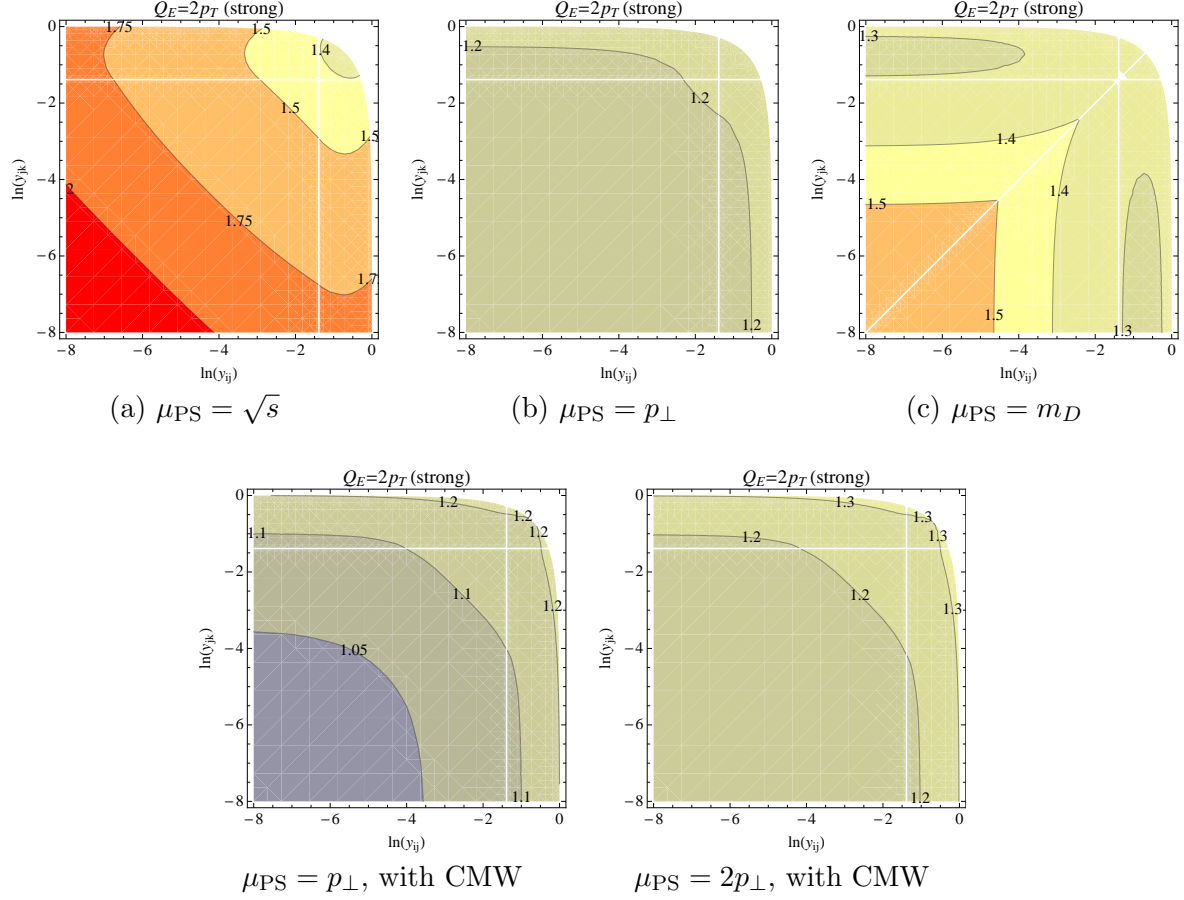


Figure 7. NLO correction factor for strong p_\perp -ordering, with GGG antennae. *Top row:* $\mu_{\text{PS}} = \sqrt{s}$ (left), $\mu_{\text{PS}} = p_\perp$ (middle), and $\mu_{\text{PS}} = m_D$ (right). *Bottom row:* using the CMW Λ_{MC} , with $\mu_{\text{PS}} = p_\perp$ (left) and $\mu_{\text{PS}} = 2p_\perp$ (right). For all plots, $\alpha_s = 0.12$, $n_F = 5$, and gluon splittings were evolved in $m_{q\bar{q}}$.

sharing variable $\zeta = \frac{s_2^2}{m_{IK}^2}$. The interesting integrals arising from expanding the Sudakov form factor then are

$$\begin{aligned}
& g_s^2 \left[C_A \int_{Q_3^2}^s d_3^0 d\Phi_{\text{ant}} - \sum_{j=1}^2 C_A \int_0^{s_j} (1 - O_{E_j}) d_3^0 d\Phi_{\text{ant}} - \sum_{j=1}^2 2T_R n_F P_{A_j} \int_0^{s_j} (1 - O_{S_j}) e_3^0 d\Phi_{\text{ant}} \right] \\
& = \frac{\alpha_s}{4\pi} \left[C_A \{ \mathcal{AE}_1(s, 1) - \mathcal{AE}_2(\min[s_{q\bar{q}}, 1], 1) - \mathcal{AE}_3(\min[s_{g\bar{q}}, 1], 1) \} \right. \\
& \quad \left. - n_F \left(\frac{P_{A_{q\bar{q}}}}{s_{q\bar{q}}} \int_{Q_3^2}^{\max(Q_3^2, s_{q\bar{q}})} ds_1 \int_0^{s_{q\bar{q}} - s_1} ds_2 + \frac{P_{A_{g\bar{q}}}}{s_{g\bar{q}}} \int_{Q_3^2}^{\max(Q_3^2, s_{g\bar{q}})} ds_1 \int_0^{s_{g\bar{q}} - s_1} ds_2 \right) e_3^0(s_1, s_2) \right] \\
& \quad (4.33)
\end{aligned}$$

with

$$\mathcal{AE}_n(m_{IK}^2, 1) = \int_{\frac{Q_3^2}{m_{IK}^2}}^1 dy_E^2 \int_0^1 d\zeta' \frac{1}{2} \mathcal{AE}_n^0(y_E^2, \zeta').$$

With $\mathcal{AE}_1^0 = a_3^0$, $\mathcal{AE}_2^0 = d_3^0$ and $\mathcal{AE}_3^0 = e_3^0$. The inner integral has been rescaled to make it independent of the outer integral with $\zeta = y_E \zeta'$. To establish the cut-off, we use the relation $4\frac{s_1 s_2}{s^2} = 4p_\perp^2/s$, which we demand to be larger than the cut-off Δ . In terms of our variables we then have the condition

$$4\zeta'(1 - \zeta') > \frac{\Delta}{y_E^2}. \quad (4.34)$$

The upper and lower limits on ζ' are then

$$\zeta'_- < \zeta' < \zeta'_+, \quad \zeta'_\pm = \frac{1}{2} \left(1 \pm \sqrt{1 - \frac{\Delta}{y_E^2}} \right). \quad (4.35)$$

Focussing on the eikonal integral

$$\frac{\alpha_s C_A}{4\pi} \int_{y_E^2 = \frac{Q_3^2}{s}}^1 \frac{dy_E^2}{y_E^2} \int_{\zeta'_-}^{\zeta'_+} \frac{d\zeta'}{\zeta'}, \quad (4.36)$$

the result for this integral is

$$\begin{aligned} & \frac{\alpha_s}{2\pi} \left[\text{Li}_2 \left(\frac{1}{2} \left(1 - \sqrt{1 - \Delta} \right) \right) - \text{Li}_2 \left(\frac{1}{2} \left(1 + \sqrt{1 - \Delta} \right) \right) + \frac{1}{2} \left[-2 \operatorname{atanh} \left(\sqrt{1 - \frac{\Delta}{y_E^2}} \right) \ln(4) \right. \right. \\ & + \operatorname{atanh} \left(\sqrt{1 - \Delta} \right) \ln(16) + \ln^2 \left(1 - \sqrt{1 - \Delta} \right) - \ln^2 \left(1 + \sqrt{1 - \Delta} \right) - \ln^2 \left(1 - \sqrt{1 - \frac{\Delta}{y_E^2}} \right) \\ & \left. \left. + \ln^2 \left(1 + \sqrt{1 - \frac{\Delta}{y_E^2}} \right) \right] - 2\text{Li}_2 \left(\frac{1}{2} \left(1 - \sqrt{1 - \frac{\Delta}{y_E^2}} \right) \right) + \text{Li}_2 \left(\frac{1}{2} \left(1 + \sqrt{1 - \frac{\Delta}{y_E^2}} \right) \right) \right] . \end{aligned} \quad (4.37)$$

In the soft limit $y_E^2 = 4y^2 \rightarrow 0$ this reduces to

$$-\frac{1}{2} \ln^2(\Delta) - \ln^2 \left(\frac{\Delta}{4y^2} \right) - 2 \ln(4y^4) \ln(2) - \text{Li}_2 \left(\frac{\Delta}{64y^2} \right) \quad (4.38)$$

Thus we see that there are explicit non-cancelling double-logarithmic terms that involve the hadronization cutoff, Δ . Depending on the ratio between the dipole mass and the cutoff, these would lead to asymptotically divergent correction factors.

One might wonder whether using a linearized form of energy ordering would make a difference, see figure 1. Rather than go through the derivations again, we merely show the full NLO corrections in figure 8, for both linear (top row) and squared (bottom row) energy ordering, for an (arbitrary) dimensionless cutoff value of $\Delta = 10^{-7}$.

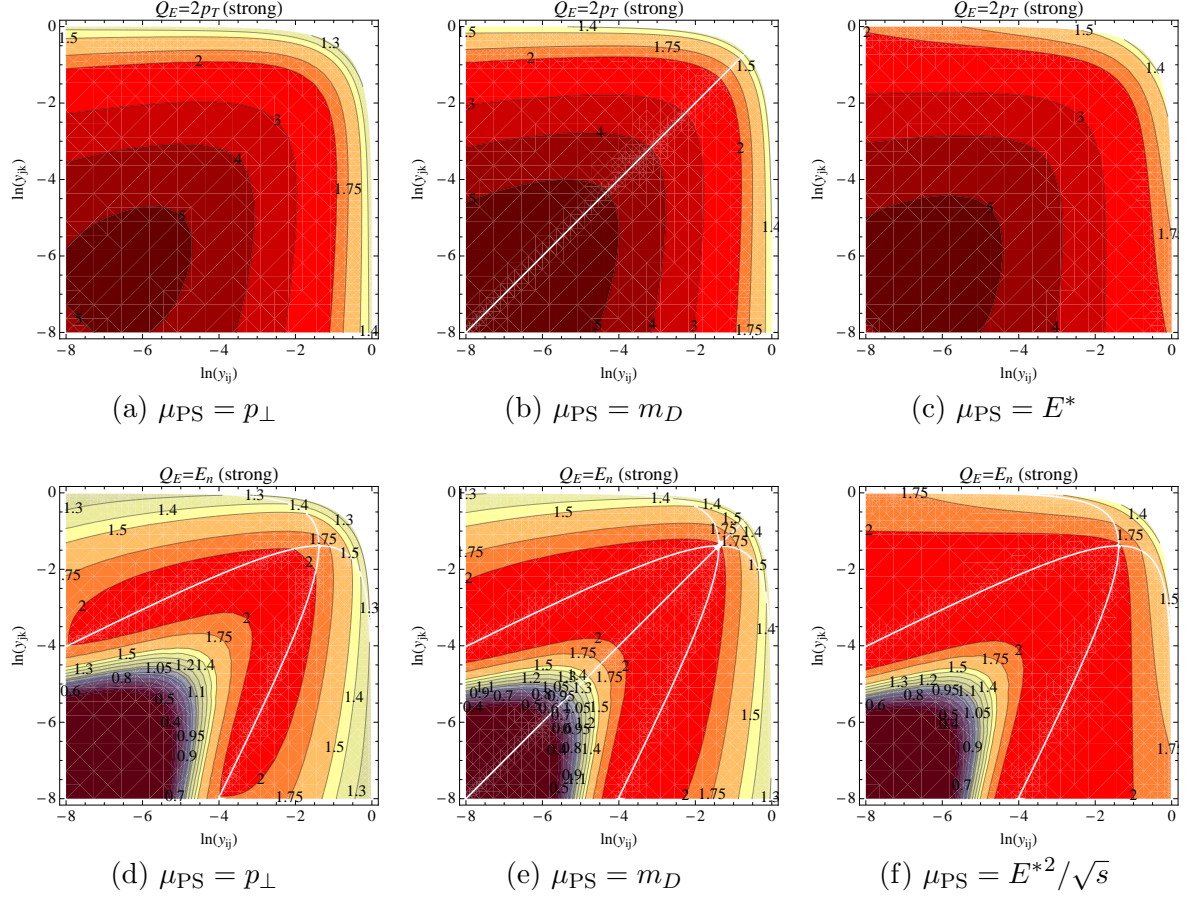


Figure 8. NLO correction factor for strong energy-ordering, with GGG antennae, for various renormalization-scale choices and linear (top row) and squared (bottom row) scaling of the evolution variable with gluon energy.

From left to right in both rows, we show the three renormalization-scale choices, $\mu_{\text{PS}} = p_{\perp}$ (left), $\mu_{\text{PS}} = m_D$ (middle), and $\mu_{\text{PS}} = Q_E$ (right), with the latter equal to linear energy in the top row and squared energy in the bottom one. Interestingly, the contours in the linear case are increasing towards the soft region, while they ultimately decrease in the squared case. It is clear, however, that no intelligent choice of renormalization scale can absorb the infrared divergences. Moreover, any other choice of Δ would have led to different contours, due to the explicit $\ln(\Delta)$ terms, hence even if a “least bad” choice was found, it would not be universal.

As mentioned above, the main point of showing these comparisons is to place the comparison between m_D and p_{\perp} in the previous subsections in perspective. Thus, while we saw that p_{\perp} was generating a better-behaved correction factor than m_D , the one for m_D is still far better behaved than is the case for energy ordering. From this perspective, we still believe it could make sense, e.g., to use m_D -ordering, with the NLO correction factor included, as a conservative uncertainty variation for a central prediction based on p_{\perp} -ordering.

4.2 Smooth Ordering

We will now discuss the same Sudakov integrals as in the previous subsections but for the case of smooth ordering (section 2.4). This is especially interesting given that smooth ordering is the way VINCIA is able to fill all of phase space without significant under- or overcounting at the LO level [24]. As discussed in section 2.4, however, this does involve some ambiguity in what Sudakov factors are associated with the unordered points, and the NLO 3-jet correction factors should tell us explicitly whether this ambiguity generates problems at this level.

The Sudakov integrations are actually more straightforward for smooth ordering than was the case for strong ordering, since the P_{imp} factor regulates the integrands on the boundaries. Therefore the integrations always run over the full phase space of the system. The $2 \rightarrow 3$ splitting generates the same terms as in the strong-ordering case, eq. (4.2). Including also the $3 \rightarrow 4$ terms, the expanded Sudakov generates the following antenna integrals,

$$g_s^2 \left[C_A \int_0^s a_3^0 d\Phi_{\text{ant}} - \sum_{j=1}^2 C_A \int_0^{s_j} \frac{Q_{E_j}^2}{Q_{E_j}^2 + Q_3^2} d_3^0 d\Phi_{\text{ant}} - \sum_{j=1}^2 2T_R n_F P_{A_j} \int_0^{s_j} \frac{m_{q\bar{q}}^2}{m_{q\bar{q}}^2 + Q_3^2} e_3^0 d\Phi_{\text{ant}} \right], \quad (4.39)$$

where Q_3 is the evolution scale evaluated on the 3-parton configuration and Q_{E_j} ($m_{q\bar{q}}$) is the scale of the $3 \rightarrow 4$ emissions (splittings) being integrated over. The full answer for the $3 \rightarrow 4$ case for gluon emission is

$$-g_s^2 \sum_{j=1}^2 C_A \int_0^{s_j} \frac{Q_{E_j}^2}{Q_{E_j}^2 + Q_3^2} d_3^0 d\Phi_{\text{ant}} = -\frac{\alpha_s C_A}{4\pi} \left(\sum_{i=1}^5 K_i L_i(s_{qg}, Q_3^2) \right) - \frac{\alpha_s C_A}{4\pi} \left(\sum_{i=1}^5 K_i L_i(s_{g\bar{q}}, Q_3^2) \right). \quad (4.40)$$

where K_i and L_i can be found in appendix C. The full answer for the $3 \rightarrow 4$ case for gluon splitting is

$$-g_s^2 \sum_{j=1}^2 n_F P_{A_j} \int_0^{s_j} \frac{m_{q\bar{q}}^2}{m_{q\bar{q}}^2 + Q_3^2} e_3^0 d\Phi_{\text{ant}} = -\frac{\alpha_s n_F}{4\pi} G(s_{qg}, Q_3^2) - \frac{\alpha_s n_F}{4\pi} G(s_{g\bar{q}}, Q_3^2). \quad (4.41)$$

where G can be found in the appendix. We will discuss the derivation of these terms in more detail in the following two subsections, for smooth m_D - and p_\perp -ordering, respectively.

4.2.1 Dipole virtuality

Since the $2 \rightarrow 3$ emission terms remain the same as in the case of strong m_D -ordering, we only need to rederive the $3 \rightarrow 4$ contributions to V_{3Z} , which are

$$\begin{aligned}
& -g_s^2 \left[\sum_{j=1}^2 C_A \int_0^{s_j} \left(1 - \frac{Q_3^2}{Q_{Ej}^2 + Q_3^2} \right) d_3^0 d\Phi_{\text{ant}} + \sum_{j=1}^2 2T_R n_F P_{A_j} \int_0^{s_j} \left(1 - \frac{Q_3^2}{m_{q\bar{q}}^2 + Q_3^2} \right) e_3^0 d\Phi_{\text{ant}} \right] \\
& = -\frac{\alpha_s}{4\pi} \left[\frac{C_A}{s_{qg}} \left(\int_0^{\frac{1}{2}s_{qg}} ds_2 \int_{s_2}^{s_{qg}-s_2} ds_1 \frac{2s_2}{Q_3^2 + 2s_2} + \int_0^{\frac{1}{2}s_{qg}} ds_1 \int_{s_1}^{s_{qg}-s_1} ds_2 \frac{2s_1}{Q_3^2 + 2s_1} \right) d_3^0 \right. \\
& \quad + \frac{C_A}{s_{g\bar{q}}} \left(\int_0^{\frac{1}{2}s_{g\bar{q}}} ds_2 \int_{s_2}^{s_{g\bar{q}}-s_2} ds_1 \frac{2s_2}{Q_3^2 + 2s_2} + \int_0^{\frac{1}{2}s_{g\bar{q}}} ds_1 \int_{s_1}^{s_{g\bar{q}}-s_1} ds_2 \frac{2s_1}{Q_3^2 + 2s_1} \right) d_3^0 \\
& \quad \left. + 2n_F \left(\frac{P_{A_1}}{s_{qg}} \int_0^{s_{qg}} ds_2 \int_0^{s_{qg}-s_2} ds_1 + \frac{P_{A_2}}{s_{g\bar{q}}} \int_0^{s_{g\bar{q}}} ds_2 \int_0^{s_{g\bar{q}}-s_2} ds_1 \right) \frac{s_1}{s_1 + Q_3^2} e_3^0 \right] \quad (4.42)
\end{aligned}$$

with $Q_3^2 = 2 \min(s_{qg}, s_{g\bar{q}})$ and e_3^0 carrying the singularity in s_1 . We will focus again on deriving the transcendentality-2 terms explicitly, with the full expressions given in the appendix. We start by recalling the expression for the strongly-ordered $2 \rightarrow 3$ branching,

$$\frac{\alpha_s C_A}{2\pi} \left[\ln \left(\frac{s}{\frac{1}{2}Q_3^2} \right) \ln \left(\frac{s - \frac{1}{2}Q_3^2}{\frac{1}{2}Q_3^2} \right) - \text{Li}_2 \left(\frac{s - \frac{1}{2}Q_3^2}{s} \right) + \text{Li}_2 \left(\frac{\frac{1}{2}Q_3^2}{s} \right) \right].$$

To this we add the results from the eikonal term $\frac{2s_{qg}}{s_1 s_2}$ of one $3 \rightarrow 4$ gluon emission, the first line in eq. (4.42),

$$\begin{aligned}
& -\frac{2\alpha_s C_A}{\pi} \int_0^{\frac{1}{2}} dy_2 \int_{y_2}^{1-y_2} dy_1 \frac{1}{y_1(y_3^2 + 2y_2)} \\
& = -\frac{\alpha_s C_A}{2\pi} \left[-\ln(4) \ln \left(1 - \frac{1}{1+y_3^2} \right) + \ln(4) \ln \left(1 + \frac{1}{1+y_3^2} \right) - 2\text{Li}_2 \left(-\frac{1}{y_3^2} \right) + 2\text{Li}_2 \left(\frac{1}{2+y_3^2} \right) \right. \\
& \quad \left. - 2\text{Li}_2 \left(\frac{2}{2+y_3^2} \right) \right] \quad (4.43)
\end{aligned}$$

where we have transformed $y_i = \frac{s_i}{s_{qg}}$ for $i = 1, 2$ and $y_3^2 = \frac{Q_3^2}{s_{qg}} = 2 \min(1, \frac{s_{g\bar{q}}}{s_{qg}})$. Taking the limit for the soft region $y_3^2 \rightarrow 2$ (since we take the invariants as vanishing simultaneously), we see that the remainder is just a finite term that contains no logarithms of the vanishing invariants,

$$\frac{\alpha_s C_A}{8\pi} \left[2\ln^2(2) + \text{Li}_2 \left(\frac{1}{4} \right) \right]. \quad (4.44)$$

We will receive this contribution twice. Including all divergent logarithmic contributions and disregarding constant terms such as in eq. (4.44), we find the same as in the strong-ordering case,

$$- \text{PS:} \quad s_{qg} = s_{g\bar{q}} = y \rightarrow 0 \quad \frac{\alpha_s C_A}{2\pi} \left[\ln^2(y) + \frac{3}{2} \ln(y) \right], \quad (4.45)$$

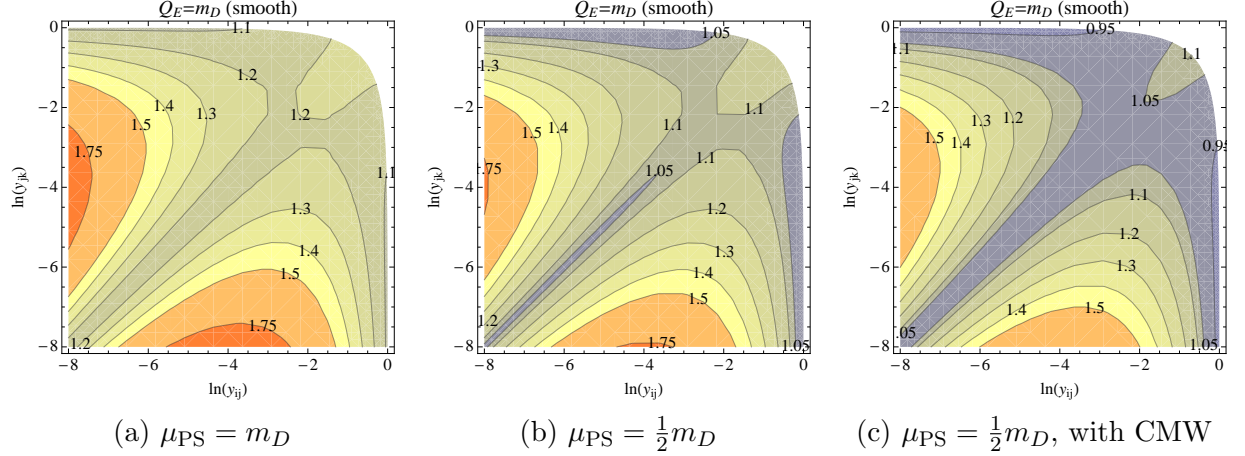


Figure 9. NLO correction factor for smooth m_D -ordering, with GGG antennae, and $\mu_{\text{PS}} = m_D$ (left), $\mu_{\text{PS}} = \frac{1}{2}m_D$ (middle), and $\mu_{\text{PS}} = \frac{1}{2}m_D$ with CMW rescaling (right). For all plots, $\alpha_s = 0.12$, $n_F = 5$, and the evolution scale for gluon splittings was $m_{q\bar{q}}$.

and hence the preferred choice of scale in the soft limit remains one which is linear in the vanishing invariants, such as $\mu_{\text{PS}} \propto m_D$.

In the hard collinear limit the Sudakov integrals plus the ‘Ariadne Log’ reduce to

$$- \text{PS:} \quad s_{qg} = y \rightarrow 0, s_{g\bar{q}} \rightarrow s \quad \frac{\alpha_s C_A}{2\pi} \left[-\frac{1}{6}C_A + \frac{1}{6}n_F \right] \ln(y) , \quad (4.46)$$

again the same as in the strongly ordered case, cf. eq. (4.24).

To summarize, we do not expect any qualitatively different limiting behaviour in the smoothly ordered case with respect to the strongly ordered one, though details may of course still vary. To illustrate this, we include the plots in figure 9. In all cases, we use a renormalization scale $\propto m_D$, but with different prefactors, from left to right: $\mu_{\text{PS}} = m_D$, $\mu_{\text{PS}} = m_D/2$, and finally $\mu_{\text{PS}} = m_D/2$ with CMW rescaling. In particular the latter gives correction factors very close to unity in both the soft and hard collinear limits, while we still see the leftover divergence inbetween those limits that was also present in the case of strong m_D -ordering, cf. figure 6. Nonetheless, it is worth noting that for a large region of phase space, say with $m_{ij} > 0.1 m$ (corresponding to $\ln(y_{ij}) > -4.6$), the corrections are still quite well behaved and relatively small, less than $\sim 20\%$.

4.2.2 Transverse momentum

Again we only need to recompute the contributions from the $3 \rightarrow 4$ Sudakov terms, as the $2 \rightarrow 3$ ones are the same as in the strongly ordered case. The $3 \rightarrow 4$ Sudakov integrals are

$$\begin{aligned}
& -g_s^2 \left[\sum_{j=1}^2 C_A \int_0^{s_j} \left(1 - \frac{Q_3^2}{Q_{Ej}^2 + Q_3^2} \right) d_3^0 d\Phi_{\text{ant}} + \sum_{j=1}^2 2T_R n_F P_{A_j} \int_0^{s_j} \left(1 - \frac{Q_3^2}{m_{q\bar{q}}^2 + Q_3^2} \right) e_3^0 d\Phi_{\text{ant}} \right] \\
& = -\frac{\alpha_s}{4\pi} \left[\left(\frac{C_A}{s_{qg}} \int_0^{s_{qg}} ds_2 \int_0^{s_{qg}-s_2} ds_1 \frac{4s_1 s_2}{Q_3^2 s_{qg} + 4s_1 s_2} + \frac{C_A}{s_{g\bar{q}}} \int_0^{s_{g\bar{q}}} ds_2 \int_0^{s_{g\bar{q}}-s_2} ds_1 \frac{4s_1 s_2}{Q_3^2 s_{g\bar{q}} + 4s_1 s_2} \right) d_3^0 \right. \\
& \quad \left. + 2n_F \left(\frac{P_{A_1}}{s_{qg}} \int_0^{s_{qg}} ds_2 \int_0^{s_{qg}-s_2} ds_1 + \frac{P_{A_2}}{s_{g\bar{q}}} \int_0^{s_{g\bar{q}}} ds_2 \int_0^{s_{g\bar{q}}-s_2} ds_1 \right) \frac{s_1}{s_1 + Q_3^2} e_3^0 \right] \quad (4.47)
\end{aligned}$$

As before we focus on explicitly calculating the transcendentality-2 contribution arising from the eikonal part of the antenna in the first term in the first line of eq. (4.47),

$$\begin{aligned}
& -\frac{\alpha_s C_A}{2\pi} \int_0^1 dy_2 \int_0^{1-y_2} dy_1 \frac{4y_1 y_2}{y_3^2 + 4y_1 y_2} \frac{1}{y_1 y_2} \\
& = -\frac{\alpha_s C_A}{2\pi} \left[-\text{Li}_2 \left(-\frac{2}{-1 + \sqrt{1 + y_3^2}} \right) - \text{Li}_2 \left(\frac{2}{1 + \sqrt{1 + y_3^2}} \right) \right] \quad (4.48)
\end{aligned}$$

where we have transformed $y_i = \frac{s_i}{s_{qg}}$ and $y_3^2 = \frac{Q_3^2}{s_{qg}}$. In the limit $s_{\min}/s, s_{\max}/s = y \rightarrow 0$ so that $y_3^2 \rightarrow 0$, this yields

$$\frac{\alpha_s C_A}{2\pi} \left[-\frac{1}{2} \ln^2(y) \right]. \quad (4.49)$$

Adding the contributions from the $2 \rightarrow 3$ splitting and transcendentality-1 terms, we find the following result for the soft limit

$$-\text{PS:} \quad s_{qg} = s_{g\bar{q}} = y \rightarrow 0 \quad \frac{\alpha_s C_A}{2\pi} \left[\ln^2(y) - \frac{1}{3} \ln(y) \right] + \frac{\alpha_s}{6\pi} n_F \ln(y), \quad (4.50)$$

as in the strongly ordered case. The double logarithm matches with SVirtual and the single logarithm can be absorbed by choosing a renormalization scale that is quadratic in the vanishing invariants, such as $\mu_{\text{PS}} \propto p_{\perp}$.

In the hard collinear limit, the shower integrals behave as

$$-\text{PS:} \quad s_{qg} = y \rightarrow 0, s_{g\bar{q}} \rightarrow s \quad \frac{\alpha_s}{2\pi} \left[-\frac{1}{6} C_A + \frac{1}{6} n_F \right] \ln(y), \quad (4.51)$$

the same as in all the other cases. This completes the argument that indeed $\mu_{\text{PS}} \propto p_{\perp}$ is the appropriate choice also for smooth p_{\perp} -ordering.

In figure 10, we show the NLO correction factors, $(1 + V_{3Z})$, for smooth p_{\perp} -ordering. The top row shows the correction factors without using the CMW rescaling of Λ_{QCD} , and the

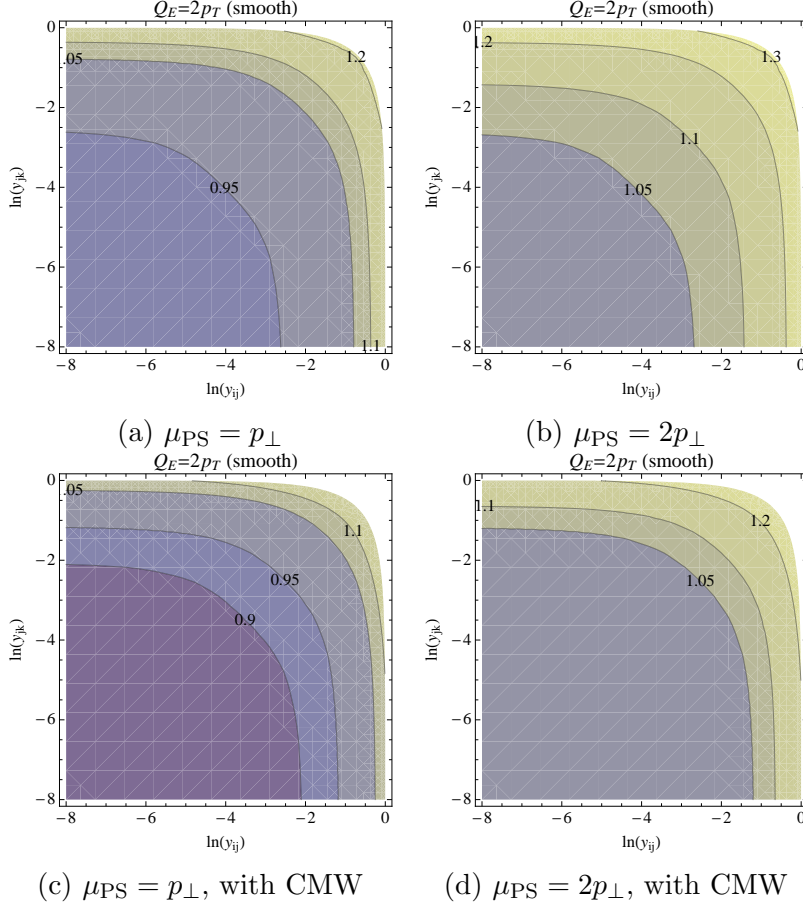


Figure 10. NLO correction factor for smooth p_\perp -ordering, with GGG antennae, without (top row) and with (bottom row) the CMW rescaling of Λ_{QCD} . The left-hand panes use $\mu_{\text{PS}} = p_\perp$ and the right-hand ones $\mu_{\text{PS}} = 2p_\perp$. For all plots, $\alpha_s = 0.12$, $n_F = 5$, and the evolution scale for gluon splittings was m_{qq} .

plots in the bottom row include it. For the left-hand panes, we used a shower renormalization scale of $\mu_{\text{PS}} = p_\perp$, and for the right-hand ones we used $\mu_{\text{PS}} = 2p_\perp$.

We see that all correction factors are essentially well-behaved, with no runaway logs, similarly to the case of strong p_\perp -ordering. However, for the case of smooth p_\perp -ordering, it looks as if the CMW rescaling (bottom row) is almost doing “too much” in the soft region. Given that the CMW arguments [35] were derived explicitly by considering the subleading behaviour of strongly ordered (coherent) parton showers, we do not perceive of this as any major drawback. Instead, one should merely be aware of the slight shifts in the NLO corrections that result from applying it or not, recalling that a rescaling of Λ by the CMW factor ~ 1.5 is within the ordinary factor 2 variation of the renormalization scale that is often taken as a standard for uncertainty estimates.

The shifts caused by CMW rescaling and/or by renormalization-scale prefactors are of

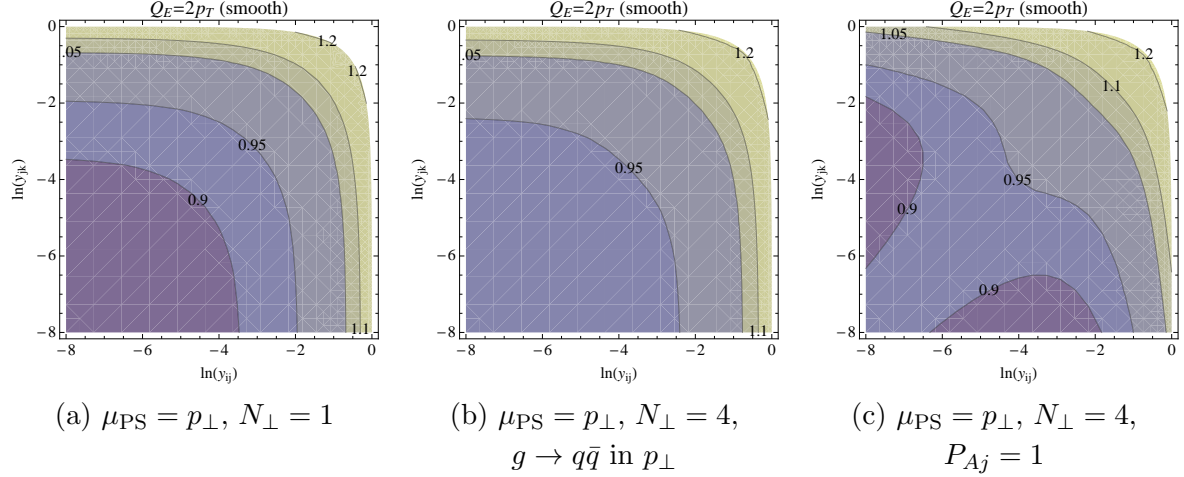


Figure 11. NLO correction factor for smooth p_{\perp} -ordering, with GGG antennae: variations of how gluon splittings are interleaved with gluon emissions, see text. We used $\alpha_s = 0.12$, $n_F = 5$, and $\mu_{\text{PS}} = p_{\perp}$.

course fully taken into account in our implementation in the VINCIA code, and are thus reabsorbed into the one-loop matching coefficient at the matched order, stabilizing the prediction. Differences at higher orders will result from the fact that the CMW rescaling, if applied, is used for all shower branchings, while the NLO correction derived here is only applied at the $Z \rightarrow 3$ stage of the calculation.

Because smooth p_{\perp} -ordering is the default in VINCIA we wish to understand this case as best as we can, and therefore we include some further comparisons with non-default settings in figure 11.

In the left figure of figure 11, we modify the normalization of the evolution variable from the VINCIA default $Q_E^2 = 4p_{\perp}^2$ to the ARIADNE choice $Q_E^2 = p_{\perp}^2$. Though the normalization factor cancels in the P_{imp} factor for sequential gluon emissions, it is relevant for deciding the relative ordering between gluon emissions and gluon splittings. As this plot shows, however, the modification only produces quite small differences in the NLO correction factor, and with the “wrong” sign. Thus, we retain $N_{\perp} = 4$ as the default in VINCIA. In middle figure of figure 11, we change the evolution variable for gluon splittings to be the same as that for gluon emissions, i.e., p_{\perp} , with similar conclusions as for the previous variation. In the right figure of figure 11, we switch off the Ariadne factor for gluon splittings. We notice that the NLO corrections get slightly larger. There is no change along the diagonal $y_{ij} = y_{jk}$ since the Ariadne factor is unity there, but along the edges of the plots, the NLO corrections become larger, which further motivates the choice of keeping the Ariadne factor switched on by default in VINCIA.

The overall result is that the infrared limits are generally well-behaved for p_{\perp} evolution with $\mu_{\text{PS}} \propto p_{\perp}$. Remaining differences amount to small finite shifts of order 10%-20% away from unity. At that level, the effective finite terms of the antenna functions also play a role,

hence it is too early to draw definite conclusions just based on the plots presented here. The impact of finite terms will be studied in section 5 in the context of matching to the LO matrix elements for $Z \rightarrow 4$ partons, which effectively fixes the finite terms with respect to the pure-shower answers studied here.

4.3 Tables of Infrared Limits

The results of the preceding subsections on the infrared limits of the pole-subtracted matrix elements and of the Sudakov integrals generated by the various evolution-scale choices are collected here, in parametric form, for easy reference. The renormalization terms, $V_{3\mu}$, are not included. Tab. 3 expresses the limits of SVirtual, while tab. 4 contains the Sudakov-integral limits.

SVirtual	soft	$\left(-L^2 - \frac{10}{3}L - \frac{\pi^2}{6}\right) C_A + \frac{1}{3}n_F L$
	hard collinear	$-\frac{5}{3}LC_A + \frac{1}{6}n_F L$

Table 3. Limits of SVirtual, with L denoting $\ln(y)$, where y parametrizes the limit in the soft region taken along the diagonal of the phase space triangle $y = s_{qg}/s = s_{g\bar{q}}/s \rightarrow 0$. The hard collinear limit only takes one invariant s_{qg}/s or $s_{g\bar{q}}/s$ to the soft limit while the other is set to 1. We have omitted an overall factor of $\alpha_s/2\pi$.

		strong	smooth	V_{3Z}
p_\perp	soft	$\left(L^2 - \frac{1}{3}L + \frac{\pi^2}{6}\right) C_A + \frac{1}{3}n_F L$	$\left(L^2 - \frac{1}{3}L - \frac{\pi^2}{6}\right) C_A + \frac{1}{3}n_F L$	$-\beta_0 L$
	hard collinear	$-\frac{1}{6}LC_A + \frac{1}{6}n_F L$	$\left(-\frac{1}{6}L - \frac{\pi^2}{6}\right) C_A + \frac{1}{6}n_F L$	$-\frac{1}{2}\beta_0 L$
m_D	soft	$\left(L^2 + \frac{3}{2}L - \frac{\pi^2}{6}\right) C_A$	$\left(L^2 + \frac{3}{2}L - \frac{\pi^2}{6}\right) C_A$	$-\frac{1}{2}\beta_0 L$
	hard collinear	$-\frac{1}{6}LC_A + \frac{1}{6}n_F L$	$\left(-\frac{1}{6}L - \frac{\pi^2}{3}\right) C_A + \frac{1}{6}n_F L$	$-\frac{1}{2}\beta_0 L$

Table 4. Limits of strong and smooth p_\perp and m_D ordering, with naming conventions as defined in tab. 3. Non divergent terms, such as π^2 have been omitted in the calculation of V_{3Z} , and the renormalization term in V_{3Z} is set to zero. An overall factor of $\alpha_s/2\pi$ is suppressed.

5 Results including both LO and NLO corrections

In the preceding section, we focussed on deriving the analytic forms of the shower integrals and comparing their infrared limits to the matrix-element expressions. It is now time to include also the finite terms arising from matching to the 4-parton tree-level matrix element, expressed by the δA terms in eq. (3.55). Our ultimate aim in this section is to include the full leading-colour one-loop corrections through second order in α_s (i.e., up to and including $Z \rightarrow 3$ partons) and combine these with the full-colour tree-level corrections through third order in α_s (i.e., up to and including $Z \rightarrow 5$ partons, the default in VINCIA). However, since we shall perform the δA integrals numerically, adding those terms to the analytic ones derived

in the previous section, we first wish to examine the numerical size and precision required on the δA terms themselves.

5.1 Finite antenna terms and LO matching corrections

Finite-term variations of the antenna functions (and in particular fixing the finite terms via unitary LO matching corrections, such as is done in VINCIA [24]) will affect the terms generated by the $3 \rightarrow 4$ Sudakov expansions in the following way. Larger finite terms will cause an increased amount of $3 \rightarrow 4$ branchings, which in turn will *decrease* the associated Sudakov factor (in the sense of driving it closer to zero). This will feed into the NLO correction factor, which compensates and drives the final answer back towards its NLO-correct value. (Note that similar variations will not occur for the $2 \rightarrow 3$ branching step, since we treat that as fixed to the LO 3-parton matrix element throughout.) This feedback mechanism is encoded in the δA terms in eq. (3.55).

Following the reasoning above, we should expect larger antenna finite terms to *increase* the NLO correction factor (since, to stabilize the 3-parton exclusive rate, it must compensate for losing more 3-parton phase-space points to 4-parton ones), and vice versa: smaller finite terms should result in a *decrease* of the NLO correction. At the pure-shower level (i.e., without LO matrix-element corrections to fix the finite terms), this is illustrated by figure 12. For ease of comparison, all plots use the CMW rescaling of Λ_{QCD} , $\mu_{\text{PS}} = p_{\perp}$, $n_F = 5$, and $\alpha_s(m_Z) = 0.12$. The default antenna functions in VINCIA¹² are shown in the middle panes, for strong (top row) and smooth (bottom row) ordering, respectively. A variation with smaller finite terms for the $3 \rightarrow 4$ antenna functions is shown to the left, and one with larger finite terms on the right. As expected, the NLO correction factors react by becoming lower for smaller finite terms and higher for larger finite terms, for both strong and smooth ordering.

We emphasise that the plots in figure 12 are shown purely for illustration, to give a feeling for the changes produced by finite-term variations. In the actual matched shower evolution, the constraint imposed by matching to the LO 4-parton matrix elements fixes the finite terms, via the unitary procedure derived in [24], which was briefly recapped in section 3.1. The effective finite terms then depend on the full LO 4-parton matrix elements, and have a more complicated structure than the simple antenna functions we have so far been playing with. We shall therefore not attempt to integrate them analytically, but prefer instead to let VINCIA compute a numerical MC estimate for us.

Each point in that MC integration will involve computing at least one LO 4-parton matrix element, hence it is crucial to know how many points will be needed to obtain sufficient accuracy. Since everything else is handled analytically, this will be the deciding factor in determining the speed of the NLO-corrected algorithm. We shall perform a speed test below in section 5.4, but first we need to determine the accuracy we need on the δA integral.

¹²Note that VINCIA was recently updated with a set of helicity-dependent antenna functions [31], so the defaults shown here are not identical to the GGG ones, but are instead helicity sums/averages over the functions defined in [31].

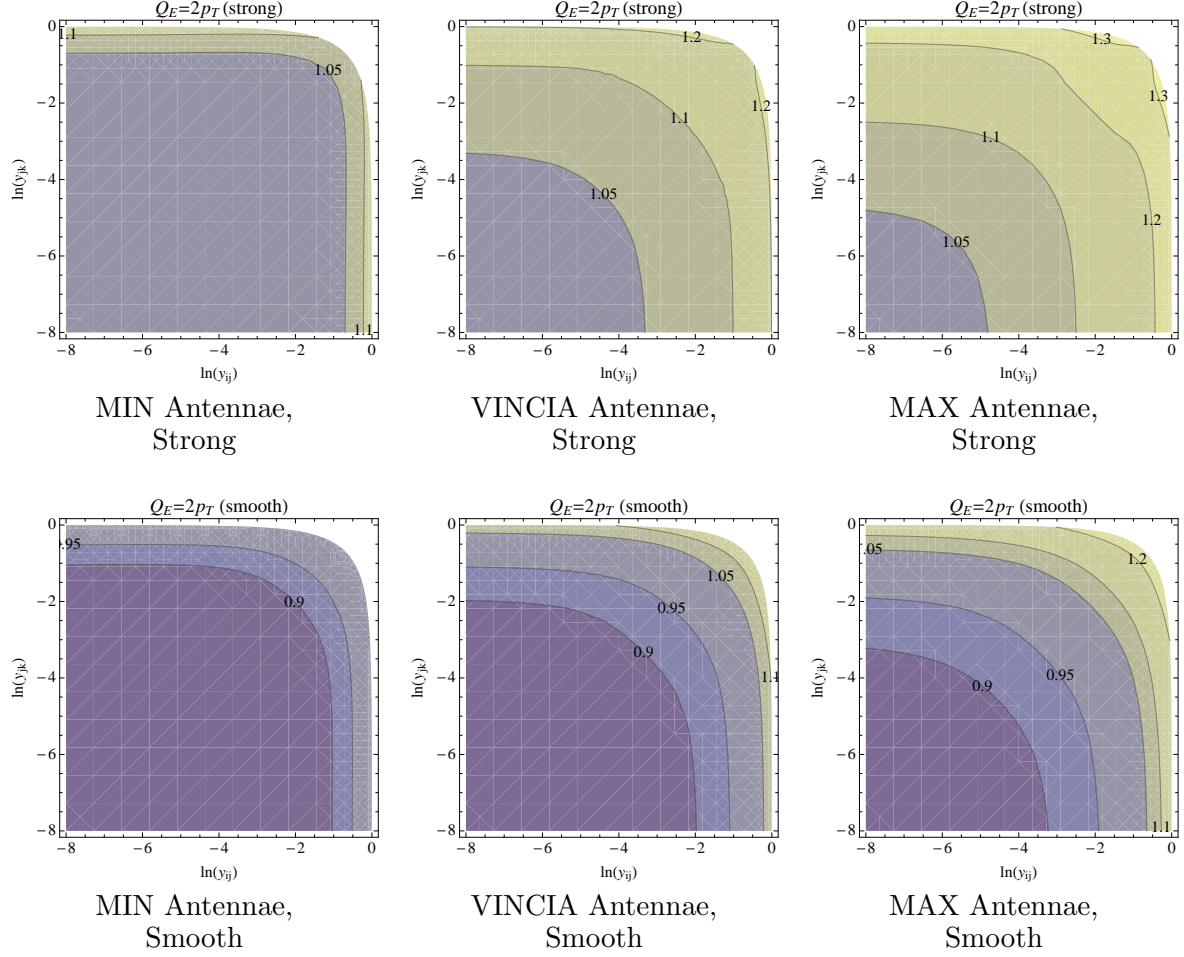


Figure 12. NLO correction factor for strong (top row) and smooth (bottom row) p_\perp -ordering, for MIN (left), VINCIA default (middle), and MAX (right) antenna functions. We use $\mu_R = p_\perp$ combined with CMW rescaling, $\alpha_s = 0.12$, and gluon splitting in m_{qq} .

A first analytic estimate of the size of the δA terms can be obtained by simply computing the ones produced by switching from GGG to the VINCIA default antennae (summed and averaged over helicities [31]), with the following $\mathcal{O}(1)$ finite-term differences:

$$qg \rightarrow qgg : F_{\text{Emit}}^{\text{VINCIA}} - F_{\text{Emit}}^{\text{GGG}} = 1.5 - (2.5 - y_{ij} - 0.5y_{jk}) = -1 + y_{ij} + 0.5y_{jk} , \quad (5.1)$$

$$qg \rightarrow q\bar{q}'q' : F_{\text{Split}}^{\text{VINCIA}} - F_{\text{Split}}^{\text{GGG}} = 0.0 - (-0.5 + y_{ij}) = 0.5 - y_{ij} , \quad (5.2)$$

with F_{Emit} and F_{Split} defined in eqs. (2.4) and (2.5). The δA terms produced by these differences are plotted in figure 13, for strong ordering in m_D (left) and p_\perp (center), and for smooth ordering in p_\perp (right), respectively. As expected, they do come out to be numerically subleading, roughly of order $\alpha_s/(2\pi)$, relative to LO (unity), yielding corrections ranging from a few permille to about a percent of the LO result.

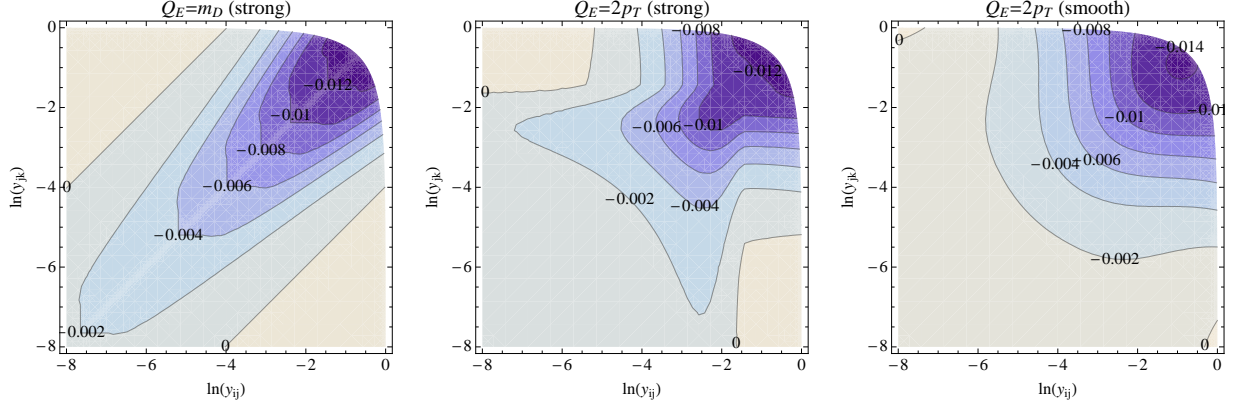


Figure 13. Size of δA terms differences between GGG and VINCIA default antennae.

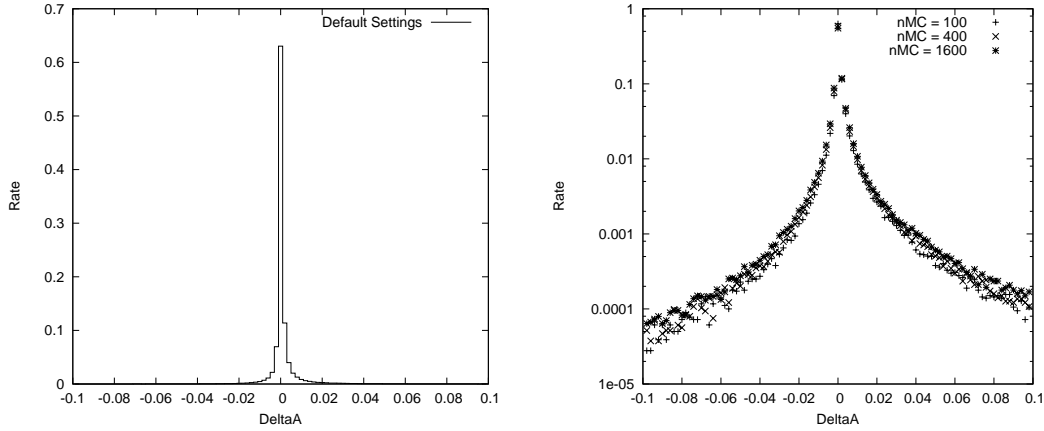


Figure 14. Distribution of the size of the δA terms (normalized so the LO result is unity) in actual VINCIA runs (v.1.1.00). *Left:* linear scale, default settings. *Right:* logarithmic scale, with variations on the minimum number of MC points used for the integrations (default is 100).

Finally, in figure 14, we include the full LO 4-parton matrix elements and plot the distribution of numerically computed δA terms during actual VINCIA runs, for 100,000 events. The result is now represented by a one-dimensional histogram, with δA on the x -axis and relative rate on the y -axis. On the left-hand pane, the δA distribution with default settings is shown on a linear scale, while the right-hand pane shows the same result on a logarithmic scale, including variations with higher numerical accuracy.

As mentioned above, the integration is done by a uniform Monte Carlo sampling of the δA integrands. We require a numerical precision better than 1% on the estimated size of the term (relative to LO) and, by default, always sample at least 100 MC points for each antenna integral. In the left-hand pane of figure 14, we see that, even with the full 4-parton LO matrix-element corrections included, the size of the δA terms remains below one percent

for the vast majority of 3-parton phase-space points.

On the logarithmic scale in the right-hand pane of figure 14, however, it is evident that there is also a tail of quite rare phase-space points which are associated with larger δA corrections. Numerical investigations reveal that this tail is mainly generated by the integrals over the $g \rightarrow q\bar{q}$ terms, in particular in phase-space points in which the gluon is collinear to one of the original quarks. This agrees with our expectation that these terms are the ones to which the pure shower gives the “worst” approximation, and hence they are the ones that receive the largest matrix-element corrections. As a test of the numerical stability of the NLO corrections for these points, we increased the minimum number of MC points used for the δA integration from the default 100 (shown with “+” symbols) to 400 (“×” symbols) and 1600 (“*” symbols), cutting the expected statistical MC error in half with each step, at the cost of increased event-generation time. Though we do observe a slight broadening of the distribution between the default and the higher-precision settings, the shifts should be interpreted horizontally and remain well under the required percent-level precision with respect to LO. The default settings are therefore kept at a minimum of 100 MC points, though we note that future investigations, in particular of more complicated partonic topologies, may require developing a better understanding of, and perhaps a better shower approximation to, these integrals, especially the $g \rightarrow q\bar{q}$ contribution.

For completeness, we note that the runs used to obtain these distributions were performed using the new default “Nikhef” tune of VINCIA’s NLO-corrected shower, which will be described in more detail in the following subsection. Parameters for the tune are given in appendix D.

5.2 LEP Results

Since we have restricted our attention to massless partons in this work, we shall mainly consider the light-flavour-tagged event-shape and fragmentation distributions produced by the L3 experiment at LEP for our validations and tuning, see [63]. We consider three possible VINCIA settings:

- New default (NLO on): uses two-loop running for α_s , with CMW rescaling of Λ_{QCD} . From the comparisons to event-shape variables presented in this section, we settled on a value of $\alpha_s(M_Z) = 0.122$. A few modifications to the string-fragmentation parameters were made, relative to the old default, to compensate for differences in the region close to the hadronization scale. The revised parameters are listed in appendix D, under the “Nikhef” tune.
- New default (NLO off). Identical to the previous bullet point, but with the NLO correction factor switched off.
- Old default (LO tune): uses one-loop running for α_s , without CMW rescaling of Λ_{QCD} , and $\alpha_s(M_Z) = 0.139$. The string-fragmentation parameters are those of the “Jeppsson 5” tune, see appendix D.

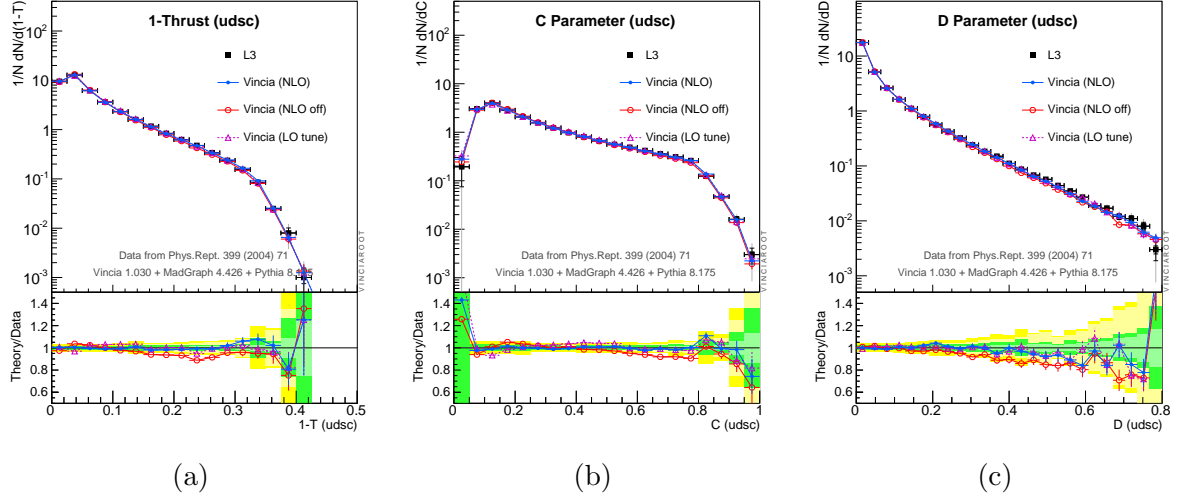


Figure 15. L3 light-flavour event shapes: Thrust, C , and D .

The three main event-shape variables that were used to determine the value of $\alpha_s(M_Z)$ are shown in figure 15, with upper panes showing the distributions themselves (data and MC) and lower panes showing the ratios of MC/data, with one- and two-sigma uncertainties on the data shown by darker (green) and lighter (yellow) shaded bands, respectively. The Thrust (*left*) and C -parameter (*middle*) distributions both have perturbative expansions that start at $\mathcal{O}(\alpha_s)$ and hence they are both explicitly sensitive to the corrections considered in this paper. The expansion of the D parameter (*right*) begins at $\mathcal{O}(\alpha_s^2)$. It is sensitive to the NLO 3-jet corrections mainly via unitarity, since all 4-jet events begin their lives as 3-jet events in our framework. It also represents an important cross-check on the value extracted from the other two variables.

For a pedagogical description of the variables, see [63]. Pencil-like 2-jet configurations are to the left (near zero) for all three observables. This region is particularly sensitive to non-perturbative hadronization corrections. More spherical events, with several hard perturbative emissions, are towards the right (near 0.5 for Thrust and 1.0 for C and D). The maximal $\tau = 1 - T$ for a 3-particle configuration is $\tau = 1/3$ (corresponding to the Mercedes configuration), beyond which only 4-particle (and higher) states can contribute. This causes a noticeable change in slope in the distribution at that point, see the left pane of figure 15. The same thing happens for the C parameter at $C = 3/4$, in the middle pane of figure 15. The D parameter is sensitive to the smallest of the eigenvalues of the sphericity tensor, and is therefore zero for any purely planar event, causing it to be sensitive only to 4- and higher-particle configurations over its entire range.

Both the new NLO tune (solid blue line with filled-dot symbols) and the old LO one (dashed magenta line with open-triangle symbols) reproduce all three event shapes very well. With the NLO corrections switched off (solid red line with open-circle symbols), the new tune produces a somewhat too soft spectrum, consistent with its low value of $\alpha_s(M_Z)$ not being

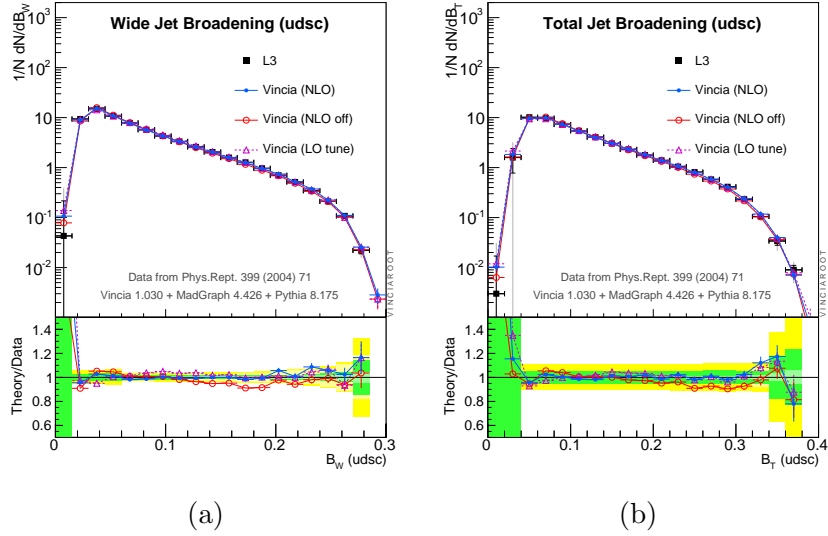


Figure 16. L3 light-flavour event shapes: jet broadening

able to describe the data without the benefit of the NLO 3-jet corrections.

As a further cross check, we show two further event-shape variables that were included in the L3 study in figure 16: the Wide and Total Jet Broadening parameters, B_W and B_T , respectively. These have a somewhat different and complementary sensitivity to the perturbative corrections, compared to the variables above, picking out mainly the transverse component of jet structure. They are equal at $\mathcal{O}(\alpha_s)$, but B_T receives somewhat larger $\mathcal{O}(\alpha_s^2)$ corrections than B_W . Again, we see that both the old (LO) and new (NLO) defaults are able to describe the data, and that the spectrum with the new default value for $\alpha_s(M_Z)$ is too soft if the NLO corrections are switched off.

Finally, as an aid to constraining the Lund fragmentation-function parameters, the L3 study also included two infrared-sensitive observables: the charged-particle multiplicity and momentum distributions, to which we compare in figure 17, with the momentum fraction defined as

$$x = \frac{2|p|}{\sqrt{s}}. \quad (5.3)$$

There is again no noteworthy differences between the old and new default tunes.

Having determined the value of $\alpha_s(M_Z)$ and the parameters of the non-perturbative fragmentation function, we extended the validations to include a set of jet-rate and jet-resolution measurements by the ALEPH experiment [64] (now without the benefit of light-flavour tagging), using the standard Durham k_T algorithm for e^+e^- collisions [65], as implemented in the FASTJET code [66]. We also compared to default PYTHIA 8 and, for completeness, checked that the relative production fractions of various meson and baryon species were indeed unchanged relative to the old VINCIA default.

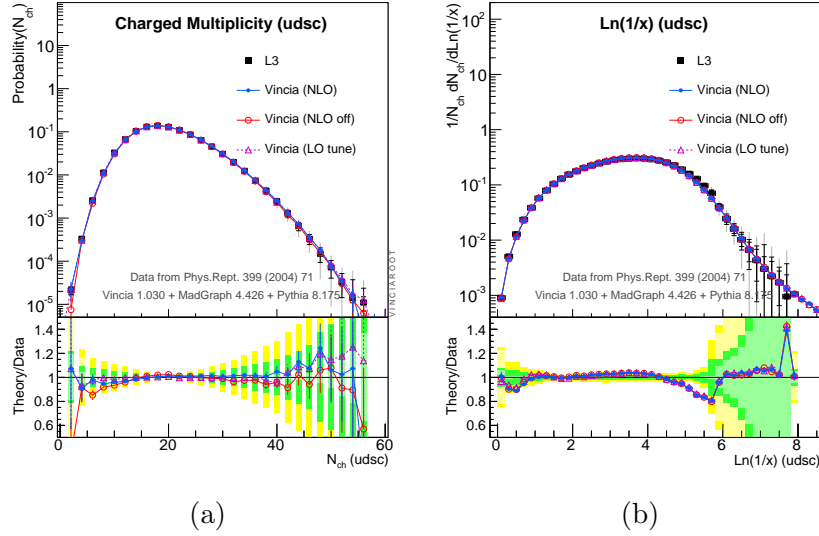


Figure 17. L3 light-flavour fragmentation observables: charged-track multiplicity and momentum distribution.

Rather than presenting all of this information in the form of many additional plots, tab. 5 instead provides a condensed summary of all the validations we have carried out, via $\langle\chi^2\rangle$ values for each of the models with respect to each of the LEP distributions, including a flat 5% “theory uncertainty” on the MC numbers. Already from this simple set of χ^2 values, it is clear that the LO models/tunes are already doing very well¹³. This agreement, however, comes at the price of using a very large (“LO”) value for α_s , which is not guaranteed to be universally applicable.

The main point of the overview in tab. 5 is that an equally good agreement can be obtained with an $\alpha_s(m_Z)$ value that is consistent with other NLO determinations [72], specifically

$$\alpha_s(m_Z) = 0.122 , \quad (5.4)$$

once the NLO 3-jet corrections are included. This should carry over to other NLO-corrected processes, and hence the fragmentation parameters we have settled on should be applicable to future NLO-corrected studies with VINCIA, and can also serve as a starting point for NLO-level matching studies with PYTHIA 8. In the latter context, the 2-loop running in particular could be retained, while the soft fragmentation parameters would presumably have to be somewhat readjusted to absorb differences between VINCIA and PYTHIA 8 near the hadronization scale¹⁴.

¹³Both VINCIA and PYTHIA are known to give quite good fits to LEP data [24, 31, 67, 68]. For comparisons including other generators and tunes, see mcplots.cern.ch [69].

¹⁴The differences in soft fragmentation parameters between existing LO VINCIA and PYTHIA-8 tunes could be used as an initial guideline for such an effort, see, e.g., appendix D.

$\langle\chi^2\rangle$ Shapes	T	C	D	B_W	B_T	$\langle\chi^2\rangle$ Frag	N_{ch}	x	Mesons	Baryons
PYTHIA 8	0.4	0.4	0.6	0.3	0.2	PYTHIA 8	0.8	0.4	0.9	1.2
VINCIA (LO)	0.2	0.4	0.4	0.3	0.3	VINCIA (LO)	0.0	0.5	0.3	0.6
VINCIA (NLO)	0.2	0.2	0.6	0.3	0.2	VINCIA (NLO)	0.1	0.7	0.2	0.6

$\langle\chi^2\rangle$ Jets	r_{1j}^{exc}	$\ln(y_{12})$	r_{2j}^{exc}	$\ln(y_{23})$	r_{3j}^{exc}	$\ln(y_{34})$	r_{4j}^{exc}	$\ln(y_{45})$	r_{5j}^{exc}	$\ln(y_{56})$	r_{6j}^{inc}
PYTHIA 8	0.1	0.2	0.1	0.2	0.1	0.3	0.2	0.3	0.2	0.4	0.3
VINCIA (LO)	0.1	0.2	0.1	0.2	0.0	0.2	0.3	0.1	0.1	0.0	0.0
VINCIA (NLO)	0.2	0.4	0.1	0.3	0.1	0.3	0.2	0.2	0.1	0.2	0.1

Table 5. $\langle\chi^2\rangle$ values for: *Top:* L3 light-flavour event shapes (*left*) and fragmentation variables [63], and LEP average meson and baryon fractions (*right*) [70, 71]. *Bottom:* Durham k_T n -jet rates, r_{nj} , and jet resolutions, y_{ij} , measured by the ALEPH experiment [64]. For the latter, the $\langle\chi^2\rangle$ calculation was restricted to the perturbative region, $\ln(y) > -8$. A flat 5% theory uncertainty was included on the MC numbers. Both default PYTHIA and the VINCIA (LO) tune use $\alpha_s(m_Z) = 0.139$ while the VINCIA (NLO) tune uses $\alpha_s(m_Z) = 0.122$.

5.3 Uncertainties

As in previous versions of VINCIA, we use the method proposed in [24] to compute a comprehensive set of uncertainty bands, which are provided in the form of a vector of alternative weights for each event. Each set is separately unitary, with average weight one¹⁵. The difference with respect to previous versions is that each variation now benefits fully from the inclusion of NLO corrections.

When setting the parameter `Vincia:uncertaintyBands = on`, the uncertainty weights are accessible through the method

```
double vincia.weight(int i=0);
```

with $i = 0$ corresponding to the ordinary event sample, normally with all weights equal to unity, and the following variations, for $i =$:

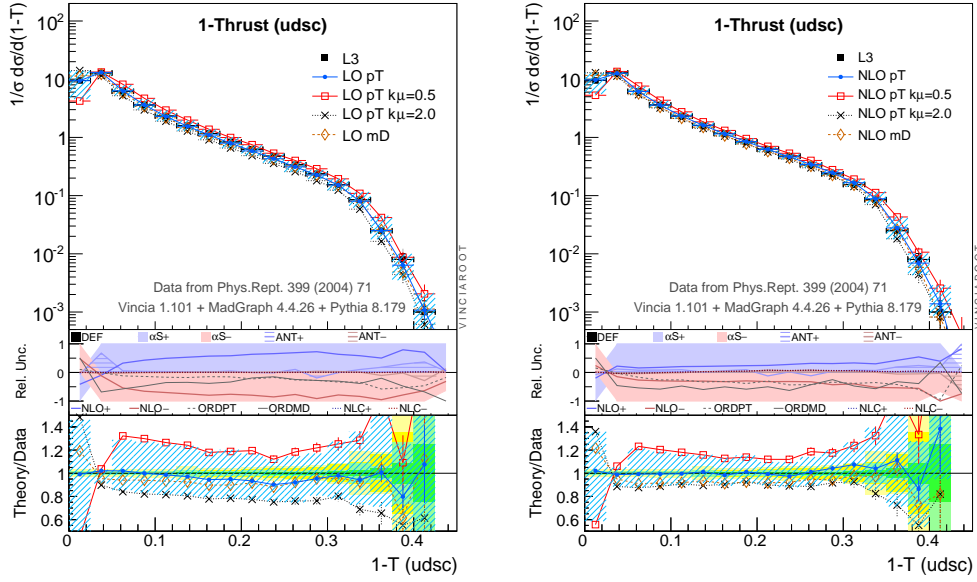
1. Default: since the user may have chosen other settings than the default, the default is included as the first variation.
2. alphaS-Hi: all renormalization scales are decreased to $\mu = \mu_{\text{def}}/k_\mu$, where $\mu_{\text{def}} = p_\perp$ for gluon emission and $\mu_{\text{def}} = m_{q\bar{q}}$ for gluon splitting. The default size of the variation ($k_\mu = 2$) can be changed by the user, if desired. A second-order compensation for this variation is provided by the renormalization-scale sensitive term $V_{3\mu}$.
3. alphaS-Lo: all renormalization scales are increased to $\mu = \mu_{\text{def}} * k_\mu$, with similar comments as for alphaS-Hi above.

¹⁵VINCIA currently does not attempt to give a separate estimate of the uncertainty on the total inclusive cross section. The uncertainties it computes only pertain to shapes of distributions and the effects of cuts on the total inclusive rate.

4. ant-Hi: antenna functions with large finite terms (MAX [31]). This variation is already compensated for by LO matching (up to the LO matched orders) and is not explicitly affected by the NLO corrections.
5. ant-Lo: antenna functions with small finite terms (MIN [31]), with similar comments as above.
6. NLO-Hi: branching probabilities are multiplied by a factor $(1+\alpha_s)$ to represent unknown (but finite) NLO corrections. Is canceled by NLO matching (up to the NLO matched order).
7. NLO-Lo: branching probabilities are divided by a factor $(1 + \alpha_s)$. Is canceled by NLO matching.
8. Ord-pT: smooth p_\perp ordering for all branchings, including $g \rightarrow q\bar{q}$ ones. Compensated at first order by LO matching, and at second order (Sudakov corrections) by NLO matching via ordering-sensitive terms in V_{3Z} .
9. Ord-mD: smooth m_D ordering for gluon emissions (with $m_{q\bar{q}}$ used for gluon splittings). Similar comments as for Ord-pT above.
10. NLC-Hi: qg emission antennae use C_A as color factor. Compensated at first order by LO matching. Not affected by NLO matching since those are so far only only done at leading color.
11. NLC-Lo: qg emission antennae use $2C_F$ as color factor, with similar comments as above.

We emphasize that these variations are not all independent (for instance the α_s and NLO variations are highly correlated) and hence the corresponding uncertainties should not be summed in quadrature. In the VINCIAROOT plotting tool included with VINCIA, the uncertainty band is constructed by taking the max and min of the variations. See the VINCIA HTML manual for more information about the uncertainty bands and [24] for details on their algorithmic construction.

To illustrate these variations, and the effect of the NLO 3-jet corrections upon them, we include the two plots shown in figure 18. We here take the Thrust observable as a representative example. (More such plots can be generated using the VINCIAROOT interface and the `vincia03-root.cc` example program included with the VINCIA code.) Similarly to previous plots in this paper, the top pane shows the normalized distribution, $1/\sigma d\sigma/d(1-T)$, and the bottom one shows the ratio of theory to data. Now, however, there is also a middle pane, which gives the relative breakdown of the automated uncertainty variations into their respective components (normalized to unity). In each plot, we compare four individual runs of VINCIA to the automated uncertainty variations, with the latter based on the central run. This provides a useful cross check of whether the variations are indeed well represented by the automated estimates, before (*left*) and after (*right*) including the NLO 3-jet corrections.



(a) $\text{NLO}_2 + \text{LO}_{2,3,4,5} + \text{shower}$

(b) $\text{NLO}_{2,3} + \text{LO}_{2,3,4,5} + \text{shower}$

Figure 18. Comparison of explicit and automated uncertainty variations without (*left*) and with (*right*) NLO 3-jet corrections. The individual curves each represents an explicit run, while the shaded blue areas represent the automated uncertainty estimates calculated from the central run.

For the individual runs, we have chosen to show the renormalization-scale ($\mu_{\text{PS}} = p_{\perp}$ for the central run and factor-2 variations) and evolution-variable (p_{\perp} for the central run and m_D as the last variation) dependence. (The antenna-function variations are canceled already at LO for this observable, so they are not interesting in the present context.) The automated uncertainty bands include all 10 variations, with the middle panes showing the contributions from each. In both plots, the scale-variation uncertainty dominates over the full range of the observable, highlighting that this is the main component that would need to be improved in order to obtain more precise results. Note, however, that both the central value at large $1 - T$ and the amount of scale variation, *are* improved by the introduction of the NLO 3-jet corrections in the right-hand pane. We also note that the distributions obtained from the explicit variation runs are faithfully reproduced by the automated variations, thus validating our confidence in the automated approach.

5.4 Speed

Although the CPU time required by matrix-element and shower/hadronization generators is still typically small in comparison to that of, say, full detector simulations, their speed and efficiency are still decisive for all generator-level studies, including tuning and validation, parameter scans, development work, phenomenology studies, comparisons to measurements corrected to the hadron level, and even studies interfaced to fast detector simulations. For this wide range of applications, the high-energy simulation itself constitutes the main part of

the calculation. An important benchmark relevant to practical work is for instance whether the calculation can be performed easily on a single machine or not.

Higher matched orders are characterized by increasing complexity and decreasing unweighting efficiencies, resulting in an extremely rapid growth in CPU requirements (see e.g. [31]). At NLO, the additional issues of negative weights and/or so-called counter-events can contribute further to the demands on computing power. With this in mind, high efficiencies and fast algorithmic structures were a primary concern in the development of the formalism for leading-order matrix-element corrections in VINCIA [24, 30, 31], and this emphasis carries through to the present work. We can make the following remarks.

- The only fixed-order phase-space generator is the Born-level one. All higher-multiplicity phase-space points are generated by (trial) showers off the lower-multiplicity ones. This essentially produces a very fast importance-sampling of phase-space that automatically reproduces the dominant QCD structures.
- Likewise, the only cross-section estimate that needs to be precomputed at initialization is the total inclusive one. Thus, initialization times remain at fractions of a second regardless of the matching order.
- The matrix-element corrected algorithm works just like an ordinary parton shower, with modified (corrected) splitting kernels. In particular, all produced events have the same weights, and no additional unweighting step is required.
- Since the corrections are performed multiplicatively, in the form of $(1 + \text{correction})$, with 1 being the LO answer, there are no negative-weight events and no counter-events. The only exception would be if the correction becomes larger than the LO answer, and negative. This would correspond to a point with a divergent fixed-order expansion, in which case the use of NLO corrections would be pointless anyway. Moreover, as demonstrated by the plots in the previous sections, our definitions of the corrections are analytically stable (and numerically subleading with respect to LO) over all of phase space, including the soft and collinear regions, for reasonable renormalization- and evolution-variable choices.
- The parameter variations described in section 5.3 can be performed together with the matching corrections to provide a set of uncertainty bands in which each variation benefits from the full corrections up to the matched orders. These are provided in the form of a vector of alternative weights for each event [24], at a cost in CPU time which is only a fraction of that of a comparable number of independent runs.

These attributes, in combination with helicity dependence in the case of the leading-order formalism [31], allow VINCIA to run comfortably on a single machine even with full-fledged matching and uncertainty variations switched on.

The inclusion of NLO corrections will necessarily slow down the calculation. The relative increase in running time relative to PYTHIA 8, is given in tab. 6, including the default level

	LO level	NLO level	Time / Event	Speed relative to PYTHIA
	$Z \rightarrow$	$Z \rightarrow$	[milliseconds]	$\frac{1}{\text{Time}} / \text{PYTHIA 8}$
PYTHIA 8	2, 3	2	0.6	1
VINCIA (NLO off)	2, 3, 4, 5	2	2.5	$\sim 1/4$
+ uncertainties	2, 3, 4, 5	2	2.9	$\sim 1/5$
VINCIA (NLO on)	2, 3, 4, 5	2, 3	3.9	$\sim 1/7$
+ uncertainties	2, 3, 4, 5	2, 3	4.0	$\sim 1/7$

Table 6. Event-generation time in default VINCIA 1.1.01 (NIKHEF tune), with and without automated uncertainty evaluations and NLO 3-jet corrections, compared to default PYTHIA 8.179.

of tree-level matching, with and without the NLO 3-jet correction¹⁶. Without it (but still including the default tree-level corrections which go up to $Z \rightarrow 5$ partons), VINCIA is 5 times slower than PYTHIA. With the NLO 3-jet correction switched on, this increases only slightly, to a factor 7. For a fully showered and hadronized calculation which includes second-order virtual and third-order tree-level corrections, we consider that to still be acceptably fast. Importantly, an event-generation time of a few milliseconds per event implies that serious studies can still be performed on an ordinary laptop computer.

6 Outlook and Conclusions

In this work, we have investigated the expansion of a Markov-chain QCD shower algorithm to second order in the strong coupling, for $e^+e^- \rightarrow 3$ partons, and made systematic comparisons to matrix-element results obtained at the same order. Using these results, we have subjected the subleading properties of shower algorithms with different evolution/ordering variables and different renormalization-scale choices to a rigorous examination. At the analytical level, we have compared the logarithmic structures at the edge of phase space, and at the numerical level we have illustrated the difference between the expanded shower algorithm and the one-loop matrix element.

We find that the choice of p_\perp -ordering, with a renormalization scale proportional to p_\perp yields the best agreement with the one-loop matrix element, over all of phase space. This elaborates on, and is consistent with, earlier findings [34, 35]. Using the antenna invariant mass, m_D , for the evolution variable still gives reasonable results in the hard regions of phase space, but leads to logarithmically divergent corrections for soft emissions, the exact form of which depends on the choice of renormalization variable. In the VINCIA code, we retain the option of using m_D mainly as a way of providing a conservative uncertainty estimate.

With the NLO 3-jet corrections included as multiplicative corrections to the shower branching probabilities, we find that we can obtain good agreement with a large set of LEP event-shape, fragmentation, and jet-rate observables with a value of the strong coupling con-

¹⁶The numbers include both showering and hadronization and were obtained on a single 2.53 GHz CPU, with gcc 4.7 -O2, using default settings for PYTHIA 8 and the “Nikhef” NLO tune for VINCIA.

stant of $\alpha_s(M_Z) = 0.122$. This is in strong contrast with earlier (LO) tunes of both PYTHIA and VINCIA which employed much larger values ~ 0.14 to obtain agreement with the LEP measurements. The parameters for the NLO tune are collected in appendix D and represent the first dedicated NLO-corrected tune to LEP data.

This paper is intended as a first step towards a systematic embedding of one-loop amplitudes within the VINCIA shower and matching formalism. To arrive at a full-fledged prescription, this will need to be extended to hadron collisions, ideally in a way that allows for convenient automation. A first step towards developing the underlying shower formalism for pp collisions was recently taken [73], and more work is in progress [74].

In addition, further studies should be undertaken of the impact of unordered sequences of radiation that can occur for the smooth-ordering case (it may be necessary to adopt a strategy similar to the truncated showers of the MC@NLO approach), and the mutually related issues of total normalization and how much of the (hard) corrections are exponentiated (similar to the differences between the POWHEG and MC@NLO formalisms, but here occurring at one additional order, where the relevant total normalization is the NNLO one). Finally, it would be interesting to develop an extension of this formalism that would allow second-order-corrected antenna functions to be used at every stage in the shower, thereby upgrading the precision of the all-orders resummation, a project that would involve examining the second-order corrections to branchings of qg and gg mother antennae as well. We look forward to following up on these issues in the near future.

Acknowledgments

We are grateful to A. Larkoski, L. Lönnblad, J. Lopez-Villarejo, S. Prestel, G. Salam, and T. Sjöstrand for discussions and comments on the manuscript. We are indebted to H. Mantler for careful cross-checks of many of the formulae in this paper, several typo corrections, and especially for providing us with alternative forms for some of the integrals listed in the appendices which are more manifestly numerically stable than those written in the original (arXiv v1 and v2) versions of our paper. We also thank C. Duncan for validating the resulting changes. PS thanks the Galileo Galilei Institute for Theoretical Physics, LH would like to thank Lund University and both of us thank CEA-Saclay for their hospitality. We also thank the INFN for partial support during the completion of this work. EL and LH have been supported by the Netherlands Foundation for Fundamental Research of Matter (FOM) programme 104, entitled “Theoretical Particle Physics in the Era of the LHC”, and the National Organization for Scientific Research (NWO).

A Infrared singular operators

Here we list the IR singularity operators from [22, 33, 59] as they are used in section 3.

$$I_{q\bar{q}}^{(1)}(\epsilon, \mu^2/s_{q\bar{q}}) = -\frac{e^{\epsilon\gamma}}{2\Gamma(1-\epsilon)} \left[\frac{1}{\epsilon^2} + \frac{3}{2\epsilon} \right] \text{Re} \left(-\frac{\mu^2}{s_{q\bar{q}}} \right)^\epsilon \quad (\text{A.1})$$

$$I_{qg}^{(1)}(\epsilon, \mu^2/s_{qg}) = -\frac{e^{\epsilon\gamma}}{2\Gamma(1-\epsilon)} \left[\frac{1}{\epsilon^2} + \frac{5}{3\epsilon} \right] \text{Re} \left(-\frac{\mu^2}{s_{qg}} \right)^\epsilon \quad (\text{A.2})$$

$$I_{qg,F}^{(1)}(\epsilon, \mu^2/s_{qg}) = \frac{e^{\epsilon\gamma}}{2\Gamma(1-\epsilon)} \frac{1}{6\epsilon} \text{Re} \left(-\frac{\mu^2}{s_{qg}} \right)^\epsilon \quad (\text{A.3})$$

B One-Loop Amplitudes

B.1 Renormalization

Because a detailed derivation of the calculation of $Z \rightarrow 3$ jets can be found in [32] we restrict ourselves to listing the result in form that is convenient for our purpose. Divergences are regulated using dimensional regularization with $d = 4 - 2\epsilon$. Our results, before ultraviolet renormalization, are cross-checked with [32] where one must undo the renormalization in their case. In order to cancel the ultraviolet poles we need to renormalize the coupling according to (see also section 3.4)

$$\alpha_s^{bare} = \alpha_s(\mu_R^2) \mu^{2\epsilon} \left[1 - \frac{\beta_0}{\epsilon} S_\epsilon \left(\frac{\alpha_s(\mu_R^2)}{4\pi} \right) \left(\frac{\mu^2}{\mu_R^2} \right)^\epsilon \right] \quad (\text{B.1})$$

where

$$\beta_0 = \frac{11N_c - 2n_F}{3} \quad (\text{B.2})$$

and $S_\epsilon = (4\pi)^\epsilon \exp(-\epsilon \gamma_E)$ contains the factors characterizing the $\overline{\text{MS}}$ scheme. Due to the renormalization, the leading order calculation will generate a term quadratic in $\alpha_s(\mu_R^2)$,

$$- \frac{\alpha_s(\mu_R)^2}{4\pi} \frac{\beta_0}{\epsilon} \left[1 + \epsilon \ln \left(\frac{\mu_R^2}{\mu^2} \right) \right] \text{Born} , \quad (\text{B.3})$$

which directly cancels the ultraviolet poles of the next-to-leading order calculation.

B.2 One-loop Matrix Element

The fixed-order expression relevant to matching in the VINCIA context is the one-loop matrix element normalized by the tree-level one. We decompose this into leading- and subleading-colour pieces, as follows:

$$\frac{2 \text{Re} [M_3^{(1)} M_3^{0*}]}{|M_3^0|^2} = \frac{\alpha_s}{2\pi} (LC + QL + SL) , \quad (\text{B.4})$$

with the LC piece containing the C_A part of the gluon loops, the QL one containing the quark loops, proportional to $n_F T_R$, and the SL piece containing the subleading gluon-loop

corrections, proportional to $-1/N_C$. As usual in MC applications, we usually refer to “Leading Colour” as including both the N_C and T_R pieces. These are both associated with so-called planar colour flows that are simple to relate to the colour-flow representations used in Monte Carlo event generators, see e.g. [1, 75]. The subleading-colour piece is included below for completeness, but has so far been left out of the NLO matching corrections implemented in the VINCIA code.

The notation of the infrared pole structure of these terms has been written similar to the integrated antenna in [22], with the difference that we have chosen to expand the scale factor μ in the integrated antenna terms in order to obtain explicitly dimensionless logarithms.

The quark has been labelled 1, the anti-quark 2 and the gluon 3.

$$\begin{aligned} \text{LC} = & N_C \left[\left(2I_{qg}^{(1)}(\epsilon, \mu^2/s_{13}) + 2I_{qg}^{(1)}(\epsilon, \mu^2/s_{23}) \right) \right. \\ & + \left(-R(y_{13}, y_{23}) + \frac{3}{2} \ln \left(\frac{s_{123}}{\mu_R^2} \right) + \frac{5}{3} \ln \left(\frac{\mu_R^2}{s_{23}} \right) + \frac{5}{3} \ln \left(\frac{\mu_R^2}{s_{13}} \right) - 4 \right) \\ & + \frac{1}{s_{123} a_3^0} \left[2 \ln(y_{13}) \left(1 + \frac{s_{13}}{s_{12} + s_{23}} - \frac{s_{23}}{s_{12} + s_{23}} - \frac{s_{23}s_{13}}{4(s_{12} + s_{23})^2} \right) \right. \\ & + 2 \ln(y_{23}) \left(1 - \frac{s_{13}}{s_{12} + s_{13}} + \frac{s_{23}}{s_{12} + s_{13}} - \frac{s_{23}s_{13}}{4(s_{12} + s_{13})^2} \right) \\ & \left. \left. + \frac{1}{2} \left(\frac{s_{13}}{s_{23}} - \frac{s_{13}}{s_{12} + s_{13}} + \frac{s_{23}}{s_{13}} - \frac{s_{23}}{s_{12} + s_{23}} + \frac{s_{12}}{s_{23}} + \frac{s_{12}}{s_{13}} + 1 \right) \right] \right] \end{aligned} \quad (\text{B.5})$$

$$\begin{aligned} \text{QL} = & 2n_F T_R \left[\left(2I_{qg,F}^{(1)}(\epsilon, \mu^2/s_{13}) + 2I_{qg,F}^{(1)}(\epsilon, \mu^2/s_{23}) \right) \right. \\ & \left. + \frac{1}{6} \left(\ln \left(\frac{s_{23}}{\mu_R^2} \right) + \ln \left(\frac{s_{13}}{\mu_R^2} \right) \right) \right] \end{aligned} \quad (\text{B.6})$$

$$\begin{aligned} \text{SL} = & \frac{1}{N_C} \left[\left(2I_{q\bar{q}}^{(1)}(\epsilon, \mu^2/s_{12}) \right) \right. \\ & - \left(4 + \frac{3}{2} \ln(y_{12}) + R(y_{12}, y_{13}) + R(y_{12}, y_{23}) \right) \\ & + \frac{1}{s_{123} a_3^0} \left[R(y_{12}, y_{13}) \left(\frac{s_{13}}{s_{23}} + 2 \frac{s_{12}}{s_{23}} \right) + R(y_{12}, y_{23}) \left(\frac{s_{23}}{s_{13}} + 2 \frac{s_{12}}{s_{13}} \right) \right. \\ & + \ln(y_{12}) \left(\frac{4s_{12}}{s_{13} + s_{23}} + \frac{2s_{12}^2}{(s_{13} + s_{23})^2} \right) \\ & + \frac{1}{2} \ln(y_{13}) \left(\frac{s_{13}}{s_{12} + s_{23}} + \frac{4s_{12}}{s_{12} + s_{23}} + \frac{s_{12}s_{13}}{(s_{12} + s_{23})^2} \right) \\ & + \frac{1}{2} \ln(y_{23}) \left(\frac{s_{23}}{s_{12} + s_{13}} + \frac{4s_{12}}{s_{12} + s_{13}} + \frac{s_{12}s_{23}}{(s_{12} + s_{13})^2} \right) \\ & \left. \left. - \frac{1}{2} \left(\frac{s_{13}}{s_{23}} - \frac{s_{23}}{s_{13}} - \frac{s_{12}}{s_{23}} - \frac{s_{12}}{s_{13}} + \frac{s_{12}}{s_{12} + s_{13}} + \frac{s_{12}}{s_{12} + s_{23}} + \frac{s_{12}}{s_{13} + s_{23}} + \frac{4s_{12}}{s_{13} + s_{23}} \right) \right] \right] \end{aligned} \quad (\text{B.7})$$

with

$$R(y, z) = \ln(y) \ln(z) - \ln(y) \ln(1-y) - \ln(z) \ln(1-z) + \frac{\pi^2}{6} - \text{Li}_2(y) - \text{Li}_2(z) , \quad (\text{B.8})$$

$$a_3^0 = \frac{|M_3^0|^2}{g_s^2 C_F |M_2^0|^2} = \frac{1}{s_{123}} \left(\frac{(1-\epsilon)s_{13}}{s_{23}} + \frac{(1-\epsilon)s_{23}}{s_{13}} + 2 \frac{s_{12}s_{123} - \epsilon s_{13}s_{23}}{s_{13}s_{23}} \right) (1-\epsilon) , \quad (\text{B.9})$$

and the infrared singular operators, $I^{(1)}$, given in appendix A.

With the one-loop matrix element expressed in this form, cancellation of the infrared poles against the integrated antennae (see below) coming from the shower will be particularly simple and will yield an expression purely dependent on the renormalization scale, μ_R , and on the kinematic invariants s_{12} , s_{23} , and s_{13} , but not on the scale factor μ .

C Antenna integrals

In this appendix we list the results of antenna integrals over phase space corresponding to the various evolution variables.

C.1 Strong Ordering Gluon Emission

The expressions for a gluon emitting antenna is given in eq. (2.4). With a redefinition the same antenna function reads

$$a_{g/IK}(y_1, y_2) = \frac{1}{m_{IK}^2} \left[\frac{2(1-y_1-y_2)}{y_1 y_2} + \frac{y_1}{y_2} + \frac{y_2}{y_1} - \delta_{Ig} \frac{y_2^2}{y_1} - \delta_K g \frac{y_1^2}{y_2} + C_{00} + C_{01} y_1 + C_{10} y_2 \right] \quad (\text{C.1})$$

where y_1, y_2 correspond to y_{ij}, y_{jk} of eq. (2.6), respectively. Recall that the last three terms serve to give a flexible and explicit way of tracking extra non-singular terms in antennae. The phase space integral over these antenna, as determined by the evolution variable, can be written as

$$\frac{1}{16\pi^2 m_{IK}^2} \int_{Q_E^2}^{m_{IK}^2} a_{g/IK} |\mathcal{J}(Q^2, \zeta)| dQ^2 d\zeta. \quad (\text{C.2})$$

All antenna integrals in eq. (3.32) have been written in such a way that they are integrated over their whole invariant mass plus a correction term running from the evolution variable to the total invariant mass. The integrals running over the whole invariant mass contain singular regions and therefore poles while the correction terms yield finite corrections. These finite corrections are discussed per evolution variable below. We define the integrals

$$\mathcal{D}_{Q\zeta} = \frac{1}{m_{IK}^4} \int dQ^2 d\zeta |J| \quad (\text{C.3})$$

$$I_1 = \mathcal{D}_{Q\zeta} \frac{1}{y_1(Q^2, \zeta) y_2(Q^2, \zeta)} \quad (\text{C.4})$$

$$I_2 = \mathcal{D}_{Q\zeta} \frac{1}{y_2(Q^2, \zeta)} = \mathcal{D}_{Q\zeta} \frac{1}{y_1(Q^2, \zeta)} \quad (\text{C.5})$$

$$I_3 = \mathcal{D}_{Q\zeta} \frac{y_1(Q^2, \zeta)}{2y_2(Q^2, \zeta)} = \mathcal{D}_{Q\zeta} \frac{y_2(Q^2, \zeta)}{2y_1(Q^2, \zeta)} \quad (\text{C.6})$$

$$I_4 = \mathcal{D}_{Q\zeta} \frac{y_2^2(Q^2, \zeta)}{2y_1(Q^2, \zeta)} = \mathcal{D}_{Q\zeta} \frac{y_1^2(Q^2, \zeta)}{2y_2(Q^2, \zeta)} \quad (\text{C.7})$$

$$I_5 = \frac{1}{2} \mathcal{D}_{Q\zeta} [C_{00} + C_{01} y_1(Q^2, \zeta) + C_{10} y_2(Q^2, \zeta)] . \quad (\text{C.8})$$

So that, in these terms, the results read

$$\frac{1}{16\pi^2 m_{IK}^2} \int_{Q_E^2}^{m_{IK}^2} dQ^2 d\zeta |J(Q^2, \zeta)| a_{g/IK} = \frac{1}{8\pi^2} \left(\sum_{i=1}^5 K_i I_i \right) \quad (\text{C.9})$$

where

$$K_1 = 1, \quad K_2 = -2, \quad K_3 = 2, \quad K_4 = -\delta_{Ig} - \delta_{Kg}, \quad K_5 = 1. \quad (\text{C.10})$$

We now turn to specific cases.

C.1.1 Dipole Virtuality

The results for the individual contributing parts of the antenna function as defined in eq. (C.4) - eq. (C.8) with $\xi = \frac{\min(s_{qg}, s_{g\bar{q}})}{m_{IK}^2 - \min(s_{qg}, s_{g\bar{q}})}$ are

$$I_1 = \frac{\pi^2}{6} + \ln^2(\xi) - \ln^2(1 + \xi) - 2 \text{Li}_2 \left[\frac{1}{1 + \xi} \right] \quad (\text{C.11})$$

$$I_2 = \frac{\xi - 1 - \ln(\xi)}{1 + \xi} \quad (\text{C.12})$$

$$I_3 = \frac{-3 + 3\xi^2 - (2 + 4\xi) \ln(\xi)}{8(1 + \xi)^2} \quad (\text{C.13})$$

$$I_4 = \frac{(\xi - 1)(11 + \xi(20 + 11\xi)) - 6(1 + 3\xi(1 + \xi)) \ln(\xi)}{36(1 + \xi)^3} \quad (\text{C.14})$$

$$I_5 = \frac{(\xi - 1)^2((C_{01} + C_{10})(1 + 2\xi) + 3C_{00}(1 + \xi))}{12(1 + \xi)^3} \quad (\text{C.15})$$

In the case of integration over the $3 \rightarrow 4$ splittings, the definition of the integrals remains the same. Only the definition of ξ changes with

$$\xi_{3 \rightarrow 4} = \frac{\min(s_{qg}, s_{g\bar{q}})}{\max(s_{qg}, s_{g\bar{q}}) - \min(s_{qg}, s_{g\bar{q}})} \quad (\text{C.16})$$

C.1.2 Transverse Momentum

The results for the individual contributing parts of the antenna function as defined in eq. (C.4) - eq. (C.8) are

$$I_1 = \frac{\pi^2}{6} + \frac{1}{2} \ln^2 \left[\frac{y_3^2}{2(1 + \sqrt{1 - y_3^2}) - y_3^2} \right] - \ln^2 \left[\frac{1}{2} \left(1 + \sqrt{1 - y_3^2} \right) \right] - 2 \text{Li}_2 \left[\frac{1}{2} \left(1 + \sqrt{1 - y_3^2} \right) \right] \quad (\text{C.17})$$

$$I_2 = - \left(\ln \left[\frac{y_3^2}{2(1 + \sqrt{1 - y_3^2}) - y_3^2} \right] + 2\sqrt{1 - y_3^2} \right) \quad (\text{C.18})$$

$$I_3 = -\frac{1}{4} \left(\ln \left[\frac{y_3^2}{2(1 + \sqrt{1 - y_3^2}) - y_3^2} \right] + 2\sqrt{1 - y_3^2} \right) \quad (\text{C.19})$$

$$I_4 = -\frac{13\sqrt{1 - y_3^2}}{36} + \frac{1}{36} y_3^2 \sqrt{1 - y_3^2} - \frac{1}{6} \ln \left[\frac{y_3^2}{2(1 + \sqrt{1 - y_3^2}) - y_3^2} \right] \quad (\text{C.20})$$

$$I_5 = \frac{1}{24} \left(2(3C_{00} + (C_{01} + C_{10})(1 - y_3^2)) \sqrt{1 - y_3^2} + 3C_{00} y_3^2 \ln \left[\frac{y_3^2}{2(1 + \sqrt{1 - y_3^2}) - y_3^2} \right] \right) \quad (\text{C.21})$$

with $y_3^2 = \frac{Q_3^2}{m_{IK}^2}$ and $m_{IK}^2 = s$. In the case of the $3 \rightarrow 4$ splittings the only adaptation takes place in the former definition where m_{IK}^2 is set equal to s_{qg} or $s_{g\bar{q}}$ dependent on which dipole is being integrated over.

C.1.3 Energy ordering

The results for this evolution parameter are

$$\begin{aligned}
I_1 = & 2 \text{Li}_2 \left[\frac{1}{2} \left(1 + \sqrt{1 - \frac{\Delta}{y_3}} \right) \right] + \ln^2 \left[\frac{1}{2} \left(1 + \sqrt{1 - \frac{\Delta}{y_3}} \right) \right] - \frac{1}{2} \ln^2 \left[\frac{\Delta}{2y_3 \left(1 + \sqrt{1 - \frac{\Delta}{y_3}} \right) - \Delta} \right] \\
& - 2 \text{Li}_2 \left[\frac{1}{2} \left(1 + \sqrt{1 - \Delta} \right) \right] - \ln^2 \left[\frac{1}{2} \left(1 + \sqrt{1 - \Delta} \right) \right] + \frac{1}{2} \ln^2 \left[\frac{\Delta}{2 \left(1 + \sqrt{1 - \Delta} \right) - \Delta} \right]
\end{aligned} \tag{C.22}$$

$$\begin{aligned}
I_2 = & 2 \left(\sqrt{y_3 - \Delta} - \sqrt{1 - \Delta} \right) + \sqrt{y_3} \ln \left[\frac{\Delta}{2y_3 \left(1 + \sqrt{1 - \frac{\Delta}{y_3}} \right) - \Delta} \right] - \ln \left[\frac{\Delta}{2 \left(1 + \sqrt{1 - \Delta} \right) - \Delta} \right]
\end{aligned} \tag{C.23}$$

$$\begin{aligned}
I_3 = & \frac{1}{4} \left(y_3 \ln \left[\frac{\Delta}{2y_3 \left(1 + \sqrt{1 - \frac{\Delta}{y_3}} \right) - \Delta} \right] - \ln \left[\frac{\Delta}{2 \left(1 + \sqrt{1 - \Delta} \right) - \Delta} \right] \right) \\
& + \frac{1}{2} \left(\sqrt{y_3(y_3 - \Delta)} - \sqrt{1 - \Delta} \right)
\end{aligned} \tag{C.24}$$

$$\begin{aligned}
I_4 = & \frac{1}{36} \left(6y_3^{\frac{3}{2}} \ln \left[\frac{\Delta}{2y_3 \left(1 + \sqrt{1 - \frac{\Delta}{y_3}} \right) - \Delta} \right] - 6 \ln \left[\frac{\Delta}{2 \left(1 + \sqrt{1 - \Delta} \right) - \Delta} \right] \right) \\
& + (13y_3 - \Delta) \sqrt{y_3 - \Delta} - (13 - \Delta) \sqrt{1 - \Delta}
\end{aligned} \tag{C.25}$$

$$\begin{aligned}
I_5 = & \frac{1}{8} C_{00} \left(\Delta \cdot \ln \left[\frac{2y_3(1 + \sqrt{1 - \frac{\Delta}{y_3}}) - \Delta}{2(1 + \sqrt{1 - \Delta}) - \Delta} \right] + 2\sqrt{1 - \Delta} - 2\sqrt{y_3(y_3 - \Delta)} \right) \\
& + \frac{1}{12} (C_{01} + C_{10}) \left((1 - \Delta)^{\frac{3}{2}} - (y_3 - \Delta)^{\frac{3}{2}} \right)
\end{aligned} \tag{C.26}$$

with Δ used as a cut-off on $4p_\perp^2$ and $y_3 = \frac{(s_{q\bar{q}} + s_{g\bar{q}})^2}{s^2}$.

C.2 Strong Ordering Gluon Splitting

The branching of a gluon splitting into a quark antiquark pair can only take place at the $3 \rightarrow 4$ level splitting. The generation of a gluon splitting takes place through an alternative form of phase space generation than the discussed m_D , p_\perp and E_n variables. Instead phase space is sampled in a triangular surface comparable to m_D ordering, yet in this case using only one cutoff, the Q^2 generated at the $2 \rightarrow 3$ level, to avoid the singular region of the gluon

splitting antenna. The gluon splitting antenna is given by

$$a_{\bar{q}/qg}(y_1, y_2) = \frac{1}{m_{IK}^2} \left(\frac{(1-2y_1)}{2y_2} + \frac{y_1^2}{y_2} + C_{00} + C_{01}y_1 + C_{10}y_2 \right). \quad (\text{C.27})$$

Because the integration surface is similar for all evolution types only depending on the cutoff Q^2 the integration is demonstrated for all types

$$\begin{aligned} H &= \frac{1}{2m_{IK}^2} \int_{Q_E^2}^{m_{IK}^2} ds_2 \int_0^{m_{IK}^2 - s_2} ds_1 a_{\bar{q}/qg}(s_1, s_2) = \frac{m_{IK}^2}{2} \int_{y_E = \frac{Q_E^2}{m_{IK}^2}}^1 dy_2 \int_0^{1-y_2} dy_1 a_{\bar{q}/qg}(y_1, y_2) \\ &= \frac{1}{2} \left[\frac{1}{3} \ln \left(\frac{1}{y_E} \right) - \frac{13}{36} + \frac{y_E}{2} - \frac{y_E^2}{4} + \frac{y_E^3}{9} + \frac{(1-y_E)^2}{2} \left(C_{00} + \frac{C_{01}}{3} (1-y_E) + \frac{C_{10}}{3} (1+2y_E) \right) \right] \end{aligned} \quad (\text{C.28})$$

where the factor a half has been added for the sake of consistency with respect to the treatment of gluon emission. The factor m_{IK}^2 needs to be replaced by either s_{qg} or $s_{g\bar{q}}$ dependent on which antenna is being integrated.

C.3 Smooth Ordering Gluon Emission

The phase space integral in the case of smooth ordering differs from strong ordering by allowing integration over the whole phase space region. The inclusion of a damping factor regulates the accessible region of phase space which generates a different phase space occupancy than in the case of strong ordering. A general form for smooth ordering integration of a gluon emission antenna is

$$\frac{1}{16\pi^2 m_{IK}^2} \int_0^{m_{IK}^2} ds_1 \int_0^{m_{IK}^2 - s_1} ds_2 \frac{Q_{E_j}^2}{Q_{E_j}^2 + Q_3^2} a_{g/IK}(s_1, s_2) \quad (\text{C.29})$$

Where we use the definition of eq. (C.1) with $s_i = y_i m_{IK}^2$, Q_3^2 denotes the branching scale and Q_{E_j} indicates the evolution variable used for gluon emission. We define the following integrals

$$\mathcal{D}_s = \frac{1}{m_{IK}^4} \int_0^{m_{IK}^2} ds_1 \int_0^{m_{IK}^2 - s_1} ds_2 \frac{Q_{E_j}^2}{Q_{E_j}^2 + Q_3^2} \quad (\text{C.30})$$

$$L_1 = \mathcal{D}_s \frac{m_{IK}^4}{s_1 s_2} \quad (\text{C.31})$$

$$L_2 = \mathcal{D}_s \frac{m_{IK}^2}{s_1} = \mathcal{D}_s \frac{m_{IK}^2}{s_2} \quad (\text{C.32})$$

$$L_3 = \mathcal{D}_s \frac{s_1}{2s_2} = \mathcal{D}_s \frac{s_2}{2s_1} \quad (\text{C.33})$$

$$L_4 = \mathcal{D}_s \frac{s_1^2}{2m_{IK}^2 s_2} = \mathcal{D}_s \frac{s_2^2}{2m_{IK}^2 s_1} \quad (\text{C.34})$$

$$L_5 = \frac{1}{2} \mathcal{D}_s \left[C_{00} + C_{01} \frac{s_1}{m_{IK}^2} + C_{10} \frac{s_2}{m_{IK}^2} \right]. \quad (\text{C.35})$$

So that, in these terms, the results read

$$\frac{1}{16\pi^2 m_{IK}^2} \int_0^{m_{IK}^2} ds_1 \int_0^{m_{IK}^2 - s_1} ds_2 \frac{Q_{E_j}^2}{Q_{E_j}^2 + Q_3^2} a_{g/IK} = \frac{1}{8\pi^2} \left(\sum_{i=1}^5 K_i L_i \right) \quad (\text{C.36})$$

where

$$K_1 = 1, \quad K_2 = -2, \quad K_3 = 2, \quad K_4 = -\delta_{Ig} - \delta_{Kg}, \quad K_5 = 1. \quad (\text{C.37})$$

We now turn to specific cases.

C.3.1 Smooth mass ordering

The only term from eq. (C.29) that requires specification is the damping factor

$$1 - P_{\text{imp}} = \frac{Q_{E_j}^2}{Q_{E_j}^2 + Q_3^2} = \frac{\min(s_1, s_2)}{\min(s_1, s_2) + \min(s_{qg}, s_{g\bar{q}})}. \quad (\text{C.38})$$

The computation of the individual antenna parts will require separating the phase space triangle in two regions ($s_1 > s_2$ and vice versa) in order to make the damping factor definite. After summing over these two regions we obtain the following values for gluon emission

contributions

$$L_1 = 2 \left[\ln(2) \ln \left(1 + \frac{2}{y_3^2} \right) - \text{Li}_2 \left(-\frac{1}{y_3^2} \right) - \text{Li}_2 \left(\frac{2}{2 + y_3^2} \right) + \text{Li}_2 \left(\frac{1}{2 + y_3^2} \right) \right] \quad (\text{C.39})$$

$$L_2 = -1 + \ln \left(2 + \frac{2}{y_3^2} \right) + y_3^2 \ln \left(1 + \frac{1}{y_3^2} \right) - \frac{1}{2} y_3^2 \ln \left(1 + \frac{2}{y_3^2} \right) \ln(2) \\ + \frac{1}{2} y_3^2 \left[\text{Li}_2 \left(-\frac{1}{y_3^2} \right) + \text{Li}_2 \left(\frac{2}{2 + y_3^2} \right) - \text{Li}_2 \left(\frac{1}{2 + y_3^2} \right) \right] \quad (\text{C.40})$$

$$L_3 = \frac{1}{8} \left(-3 + 2 \ln \left(\frac{2 + 2y_3^2}{y_3^2} \right) + 2y_3^2 \ln \left(\frac{1 + y_3^2}{2y_3^2} \right) + y_3^4 \ln \left(1 + \frac{2}{y_3^2} \right) \ln(2) \right. \\ \left. - y_3^4 \left[\text{Li}_2 \left(-\frac{1}{y_3^2} \right) + \text{Li}_2 \left(\frac{2}{2 + y_3^2} \right) - \text{Li}_2 \left(\frac{1}{2 + y_3^2} \right) \right] \right) \quad (\text{C.41})$$

$$L_4 = \frac{1}{72} \left[-22 + 12 \ln \left(\frac{2 + 2y_3^2}{y_3^2} \right) - 3y_3^2 + 18y_3^2 \ln \left(\frac{1 + y_3^2}{\sqrt{2}y_3^2} \right) - 3y_3^4 + 9y_3^4 \ln \left(\frac{2 + 2y_3^2}{y_3^2} \right) \right] \\ + \frac{1}{24} y_3^6 \ln \left(\frac{1 + y_3^2}{y_3^2} \right) - \frac{1}{16} y_3^6 \ln \left(\frac{2 + y_3^2}{y_3^2} \right) \ln(2) \\ + \frac{1}{16} y_3^6 \left[\text{Li}_2 \left(-\frac{1}{y_3^2} \right) + \text{Li}_2 \left(\frac{2}{2 + y_3^2} \right) - \text{Li}_2 \left(\frac{1}{2 + y_3^2} \right) \right] \quad (\text{C.42})$$

$$L_5 = \frac{1}{48} \left[4(3C_{00} + C_{01} + C_{10}) + 3(8C_{00} + C_{01} + C_{10})y_3^2 - 6(C_{01} + C_{10})y_3^4 \right. \\ \left. - 6y_3^2(1 + y_3^2)(4C_{00} + C_{01} + C_{10} - (C_{01} + C_{10})y_3^2) \ln \left(\frac{1 + y_3^2}{y_3^2} \right) \right] \quad (\text{C.43})$$

with $y_3^2 = \frac{2 \min(s_{qg}, s_{g\bar{q}})}{m_{IK}^2}$.

C.3.2 Smooth transverse momentum ordering

In the case of smooth ordering for transverse momentum we find the following result for the ordering requirement

$$1 - P_{\text{imp}} = \frac{Q_{E_j}^2}{Q_{E_j}^2 + Q_3^2} = \frac{\frac{s_1 s_2}{m_{IK}^2}}{\frac{s_1 s_2}{m_{IK}^2} + \frac{s_{qg} s_{g\bar{q}}}{s}}. \quad (\text{C.44})$$

Where m_{IK}^2 should be replaced by s_{qg} or $s_{g\bar{q}}$ dependent on the dipole of integration. In combination with eq. (C.29) we find the following results for the partial gluon emission antenna

parts

$$L_1 = \frac{1}{2} \ln^2 \left(\frac{y_3^2}{2(1 + \sqrt{1 + y_3^2}) + y_3^2} \right) \quad (\text{C.45})$$

$$L_2 = -2 - \sqrt{1 + y_3^2} \cdot \ln \left(\frac{y_3^2}{2(1 + \sqrt{1 + y_3^2}) + y_3^2} \right) \quad (\text{C.46})$$

$$L_3 = -\frac{1}{2} - \frac{1}{4} \sqrt{1 + y_3^2} \cdot \ln \left(\frac{y_3^2}{2(1 + \sqrt{1 + y_3^2}) + y_3^2} \right) \quad (\text{C.47})$$

$$L_4 = -\frac{13}{36} - \frac{1}{12} y_3^2 - \frac{1}{24} (4 + y_3^2) \sqrt{1 + y_3^2} \ln \left(\frac{y_3^2}{2(1 + \sqrt{1 + y_3^2}) + y_3^2} \right) \quad (\text{C.48})$$

$$\begin{aligned} L_5 = & (C_{01} + C_{10}) \left(\frac{1}{12} + \frac{1}{4} y_3^2 + \frac{1}{8} y_3^2 \sqrt{1 + y_3^2} \ln \left(\frac{y_3^2}{2(1 + \sqrt{1 + y_3^2}) + y_3^2} \right) \right) \\ & + C_{00} \left(\frac{1}{4} - \frac{1}{16} y_3^2 \ln^2 \left(\frac{y_3^2}{2(1 + \sqrt{1 + y_3^2}) + y_3^2} \right) \right) \end{aligned} \quad (\text{C.49})$$

with $y_3^2 = 4 \frac{s_{qg} s_{g\bar{q}}}{s m_{IK}^2} = \frac{4}{N_\perp} \frac{Q_3^2}{m_{IK}^2}$, so that $y_3^2 = 4s_{qg}/s$ for $m_{IK}^2 = s_{g\bar{q}}$, and $y_3^2 = 4s_{g\bar{q}}/s$ for $m_{IK}^2 = s_{qg}$.

C.4 Smooth Ordering Gluon Splitting

Additionally we also need to consider the gluon splitting antenna function for smooth ordering. Similar to the strong ordering case, the separate generation of gluon splitting variables allows for a new choice for evolution variable and thereby a different phase space surface. As in the case of gluon emission we allow for integration over the whole phase space, using the damping factor to limit the accessible area. A general notation is the following

$$G = \frac{1}{2m_{IK}^2} \int_0^{m_{IK}^2} ds_2 \int_0^{m_{IK}^2 - s_2} ds_1 \frac{Q_{Ej}^2}{Q_{Ej}^2 + Q_3^2} a_{\bar{q}/qg}(s_1, s_2), \quad (\text{C.50})$$

with the definition for the gluon splitting antenna as in eq. (C.27) and the default choice of evolution variable for gluon splittings being $Q_{Ej}^2 = m_{q\bar{q}}^2 = s_2$.

C.4.1 Emissions ordered in m_D , splittings in $m_{q\bar{q}}$

With the gluon splitting antenna as defined in eq. (C.27) and the phase space integral eq. (C.50) we find the following result for $Q_3^2 = N' \min(s_{qg}, s_{g\bar{q}})$:

$$\begin{aligned}
G = & \frac{1}{72s_P^3} \left(-12(s_P^3 + 3(-1 + 2C_{00} + C_{10})y_3^2s_P^2 + 3(-1 + 2C_{00} - 2C_{01} + 2C_{10} + 2C_{10})y_3^4s_P \right. \\
& + (-2 - 6C_{01} + 3C_{10})y_3^6) \operatorname{arctanh} \left(\frac{s_P}{2y_3^2 + s_P} \right) \\
& + s_P \left((-13 + 18C_{00} + 6C_{01} + 6C_{10})s_P^2 + 3(-4 + 12C_{00} - 6C_{01} + 9C_{10})y_3^2s_P \right. \\
& \left. \left. - 6(2 + 6C_{01} - 3C_{10})y_3^4 + 18s_P^2 \ln \left(\frac{s_P + y_3^2}{y_3^2} \right) \right) \right), \tag{C.51}
\end{aligned}$$

with $y_3 = \frac{N' \min(s_{qg}, s_{g\bar{q}})}{s}$ and $s_P = \max(s_{qg}, s_{g\bar{q}})/s$. Note that the gluon splitting antenna has been defined with the singularity in y_2 which determines the form of the damping factor.

C.4.2 Emissions ordered in \mathbf{p}_\perp , splittings in $\mathbf{m}_{q\bar{q}}$

With the gluon splitting antenna defined in eq. (C.27) and the phase space integral eq. (C.50) we find the following result for $Q_3^2 = N_\perp s_{qg} s_{g\bar{q}}/s$:

$$\begin{aligned}
G = & \frac{1}{72} \left(-13 + 18C_{00} + 6C_{01} + 6C_{10} + 3(-4 + 12C_{00} - 6C_{01} + 9C_{10})y_3^2 \right. \\
& - 6(2 + 6C_{01} - 3C_{10})y_3^4 + 36y_3^2 \operatorname{acoth}(1 + 2y_3^2) - 6(-2 + y_3^2(6C_{00}(1 + y_3^2) \\
& \left. + 3C_{10}(1 + y_3^2)^2 - y_3^2(3 + 2y_3^2 + 6C_{01}(1 + y_3^2)))) \ln \left(1 + \frac{1}{y_3^2} \right) \right), \tag{C.52}
\end{aligned}$$

with $y_3^2 = N_\perp \frac{s_{qg} s_{g\bar{q}}}{s m_{IK}^2} = Q_3^2/m_{IK}^2$, so that $y_3^2 = N_\perp s_{qg}/s$ for $m_{IK}^2 = s_{g\bar{q}}$, and $y_3^2 = N_\perp s_{g\bar{q}}/s$ for $m_{IK}^2 = s_{qg}$.

D NLO Tune Parameters

In tab. 7 below, we list the perturbative and non-perturbative fragmentation parameters for the Nikhef NLO tune of VINCIA. For reference, we compare them to the current (LO) default Jeppsson 5 tune, which was used for comparisons to LO VINCIA in this paper.

References

- [1] **MCnet** Collaboration, A. Buckley, J. Butterworth, S. Gieseke, D. Grellscheid, S. Höche, et al., *General-purpose event generators for LHC physics*, *Phys.Rept.* **504** (2011) 145, [[arXiv:1101.2599](#)].
- [2] S. Frixione and B. R. Webber, *Matching NLO QCD computations and parton shower simulations*, *JHEP* **06** (2002) 029, [[hep-ph/0204244](#)].
- [3] S. Frixione, P. Nason, and B. R. Webber, *Matching NLO QCD and parton showers in heavy flavour production*, *JHEP* **08** (2003) 007, [[hep-ph/0305252](#)].

Parameter	NLO Tune (Nikhef)	LO Tune (Jeppsson 5)	Comment
! * alphaS			
Vincia:alphaSvalue	= 0.122	= 0.139	! alphaS(mZ) value
Vincia:alphaSkMu	= 1.0	= 1.0	! Renormalization-scale prefactor
Vincia:alphaSorder	= 2	= 1	! Running order
Vincia:alphaSmode	= 1	= 1	! muR = pT:emit and Q:split
Vincia:alphaScmw	= on	= off	! CMW rescaling of Lambda on/off
! * Shower evolution and IR cutoff			
Vincia:evolutionType	= 1	= 1	! pT-evolution
Vincia:orderingMode	= 2	= 2	! Smooth ordering
Vincia:pTnormalization	= 4.	= 4.	! QT = 2pT
Vincia:cutoffType	= 1	= 1	! Cutoff taken in pT
Vincia:cutoffScale	= 0.8	= 0.6	! Cutoff value (in GeV)
! * Longitudinal string fragmentation parameters			
StringZ:aLund	= 0.40	= 0.38	! Lund FF a (hard fragmentation supp)
StringZ:bLund	= 0.85	= 0.90	! Lund FF b (soft fragmentation supp)
StringZ:aExtraDiquark	= 1.0	= 1.0	! Extra a to suppress hard baryons
! * pT in string breakups			
StringPT:sigma	= 0.29	= 0.275	! Soft pT in string breaks (in GeV)
StringPT:enhancedFraction	= 0.01	= 0.01	! Fraction of breakups with enhanced pT
StringPT:enhancedWidth	= 2.0	= 2.0	! Enhancement factor
! * String breakup flavour parameters			
StringFlav:probStoUD	= 0.215	= 0.215	! Strangeness-to-UD ratio
StringFlav:mesonUDvector	= 0.45	= 0.45	! Light-flavour vector suppression
StringFlav:mesonSvector	= 0.65	= 0.65	! Strange vector suppression
StringFlav:mesonCvector	= 0.80	= 0.80	! Charm vector suppression
StringFlav:probQQtoQ	= 0.083	= 0.083	! Diquark rate (for baryon production)
StringFlav:probSQtoQQ	= 1.00	= 1.00	! Optional Strange diquark suppression
StringFlav:probQQ1toQQ0	= 0.031	= 0.031	! Vector diquark suppression
StringFlav:etaSup	= 0.68	= 0.68	! Eta suppression
StringFlav:etaPrimeSup	= 0.11	= 0.11	! Eta' suppression
StringFlav:decupletSup	= 1.0	= 1.0	! Optional Spin-3/2 Baryon Suppression

Table 7. Parameters of the “Nikhef” NLO tune, compared to those of the “Jeppsson 5” LO tune.

- [4] V. Hirschi, R. Frederix, S. Frixione, M. V. Garzelli, F. Maltoni, et al., *Automation of one-loop QCD corrections*, *JHEP* **1105** (2011) 044, [[arXiv:1103.0621](#)].
- [5] R. Frederix, S. Frixione, F. Maltoni, and T. Stelzer, *Automation of next-to-leading order computations in QCD: The FKS subtraction*, *JHEP* **0910** (2009) 003, [[arXiv:0908.4272](#)].
- [6] R. Frederix, S. Frixione, V. Hirschi, F. Maltoni, R. Pittau, et al., *Four-lepton production at hadron colliders: aMC@NLO predictions with theoretical uncertainties*, *JHEP* **1202** (2012) 099, [[arXiv:1110.4738](#)].
- [7] P. Nason, *A New method for combining NLO QCD with shower Monte Carlo algorithms*, *JHEP* **0411** (2004) 040, [[hep-ph/0409146](#)].
- [8] S. Frixione, P. Nason, and C. Oleari, *Matching NLO QCD computations with Parton Shower simulations: the POWHEG method*, *JHEP* **11** (2007) 070, [[arXiv:0709.2092](#)].
- [9] S. Alioli, P. Nason, C. Oleari, and E. Re, *A general framework for implementing NLO calculations in shower Monte Carlo programs: the POWHEG BOX*, *JHEP* **1006** (2010) 043, [[arXiv:1002.2581](#)].
- [10] N. Lavesson and L. Lönnblad, *Extending CKKW-merging to One-Loop Matrix Elements*, *JHEP* **0812** (2008) 070, [[arXiv:0811.2912](#)].
- [11] S. Plätzer and S. Gieseke, *Dipole Showers and Automated NLO Matching in Herwig++*, *Eur.Phys.J.* **C72** (2012) 2187, [[arXiv:1109.6256](#)].
- [12] S. Höche, F. Krauss, M. Schönherr, and F. Siegert, *QCD matrix elements + parton showers: The NLO case*, *JHEP* **1304** (2013) 027, [[arXiv:1207.5030](#)].
- [13] T. Gehrmann, S. Höche, F. Krauss, M. Schönherr, and F. Siegert, *NLO QCD matrix elements + parton showers in $e^+e^- \rightarrow \text{hadrons}$* , *JHEP* **1301** (2013) 144, [[arXiv:1207.5031](#)].
- [14] R. Frederix and S. Frixione, *Merging meets matching in MC@NLO*, *JHEP* **1212** (2012) 061, [[arXiv:1209.6215](#)].
- [15] L. Lönnblad and S. Prestel, *Unitarising Matrix Element + Parton Shower merging*, *JHEP* **1302** (2013) 094, [[arXiv:1211.4827](#)].
- [16] S. Plätzer, *Controlling inclusive cross sections in parton shower + matrix element merging*, [[arXiv:1211.5467](#)].
- [17] S. Alioli, C. W. Bauer, C. J. Berggren, A. Hornig, F. J. Tackmann, et al., *Combining Higher-Order Resummation with Multiple NLO Calculations and Parton Showers in GENEVA*, [[arXiv:1211.7049](#)].
- [18] L. Lönnblad and S. Prestel, *Merging Multi-leg NLO Matrix Elements with Parton Showers*, [[arXiv:1211.7278](#)].
- [19] K. Hamilton, P. Nason, C. Oleari, and G. Zanderighi, *Merging $H/W/Z + 0$ and 1 jet at NLO with no merging scale: a path to parton shower + NNLO matching*, [[arXiv:1212.4504](#)].
- [20] G. Gustafson and U. Pettersson, *Dipole formulation of QCD cascades*, *Nucl. Phys.* **B306** (1988) 746.
- [21] D. A. Kosower, *Antenna factorization of gauge-theory amplitudes*, *Phys. Rev.* **D57** (1998) 5410, [[hep-ph/9710213](#)].

- [22] A. Gehrmann-De Ridder, T. Gehrmann, and E. W. N. Glover, *Antenna Subtraction at NNLO*, *JHEP* **09** (2005) 056, [[hep-ph/0505111](#)].
- [23] W. T. Giele, D. A. Kosower, and P. Z. Skands, *A Simple shower and matching algorithm*, *Phys. Rev.* **D78** (2008) 014026, [[arXiv:0707.3652](#)].
- [24] W. Giele, D. Kosower, and P. Skands, *Higher-Order Corrections to Timelike Jets*, *Phys. Rev.* **D84** (2011) 054003, [[arXiv:1102.2126](#)].
- [25] D. A. Kosower, *Antenna factorization in strongly-ordered limits*, *Phys. Rev.* **D71** (2005) 045016, [[hep-ph/0311272](#)].
- [26] P. Skands, *QCD for Collider Physics*, [arXiv:1104.2863](#).
- [27] Z. Nagy and D. E. Soper, *Final state dipole showers and the DGLAP equation*, *JHEP* **0905** (2009) 088, [[arXiv:0901.3587](#)].
- [28] P. Z. Skands and S. Weinzierl, *Some remarks on dipole showers and the DGLAP equation*, *Phys. Rev.* **D79** (2009) 074021, [[arXiv:0903.2150](#)].
- [29] B. Andersson, G. Gustafson, and C. Sjögren, *Comparison of the dipole cascade model versus $O(\alpha_s^{**2})$ matrix elements and color interference in e^+e^- annihilation*, *Nucl. Phys.* **B380** (1992) 391.
- [30] J. Lopez-Villarejo and P. Skands, *Efficient Matrix-Element Matching with Sector Showers*, *JHEP* **1111** (2011) 150, [[arXiv:1109.3608](#)].
- [31] A. J. Larkoski, J. J. Lopez-Villarejo, and P. Skands, *Helicity-Dependent Showers and Matching with VINCIA*, *Phys. Rev.* **D87** (2013) 054033, [[arXiv:1301.0933](#)].
- [32] R. K. Ellis, D. A. Ross, and A. E. Terrano, *The Perturbative Calculation of Jet Structure in e^+e^- Annihilation*, *Nucl. Phys.* **B178** (1981) 421.
- [33] A. Gehrmann-De Ridder, T. Gehrmann, and E. Glover, *Infrared structure of $e^+e^- \rightarrow 2$ jets at NNLO*, *Nucl. Phys.* **B691** (2004) 195, [[hep-ph/0403057](#)].
- [34] D. Amati, A. Bassetto, M. Ciafaloni, G. Marchesini, and G. Veneziano, *A Treatment of Hard Processes Sensitive to the Infrared Structure of QCD*, *Nucl. Phys.* **B173** (1980) 429.
- [35] S. Catani, B. Webber, and G. Marchesini, *QCD coherent branching and semiinclusive processes at large x* , *Nucl. Phys.* **B349** (1991) 635.
- [36] T. Sjöstrand, S. Mrenna, and P. Z. Skands, *A Brief Introduction to PYTHIA 8.1*, *Comput. Phys. Commun.* **178** (2008) 852, [[arXiv:0710.3820](#)].
- [37] G. Altarelli and G. Parisi, *Asymptotic Freedom in Parton Language*, *Nucl. Phys.* **B126** (1977) 298.
- [38] M. Bengtsson and T. Sjöstrand, *Coherent Parton Showers Versus Matrix Elements: Implications of PETRA - PEP Data*, *Phys. Lett.* **B185** (1987) 435.
- [39] A. Gehrmann-De Ridder, M. Ritzmann, and P. Skands, *Timelike Dipole-Antenna Showers with Massive Fermions*, *Phys. Rev.* **D85** (2012) 014013, [[arXiv:1108.6172](#)]. 50 pages.
- [40] G. Marchesini and B. Webber, *Simulation of QCD Jets Including Soft Gluon Interference*, *Nucl. Phys.* **B238** (1984) 1.

- [41] G. Marchesini and B. Webber, *Monte Carlo Simulation of General Hard Processes with Coherent QCD Radiation*, *Nucl.Phys.* **B310** (1988) 461.
- [42] S. Gieseke, P. Stephens, and B. Webber, *New formalism for QCD parton showers*, *JHEP* **0312** (2003) 045, [[hep-ph/0310083](#)].
- [43] G. Corcella, I. Knowles, G. Marchesini, S. Moretti, K. Odagiri, et al., *HERWIG 6: An Event generator for hadron emission reactions with interfering gluons (including supersymmetric processes)*, *JHEP* **0101** (2001) 010, [[hep-ph/0011363](#)].
- [44] M. Bähr, S. Gieseke, M. Gigg, D. Grellscheid, K. Hamilton, et al., *Herwig++ Physics and Manual*, *Eur.Phys.J.* **C58** (2008) 639.
- [45] M. Bengtsson and T. Sjöstrand, *A Comparative Study of Coherent and Noncoherent Parton Shower Evolution*, *Nucl. Phys.* **B289** (1987) 810.
- [46] T. Sjöstrand, S. Mrenna, and P. Z. Skands, *PYTHIA 6.4 Physics and Manual*, *JHEP* **0605** (2006) 026, [[hep-ph/0603175](#)].
- [47] S. Catani and M. Seymour, *A General algorithm for calculating jet cross-sections in NLO QCD*, *Nucl.Phys.* **B485** (1997) 291, [[hep-ph/9605323](#)].
- [48] G. Gustafson, *Multiplicity distributions in QCD cascades*, *Nucl.Phys.* **B392** (1993) 251.
- [49] F. A. Berends and W. Giele, *Multiple Soft Gluon Radiation in Parton Processes*, *Nucl.Phys.* **B313** (1989) 595.
- [50] L. Lönnblad, *ARIADNE version 4: A Program for simulation of QCD cascades implementing the color dipole model*, *Comput. Phys. Commun.* **71** (1992) 15.
- [51] T. Sjöstrand, *A Model for Initial State Parton Showers*, *Phys.Lett.* **B157** (1985) 321.
- [52] T. Sjöstrand and M. van Zijl, *A Multiple Interaction Model for the Event Structure in Hadron Collisions*, *Phys.Rev.* **D36** (1987) 2019.
- [53] S. Frixione, Z. Kunszt, and A. Signer, *Three jet cross-sections to next-to-leading order*, *Nucl.Phys.* **B467** (1996) 399–442, [[hep-ph/9512328](#)].
- [54] Z. Nagy, *Next-to-leading order calculation of three jet observables in hadron hadron collision*, *Phys.Rev.* **D68** (2003) 094002, [[hep-ph/0307268](#)].
- [55] J. Lopez-Villarejo and P. Skands, *Strong and Smooth Ordering in Antenna Showers*, [arXiv:1203.6803](#). In Les Houches SM and NLO Multileg and SM MC Working Groups: Summary Report.
- [56] M. H. Seymour, *Matrix element corrections to parton shower algorithms*, *Comp. Phys. Commun.* **90** (1995) 95, [[hep-ph/9410414](#)].
- [57] S. Catani, F. Krauss, R. Kuhn, and B. R. Webber, *QCD Matrix Elements + Parton Showers*, *JHEP* **11** (2001) 063, [[hep-ph/0109231](#)].
- [58] L. Lönnblad, *Correcting the colour-dipole cascade model with fixed order matrix elements*, *JHEP* **05** (2002) 046, [[hep-ph/0112284](#)].
- [59] A. Gehrmann-De Ridder, T. Gehrmann, E. Glover, and G. Heinrich, *Infrared structure of $e^+ e^- \rightarrow 3$ jets at NNLO*, *JHEP* **0711** (2007) 058, [[arXiv:0710.0346](#)].

- [60] R. K. Ellis, D. A. Ross, and A. E. Terrano, *Calculation of Event Shape Parameters in e^+e^- Annihilation*, *Phys. Rev. Lett.* **45** (1980) 1226.
- [61] A. J. Larkoski and M. E. Peskin, *Spin-Dependent Antenna Splitting Functions*, *Phys. Rev.* **D81** (2010) 054010, [[arXiv:0908.2450](#)].
- [62] Y. Dokshitzer and G. Marchesini, *Monte Carlo and large angle gluon radiation*, *JHEP* **0903** (2009) 117, [[arXiv:0809.1749](#)].
- [63] **L3** Collaboration, P. Achard et al., *Studies of hadronic event structure in e^+e^- annihilation from 30-GeV to 209-GeV with the L3 detector*, *Phys.Rept.* **399** (2004) 71, [[hep-ex/0406049](#)].
- [64] **ALEPH** Collaboration, A. Heister et al., *Studies of QCD at e^+e^- centre-of-mass energies between 91-GeV and 209-GeV*, *Eur. Phys. J.* **C35** (2004) 457.
- [65] W. J. Stirling, *Hard QCD working group: Theory summary*, *J.Phys.* **G17** (1991) 1567–1574.
- [66] M. Cacciari, G. P. Salam, and G. Soyez, *FastJet User Manual*, *Eur.Phys.J.* **C72** (2012) 1896, [[arXiv:1111.6097](#)].
- [67] A. Buckley, H. Hoeth, H. Lacker, H. Schulz, and J. E. von Seggern, *Systematic event generator tuning for the LHC*, *Eur.Phys.J.* **C65** (2010) 331, [[arXiv:0907.2973](#)].
- [68] J. Alcaraz Maestre et al., *The SM and NLO Multileg and SM MC Working Groups: Summary Report*, [arXiv:1203.6803](#).
- [69] A. Karneyeu, L. Mijovic, S. Prestel, and P. Skands, *MCPLOTS: a particle physics resource based on volunteer computing*, [arXiv:1306.3436](#), <http://mcplots.cern.ch>.
- [70] A. Buckley and M. Whalley, *HepData reloaded: Reinventing the HEP data archive*, *PoS ACAT2010* (2010) 067, [[arXiv:1006.0517](#)].
- [71] **Particle Data Group** Collaboration, J. Beringer et al., *Review of Particle Physics (RPP)*, *Phys.Rev.* **D86** (2012) 010001.
- [72] A. Pich, *Review of α_s determinations*, [arXiv:1303.2262](#).
- [73] M. Ritzmann, D. Kosower, and P. Skands, *Antenna Showers with Hadronic Initial States*, *Phys.Lett.* **B718** (2013) 1345–1350, [[arXiv:1210.6345](#)].
- [74] W. T. Giele, L. Hartgring, D. A. Kosower, E. Laenen, A. J. Larkoski, et al., *The Vincia Parton Shower*, [arXiv:1307.1060](#).
- [75] E. Boos, M. Dobbs, W. Giele, I. Hinchliffe, J. Huston, et al., *Generic user process interface for event generators*, [hep-ph/0109068](#).